UNIV. OF MICHIGAN
MAY 7 1953

Electrochemical Society

ELECTROCHEMICAL INDUSTRY

The Pittsburgh Area

The De Nora Cells At
MUSCLE SHOALS

The De Nora cells at the new Government-owned, Monsanto-operated chlorine plant, Muscle Shoals, Alabama, are eloquent testimony to chemical engineering progress.

Uniformly high quality GLC GRAPHITE ANODES are doing their share to help the electrolytic industry meet the ever-increasing civilian and defense demands for chlorine and caustic soda.

ELECTRODE DIVISION

Great Lakes Carbon Corporation

Niagara Falls, N. Y. GLC Morganton, N. C.

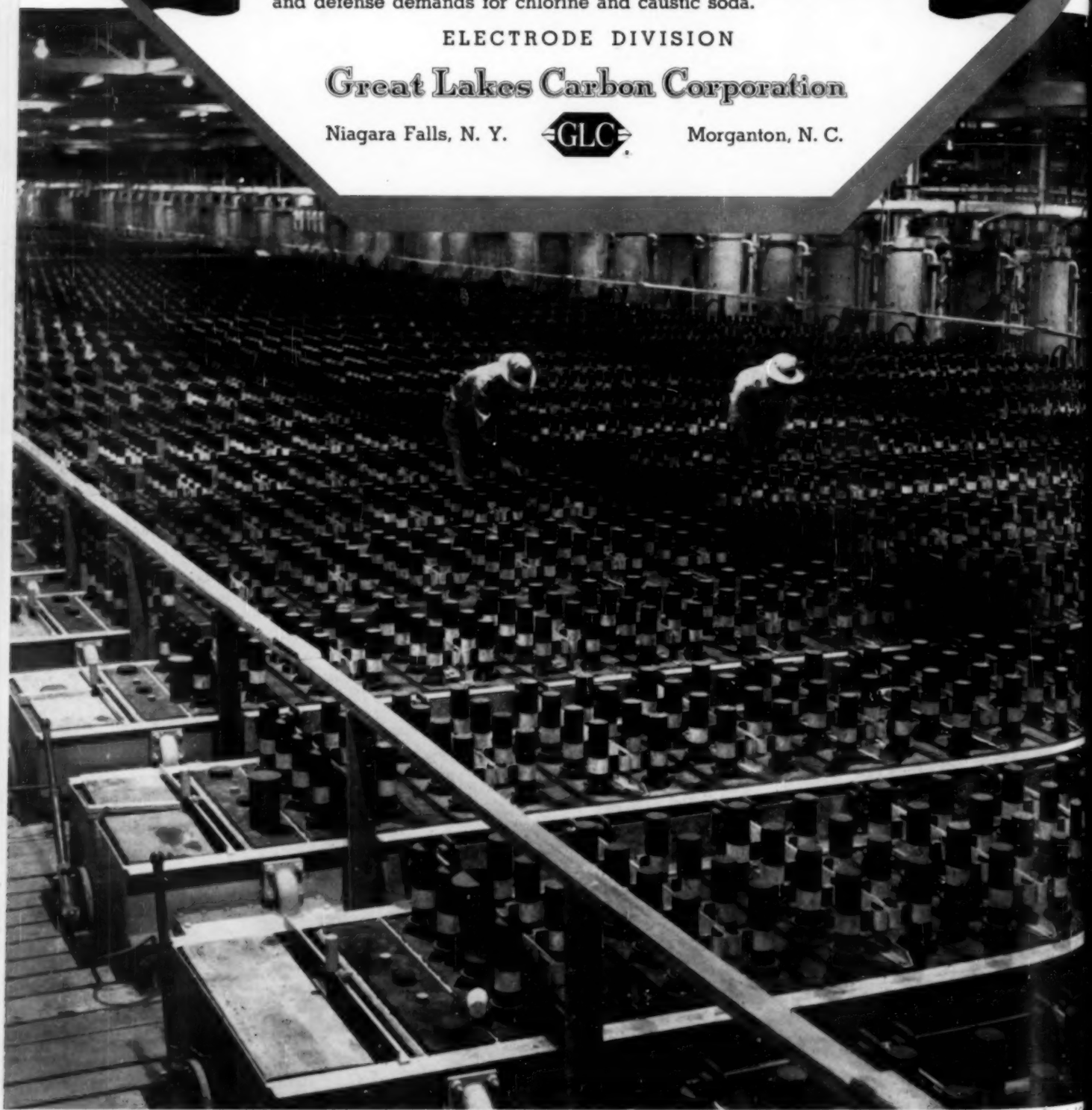

Courtesy Monsanto Chemical Co.

Graphite Anodes, Electrodes and Specialties

Sales office: Niagara Falls, N. Y. **Other offices:** New York, N. Y., Chicago, Ill., Pittsburgh, P

Sales Agents: J. B. Hayes, Birmingham, Ala., George O'Hara, Long Beach, Cal., Great Northern Carbon & Chemical Co. Ltd., Montreal, Can

EDITORIAL STAFF

R. M. Burns, *Chairman*
Norman Hackerman, *Technical Editor*
Ruth G. Sterns, *Managing Editor*
Cecil V. King, *Associate Editor*
U. B. Thomas, *News Editor*
Mary F. Murray, *Assistant Editor*

DIVISIONAL EDITORS

M. A. Streicher, *Corrosion*
Abner Brenner, *Electrodeposition*
N. C. Cahoon, *Battery*
H. C. Froelich, *Electronics*
W. C. Gardiner, *Industrial Electrolytic*
S. J. Sindeband, *Electrothermic*
John J. Chapman, *Electric Insulation*
L. B. Rogers, *Theoretical*
Sherlock Swann, Jr., *Electro-Organic*

REGIONAL EDITORS

Joseph Schulein, *Pacific Northwest*
J. C. Schumacher, *Los Angeles*
O. W. Storey, *Chicago*
G. W. Heise, *Cleveland*
Paul S. Brallier, *Niagara Falls*
Oliver Osborn, *Houston*
Earl A. Gulbransen, *Pittsburgh*
A. C. Holm, *Canada*
J. W. Cuthbertson, *Great Britain*
T. L. Rama Char, *India*

ADVERTISING OFFICE

Jack Bain
Advertising Manager
545 Fifth Avenue
New York 17, N. Y.
PHONE—*Murray Hill 2-3345*

Journal of the
Electrochemical Society

MAY, 1953 VOL. 100 • NO. 5

CONTENTS

Regional Features

The Need to be Different—Editorial. *Earl A. Gulbransen*... 113*C*
Electrochemical Industry: The Pittsburgh Area. *Paul Fugassi* 117*C*

Technical Papers

The Inhibition of the Corrosion of Iron by Some Anodic Inhibitors. *M. J. Pryor and M. Cohen*..... 203
Amount of Oxygen on the Surface of Passive Stainless Steel. *Herbert H. Uhlig and Samuel S. Lord, Jr*..... 216
Distribution of Conductivity within Dielectric Films on Aluminum. *J. E. Lilienfeld and Charles Miller*..... 222
Electrodeposition of Copper from the Monoethanolamine Bath. *T. L. Rama Char and N. B. Shivaraman*..... 227
Electrodeposition of Cadmium from Fluoborate Solutions. *T. R. Anantharaman and J. Balachandra*..... 232
Electrogalvanizing from Fluoborate Solutions. *T. R. Anantharaman and J. Balachandra*..... 237
Factors Controlling the Combustion of Zirconium Powders. *Holger C. Andersen and Lawrence H. Belz*..... 240
Alkaline Earth Orthophosphate Phosphors. *Keith H. Butler*. 250
Copper-Activated Zinc Sulfide Phosphors with Yellow and Red Emission. *H. C. Froelich*..... 256

Feature Section

Electrolytic Grinding or Machining of Metals. *O. W. Storey*. 125*C*

Current Affairs

News in the Electrochemical Field..... 127*C*
Section News..... 129*C* Publishers' Announcements 132*C*
Personals..... 131*C* New Products..... 133*C*
New Members..... 132*C* Literature from Industry.. 133*C*
Highlights of Board of Directors' Meeting and Auditor's Report 135*C*

Published monthly by The Electrochemical Society, Inc., Mount Royal and Guilford Aves., Baltimore 2, Md., combining the JOURNAL and TRANSACTIONS OF THE ELECTROCHEMICAL SOCIETY. Editorial offices: 235 West 102nd Street, New York 25, N. Y. Statements and opinions given in articles and papers in the JOURNAL OF THE ELECTROCHEMICAL SOCIETY are those of the contributors, and The Electrochemical Society assumes no responsibility for them. Subscription $11.25 to members, $15.00 to nonmembers. Single copies $1.25 to members, $1.50 to nonmembers. Copyright 1953 by The Electrochemical Society, Inc. Entered as second-class matter November 15, 1947, at the Post Office at Baltimore, Md., under the act of August 24, 1912.

Pipes that grew without getting bigger

Cross-section of coaxial cable. To triple capacity, Bell Laboratories and Western Electric engineers had to make 1000 amplifiers work perfectly in tandem... feed repeater power along the same cable that carries messages . . . put signals on and off the line at numerous cities along the route without distortion.

Pencil-size pipes carry telephone messages and television across country through the Bell System's coaxial cable. Once, each pipe could carry 600 voices, or one television program. Now it can carry 1800 voices, or 600 voices *plus* a broadcast quality television program.

Yet the pipes aren't any larger. They are being made into triple-duty voiceways by new repeaters, new terminal equipment and other transmission advances developed by Bell Laboratories engineers.

The conversion expense is less than the cost of laying extra coaxial cables. But it calls for highly refined manufacturing procedures, made possible only by close co-operation of Bell Laboratories and Western Electric, manufacturing unit of the Bell System.

In improving the coaxial cable system they created more than 20 years ago, engineers at Bell Telephone Laboratories devised a new way to give America still better telephone service, while the cost stays low.

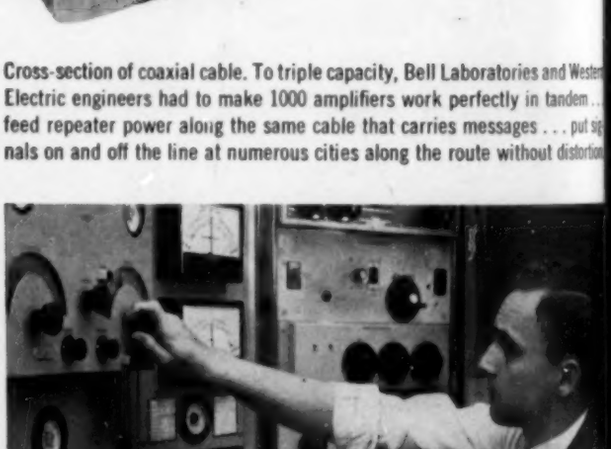

Laboratories engineer tests new triple-duty coaxial system. It marks the first time that telephone conversations and television can travel through the same pipes at the same time. With a wider frequency band being transmitted, the problem was to eliminate interference between the two types of signals.

BELL TELEPHONE LABORATORIES

IMPROVING TELEPHONE SERVICE FOR AMERICA PROVIDES CAREERS FOR CREATIVE MEN IN SCIENTIFIC AND TECHNICAL FIELDS

The Inhibition of the Corrosion of Iron by Some Anodic Inhibitors[1]

M. J. Pryor and M. Cohen
National Research Council, Ottawa, Canada

ABSTRACT

Inhibitors having relatively strong oxidizing anions, such as sodium chromate and nitrite, passivate iron both in the presence of air and in deaerated solutions. Much weaker oxidizing agents such as sodium tungstate and molybdate behave similarly to chromate and nitrite in the presence of air but do not prevent corrosion in deaerated solutions despite the fact that potential/time and polarization curves indicate that slow film formation is occurring. Tungstate ions, however, are effective oxidizing agents toward iron when discharged anodically at high current density.

Solutions of sodium acetate, benzoate, carbonate, hydroxide, orthophosphate, and silicate, which do not contain oxidizing anions, passivate iron only when they contain dissolved air. When these solutions are deaerated they attack iron very slowly, potential/time and polarization curves indicating that this attack is mainly under cathodic control.

It is postulated that oxygen dissolved in solution is mainly responsible for passivity by virtue of its heterogeneous reaction with surface iron atoms to form a thin film of γ-Fe_2O_3, approximately 200 Å[2] thick, in a manner similar to that by which oxide films are formed in air. This film, if kept in constant repair, prevents iron ions from the metal passing into solution. It is considered that, in inhibitors containing oxidizing anions, the passivity film is formed mainly by dissolved oxygen, whereas in other inhibitors, which do not contain oxidizing anions, the oxide is formed entirely by dissolved oxygen.

Introduction

Previous research was carried out in order to obtain more comprehensive information concerning the reactions occurring when solutions of sodium nitrite (1, 7, 8), sodium chromate (2), sodium hydroxide (3), and sodium orthophosphate (4, 5, 6), saturated with dissolved air, inhibit the corrosion of iron. In all cases passivation of initially film-free iron resulted in the formation of a thin invisible film which was mainly composed of γ-Fe_2O_3. It was suggested that the oxide resulted from the adsorption of oxygen dissolved in solution followed by reaction with the iron surface and growth of the film, until a limiting thickness was obtained. Chromate and nitrite, which are themselves oxidizing agents, were believed to contribute to the formation of oxide by adsorption on the surface followed by oxidation of the iron and reduction of the inhibitor anion. This contention was supported by the observation that, in deaerated solution, iron was still passivated by chromate (3) but suffered slow corrosion in sodium phosphate (5) and sodium hydroxide (3) which are not oxidizing agents with respect to iron.

Since the formation of a protective oxide film was not instantaneous, very slow corrosion initially accompanied the growth of oxide. The corrosion was believed to be localized, presumably at discontinuities in the oxide film, and was mainly under anodic control. This was supported by the detection of small inclusions of corrosion product in the passivity film, lepidocrocite (γ-FeO·OH) in the case of sodium hydroxide (3) and sodium nitrite (8), and strengite ($FePO_4 \cdot 2H_2O$) in the case of sodium phosphate (9) by the combined use of electron microscopy and electron diffraction. The detection of phosphate was later confirmed by a radioactive tracer method (6). The mechanism of inhibition put forward for these four inhibitors was essentially similar, bearing in mind the one major difference that chromate and nitrite ions are oxidizing agents with respect to iron and that chromate, at least, can passivate this metal in deaerated solutions, whereas phosphate and hydroxyl ions are nonoxidizing agents and attack iron very slowly in deaerated solutions.

Lochte and Paul (10) previously pointed out that sodium phosphate, hydroxide, carbonate, and borate behaved similarly in that the electrode potential of iron exposed to deaerated solutions of these compounds was much more negative than in similar solutions containing dissolved air. Furthermore, Robertson (11) showed that sodium chromate, nitrite, tungstate, and molybdate passivated iron at similar concentrations in the presence of air.

[1] Manuscript received June 19, 1952. This paper was prepared for delivery before the Montreal Meeting, October 26 to 30, 1952.

[2] Estimated on the apparent surface area of the specimens.

The purpose of the research described below was to determine whether one mechanism of inhibition could be advanced to explain the passivation of iron by anodic inhibitors in general, since their behavior toward iron was similar in so many aspects. The inhibitors investigated were sodium acetate, benzoate, silicate, carbonate, tungstate, and molybdate in addition to the four inhibitors sodium chromate, nitrite, hydroxide, and phosphate previously investigated.

The major part of the research was directed toward investigating the effect of deaeration on the weight losses of iron specimens, the weight loss/concentration curves, and the potential/time curves. Polarization curves, determined in deaerated solutions, indicated whether the corrosion was under

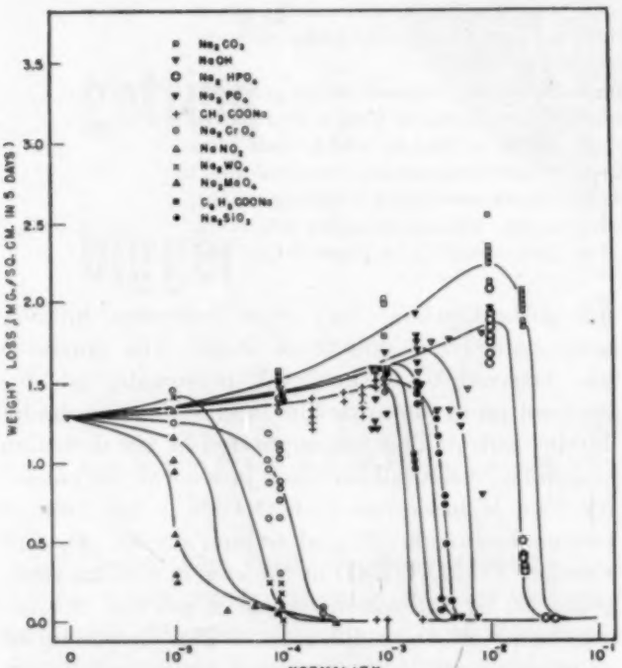

FIG. 1. Variation of weight loss/cm² in 5 days with concentration of 11 inhibitors in the presence of air.

anodic or cathodic control. Experiments were also carried out to ascertain whether inhibitors that were extremely effective in distilled water were, of necessity, also very effective in solutions containing potassium chloride. The effect of carbon dioxide on the corrosion rate was also determined.

EXPERIMENTAL AND RESULTS

Materials.—The iron was in the form of annealed sheet 0.02 cm thick and had the following analysis: C, 0.052 per cent; Si, trace; S, 0.013 per cent; P, 0.028 per cent; Mn, 0.20 per cent; Ni, 0.04 per cent; Cr and Cu, not determinable.

This sheet was used in all experiments except those carried out to determine the effect of concentration on weight loss in the presence of air and the effects of chloride and carbon dioxide. The sheet used in these experiments was on auto-body steel 0.1 cm thick having the analysis: C, 0.12 per cent; Mn, 0.32 per cent; Si, 0.02 per cent; S, 0.01 per cent; P, 0.014 per cent. Specimens, 2.5 x 2.5 cm, cut from these sheets were thoroughly degreased with benzene, abraded with 3/0 emery paper, swabbed with acetone, dried, weighed, and exposed to the solutions as quickly as possible.

The inhibitor solutions under investigation were made from C.P. chemicals and distilled water.

Variation of Weight Loss with Concentration in the Presence of Dissolved Air

The relationship between weight loss and concentration was determined in aqueous solutions of the following compounds: sodium carbonate, hydroxide, dibasic and tribasic phosphate, acetate, benzoate, nitrite, chromate, tungstate, molybdate, and silicate.

The specimens were suspended from glass hooks, by a hole near the center of the top edge, in 200 ml of the solution under investigation in such a manner that their upper edges were 1 cm below the water line of the solution. Experiments were carried out for five days at 25° ± 0.5°C with a high relative humidity to reduce evaporation from the solutions. At the end of the experiment the specimens were removed from the solutions; adherent corrosion products were removed, carefully washed with distilled water, and dried in a desiccator. The specimens were then pickled for 2 minutes in inhibited 1:1 hydrochloric acid; exposure of a clean panel to this treatment resulted in a weight loss of less than 0.2 mg. The specimens were finally washed with water, dried with acetone, and reweighed, the results being expressed as weight loss/cm² in five days (Fig. 1).

The corrosion products were subjected to x-ray analysis using a cobalt target and an iron filter. The results are shown in Table I.

Variation in Weight Loss with Concentration in Deaerated Solutions

This examination was carried out as previously described (5) using the deaeration technique involving the very large decrease in gaseous solubility on freezing an aqueous solution. The apparatus previously used was modified so that specimens measuring 4 x 3 cm and 50 ml of solution could be used. In a typical experiment a specimen was exposed to 50 ml of deaerated solution for five days, the apparatus being placed in a water bath maintained at 25° ± 0.05°C. At the end of this period the apparatus was removed from the bath and opened to

the air; the specimen was removed from solution, cleaned 5 seconds with inhibited 1:1 hydrochloric acid, washed, dried, and reweighed; exposure of a clean specimen to this treatment resulted in a weight loss of less than 0.1 mg.

to determine them with any degree of accuracy by this method, but the solutions, on subsequent exposure to air, became yellowish and later minute quantities of brown hydrated ferric oxide were precipitated. This indicated that, although the

TABLE I

Inhibitor	Conc N	Form of corrosion	Corrosion product	Relative intensities of strongest lines for corrosion products containing more than one compound
NaOH	10^{-3}	General attack	γ-FeO·OH, Fe_3O_4 and α-FeO·OH	100:25:10
	10^{-4}	General attack	γ-FeO·OH, Fe_3O_4 and α-FeO·OH	100:40:1
Na_2CO_3	10^{-2}	Localized attack	α-FeO·OH	—
	10^{-3}	General attack	γ-FeO·OH	—
Na_2HPO_4	10^{-2}	Localized attack	$Fe_3(PO_4)_2 8H_2O$	—
	10^{-3}	General attack	γ-FeO·OH	—
Na_3PO_4	10^{-3}	General attack	γ-FeO·OH	—
	10^{-4}	General attack	γ-FeO·OH and Fe_3O_4	100:5
CH_3COONa	10^{-3}	General attack	γ-FeO·OH and Fe_3O_4	100:80
	10^{-4}	General attack	γ-FeO·OH and Fe_3O_4	100:100
C_6H_5COONa	10^{-3}	General attack	Fe_3O_4 and γ-FeO·OH	100:90
	10^{-4}	General attack	Fe_3O_4 and γ-FeO·OH	100:90
Na_2CrO_4	10^{-4}	General attack	γ-FeO·OH, Fe_3O_4 and α-FeO·OH	100:80:1
	10^{-5}	General attack	Fe_3O_4 and γ-FeO·OH	100:90
$NaNO_2$	10^{-4}	General attack	Fe_3O_4, γ-FeO·OH and α-FeO·OH	100:90:3
Na_2MoO_4	10^{-4}	General attack	α-FeO·OH, γ-FeO·OH and Fe_3O_4	100:75:10

The concentration range examined was $10^{-5}N$ to $1.0N$ for the two inhibitors, disodium phosphate and sodium acetate; blank experiments were carried out to determine the weight loss in distilled water. The results are shown in Fig. 2. Even at the lowest concentration of phosphate examined ($10^{-5}N$) small quantities of crystalline ferrous phosphate were observed adhering firmly to the iron. On the other hand, specimens immersed in the acetate solutions had a slightly dulled appearance and no solid corrosion product could be seen. However, on admitting air to the apparatus the sodium acetate solution first became a brownish-yellow color and later a small quantity of brown hydrated oxide of iron was precipitated.

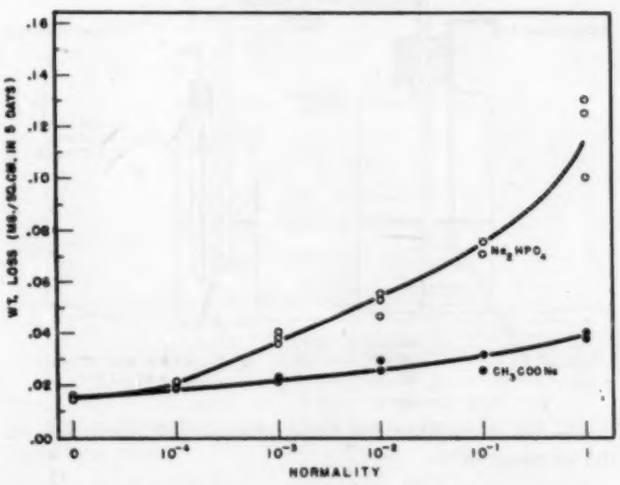

FIG. 2. Variation of weight loss/cm² in 5 days with concentration in deaerated solutions of disodium phosphate and sodium acetate.

Weight Loss Determinations in Deaerated Solutions

These determinations were carried out as described above in deaerated $0.1N$ solutions of all inhibitors under investigation in this research. It was found that iron suffered slow corrosion in deaerated $0.1N$ solutions of all inhibitors with the exception of sodium chromate and sodium nitrite. However, weight losses were so low in solutions with pH values higher than about 10.5 that it was not possible

weight losses were too small to measure accurately, the specimens had undoubtedly undergone very slow corrosion. The weight losses in deaerated solutions with pH values below 10.5 were such that they could be measured to a reasonable degree of accuracy (see Table II). Portions of the original air-

formed oxide film were frequently undermined and could be observed suspended in the solutions. Under the microscope the films exhibited abrasion marks. Specimens immersed in sodium molybdate solution grew films of interference color thickness but, in addition, iron also passed into solution. Only specimens immersed in deaerated solutions of disodium phosphate had a visible solid corrosion product [$Fe_3(PO_4)_2 8H_2O$] adhering to the iron. In all other

TABLE II

Solution *N*	Wt loss/cm² in 5 days (mg)	*p*H value
0.1 Na_2HPO_4	0.075, 0.070	8.5
0.1 CH_3COONa	0.025, 0.031	8.5
0.1 C_6H_5COONa	0.027, 0.033	8.6
0.1 Na_2MoO_4	0.021, 0.029†	8.7
0.1 Na_2WO_4	0.021, 0.016	9.2
0.1 Na_2CO_3	Very small*	10.6
0.1 Na_3PO_4	" "	11.7
0.1 Na_2SiO_3	" "	12.5
0.1 NaOH	" "	12.8
0.1 Na_2CrO_4	Passive	8.5
0.1 $NaNO_2$	"	8.7
0.1 KCl	0.021, 0.019	
H_2O	0.015, 0.017	

† First order interference colors observed on the specimens.

* Weight loss too small to determine accurately but iron passes into solution and precipitates out as hydrated oxide on exposure of solution to air.

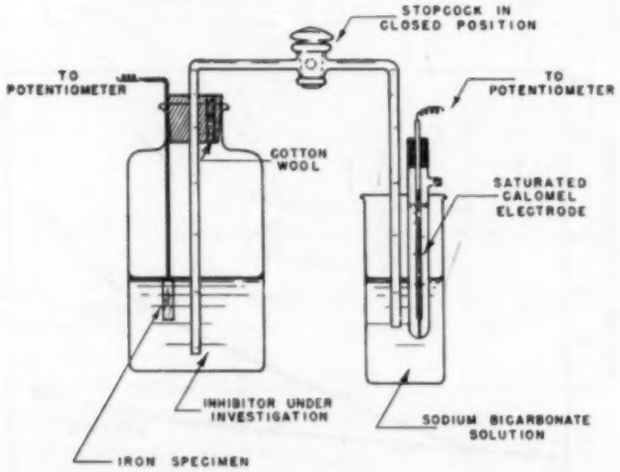

FIG. 3. Apparatus for determination of potentials in the presence of air.

cases, with the exception of sodium molybdate, the specimens either appeared bright or had a slightly etched appearance despite the fact that appreciable dissolution of iron had occurred.

Potential Measurements in the Presence of Air

The variation of the electrode potential of abraded iron specimens with time was determined continuously over a five-day period in 0.1*N* inhibitor solutions.

The apparatus used for these determinations is shown in Fig. 3. Specimens were in the form of strip 0.5 cm wide with a total of 2.5 cm² area exposed to the electrolyte. 300 ml of the solution under investigation were placed in a 600-ml glass bottle and shaken thoroughly in contact with the atmosphere in order to ensure saturation with respect to dissolved air. A small hole through the cork for the bottle was loosely packed with cotton wool to reduce evaporation while still permitting access to the air. Electrolytic contact to a saturated calomel electrode placed in an auxiliary vessel containing saturated sodium bicarbonate solution was effected through a stopcock kept in the closed position. This stopcock was greased with a stiff paste consisting of a mixture of bentonite,[3] glycerine, and water which prevented contamination of the inhibitor solution but maintained excellent electrolytic contact. Separate experiments showed that the resistance of a stopcock treated in this manner was initially of the order of two megohms, but fell in a few hours to a value of approximately 250,000 ohms and remained constant for several weeks; furthermore no diffusion of colored solutions through the stopcock could be detected in one month under a hydrostatic head of one foot.

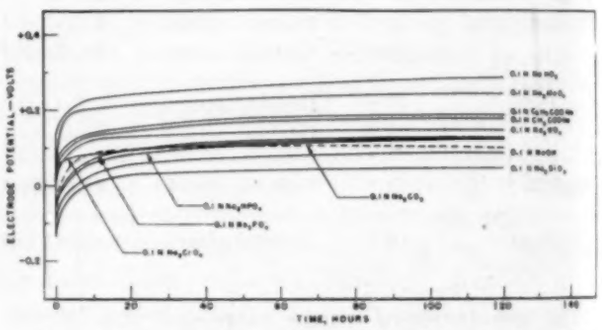

FIG. 4. Potential/time curves for 0.1*N* solutions of 11 inhibitors in the presence of air.

In a typical experiment the specimen was degreased and abraded as described previously; it was then exposed to the solution under examination; potential difference readings were recorded continuously over the five-day period of the experiment by means of a Leeds and Northrup "Micromax" recording potentiometer.

Potential/time curves,[4] determined at 25° ± 0.5°C in 0.1*N* inhibitor solutions are shown in Fig. 4. Experiments were carried out either in duplicate or

[3] A hydrous aluminum silicate which swells on the addition of water.

[4] All potentials in this paper are expressed in relation to the Standard Hydrogen scale.

in triplicate with a control in each series—consisting usually of a redetermination of the curve for 0.1*N* sodium chromate. The results obtained were reasonably reproducible (±10 mv) if careful attention was paid to such factors as saturation of the solutions with dissolved air, absence of vibration, and similarity of surface treatment of the specimens.

Potential/time measurements were also carried out in more dilute solutions of these inhibitors. Fig. 5 and 6 show some typical results. In all cases, dilution of the inhibitor resulted in a more positive (noble) potential as long as the specimens did not corrode. When the final potentials are plotted against the *p*H value of the solution it can be seen that the steady values to which the passive potentials settle become more negative with a rise in *p*H (Fig. 7). The points not lying on the curve are the phosphates and sodium silicate.

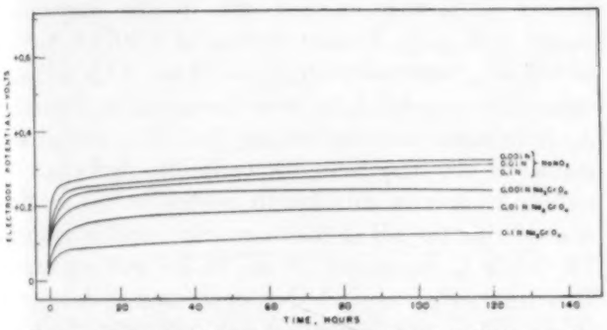

FIG. 5. Potential/time curves in diluted inhibitor solutions in the presence of air.

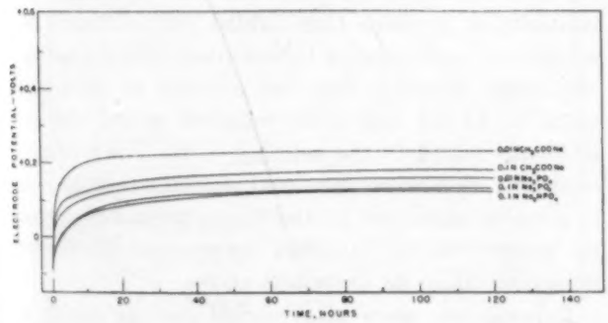

FIG. 6. Potential/time curves in diluted inhibitor solutions in the presence of air.

Potential Measurements in Deaerated Solutions

Potential measurements in deaerated solutions were carried out using the method and apparatus described in a previous paper (5). Specimens measuring 2.5 x 0.5 cm which had been degreased and abraded as described above were exposed to 5 ml of the deaerated 0.1*N* inhibitor solution to which had been added 10 ppm chloride ion, in the form of potassium chloride, so that the chloridized silver wire could take up a steady potential characteristic of the concentration of chloride ions in solution. Potential difference measurements were recorded continuously for the five-day period of the experiments in all 0.1*N* inhibitor solutions with the exception of sodium chromate in which the silver/silver chloride electrode was not stable. Previous work (3), however, had shown that the potential of iron in deaerated 0.1*N* K_2CrO_4 was initially zero and became slowly more positive (noble) with time. The potential of the chloridized silver wire was determined separately at the end of each run and the electrode potential of the specimens calculated. The original air-formed oxide film appeared more stable at *p*H values above 11.0 and was therefore first destroyed by two minutes' treatment with deaerated 0.1*N* hydrochloric acid. The results are shown in Fig. 8.

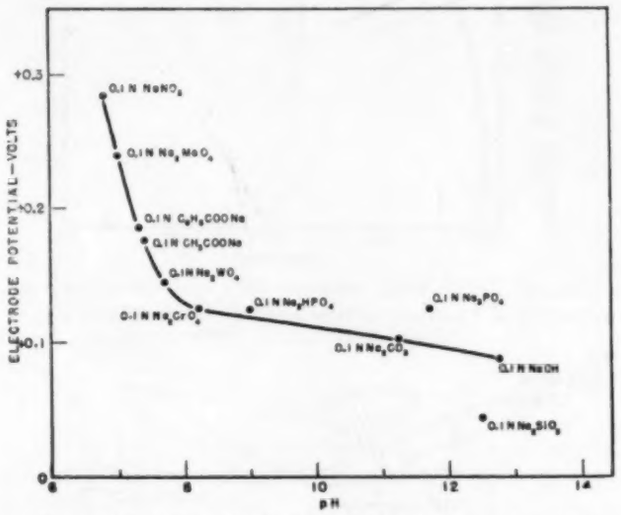

FIG. 7. Relationship between the steady value of the passive potentials and the *p*H of the solutions.

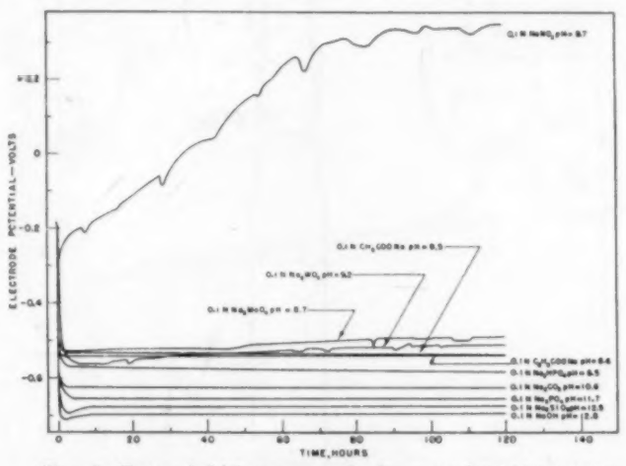

FIG. 8. Potential/time curves in deaerated 0.1*N* inhibitor solutions.

It can be seen that, with the exception of sodium nitrite, tungstate, and molybdate, the potential/time curves are either flat or become slightly more negative (active) with time. Chromate and nitrite are

known to be oxidizing agents with respect to iron, but recently doubt has been raised as to whether tungstate and molybdate behave in a similar manner (11). Accordingly, experiments were carried out to investigate this point.

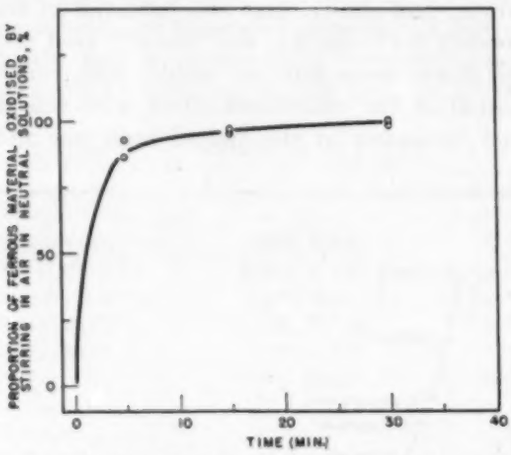

FIG. 9. Relationship between time and the percentage oxidation of a neutral ferrous solution by dissolved air.

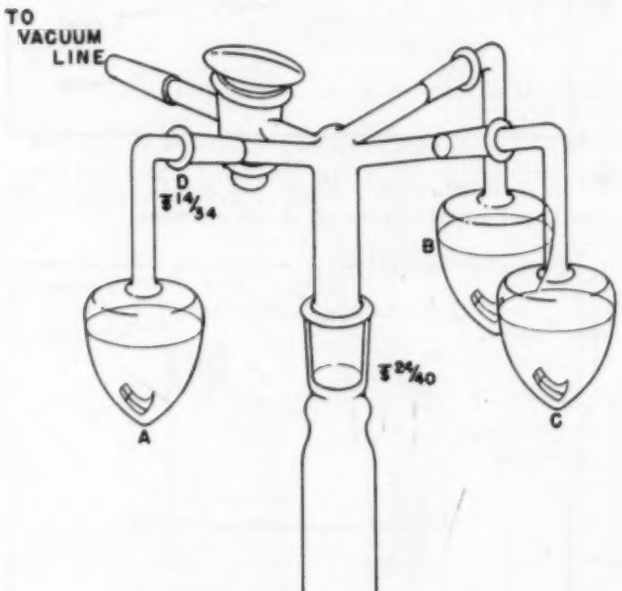

FIG. 10. Apparatus for determining the rates of oxidation of deaerated ferrous solutions.

Rate of Oxidation of Ferrous Solutions at Neutral pH Values by Sodium Tungstate, Molybdate, and Dissolved Air

The rate of oxidation of ferrous ions by dissolved air was determined by stirring 25 ml of acidified 0.0072*N* $FeSO_4$ solution, neutralized to a *p*H value of approximately 7.0 by the addition of strong NaOH solution. The concentration of residual Fe^{++} in solution was determined at different intervals of time by acidifying the solution with concentrated sulfuric acid, which dissolved the hydrated oxides of iron and stopped further oxidation of the ferrous ions, the concentration of which was then determined by an electrometric titration with 0.1*N* $KMnO_4$ from a microburette. The results (Fig. 9) show that oxidation is 95 per cent complete in five minutes and 100 per cent complete in thirty minutes.

Since the rate of oxidation of ferrous ions by air in neutral solution is so high, any attempt to determine the rate of oxidation by tungstate and molybdate must be carried out in the absence of air. Accordingly experiments to this end, the preliminary results of which have been previously reported (12), were carried out in the apparatus shown in Fig. 10. Twenty five ml of 0.0072*N* $FeSO_4$ in NH_2SO_4, together with excess (4 ml) 0.1*N* sodium tungstate or molybdate, were contained in the bulb, A. Robertson (11) has shown that this mixture is stable in air. The bulb, B, contained sufficient *N* sodium hydroxide solution to neutralize the acid in A and bring the *p*H of the mixture to approximately 7.0, while C contained 20 ml of 3*N* sulfuric acid. The three solutions were then deaerated as described above. When the deaeration was complete, the contents of A were transferred to the reaction chamber, R, by rotating the bulb about the joint D. The contents of B were then added to neutralize the excess acid and to bring the solution into the neutral *p*H range. Reaction was then allowed to take place at 25°C. At the end of the required period the acid in C was added to the solution in R. The hydrated oxides of iron were dissolved and the ferrous ions in solution stabilized by the excess acid. The ferrous ion concentration was then determined by electrometric titration as described above.

Experiments were also carried out in which no oxidant was added to the ferrous solution. Owing to incomplete drainage and perhaps to some decomposition of the ferrous hydroxide (13, 14), although this point is very doubtful (15), a small decrease in the ferrous ion content of the final solution was observed. This blank reading, which appeared to be independent of time, was subtracted from all values obtained with tungstate and molybdate present. The results, expressed as the percentage of weight of ferrous material oxidized, are shown in Fig. 11. They demonstrate that both tungstate and molybdate are very mild oxidizing agents with respect to ferrous compounds; the effect, however, would be masked in neutral solutions by oxidation with dissolved air, if this was present. It was also observed that excess potassium chromate completely oxidized

ferrous ions in the presence of 1*N* sulfuric acid extremely rapidly.

Determination of Polarization Curves

Anodic and cathodic polarization curves were determined in deaerated 0.1*N* solutions of some anodic inhibitors using the method described in a previous paper (5). The iron electrodes, measuring 2.5 x 0.5 cm were suspended 1 cm apart in 5 ml of the deaerated inhibitor solution containing 10 ppm chloride ion in the form of potassium chloride. The potentials were measured against a chloridized silver wire also suspended in the solution. The applied current ranged between 0–10 microamps/cm² of specimen. The results are shown in Fig. 12. It can be seen that the slopes of the cathodic polarization curves increase with a rise in *p*H and in all cases are greater than those of the anodic polarization curves. The slope of the anodic polarization curve for sodium tungstate is, however, somewhat greater than that of other inhibitors at a similar *p*H value.

A further investigation of the anodic curve for sodium tungstate was, therefore, carried out as follows. At the end of one determination the current was switched off and the specimen left in contact with the solution for 24 hours. The anodic curve was then redetermined in a similar manner and the current switched off once more. The procedure was repeated several times over a period of five days. The rise in potential of the specimen, with time, following anodic polarization was much more rapid than that of a specimen simply exposed to deaerated 0.1*N* sodium tungstate as shown in Fig. 8. After several redeterminations the anode became passive (Fig. 13), whereas the potential of the cathode remained close to the original value. This behavior is quite different from that exhibited by deaerated 0.1*N* disodium phosphate in which the anodic

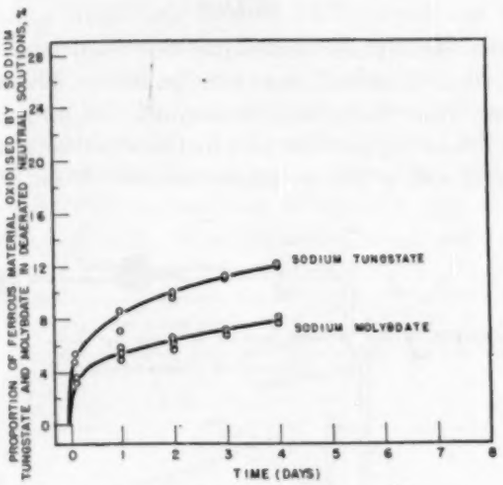
PROPORTION OF FERROUS MATERIAL OXIDISED BY SODIUM TUNGSTATE AND MOLYBDATE IN DEAERATED NEUTRAL SOLUTIONS, %
SODIUM TUNGSTATE
SODIUM MOLYBDATE
TIME (DAYS)

FIG. 11. Relationship between time and the percentage oxidation of deaerated neutral ferrous solutions by excess sodium tungstate and sodium molybdate.

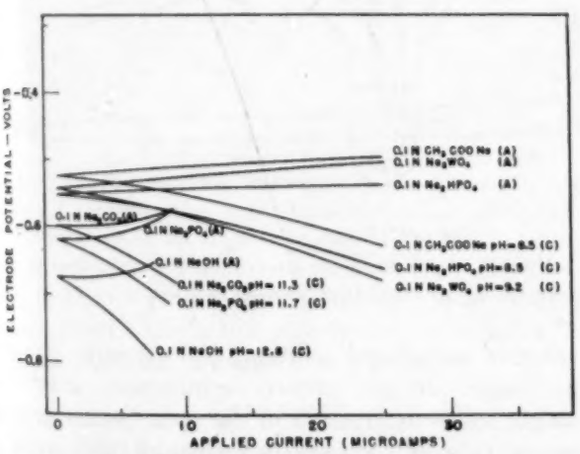
ELECTRODE POTENTIAL — VOLTS
APPLIED CURRENT (MICROAMPS)
0.1 N CH₃COONa (A)
0.1 N Na₂WO₄ (A)
0.1 N Na₂HPO₄ (A)
0.1 N Na₃PO₄ (A)
0.1 N NaOH (A)
0.1 N CH₃COONa pH=8.5 (C)
0.1 N Na₂HPO₄ pH=8.5 (C)
0.1 N Na₂WO₄ pH=9.2 (C)
0.1 N Na₂CO₃ pH= 11.3 (C)
0.1 N Na₃PO₄ pH= 11.7 (C)
0.1 N NaOH pH=12.8 (C)

FIG. 12. Anodic and cathodic polarization curves in some deaerated 0.1*N* inhibitor solutions. A, anodic polarization curves; C, cathodic polarization curves.

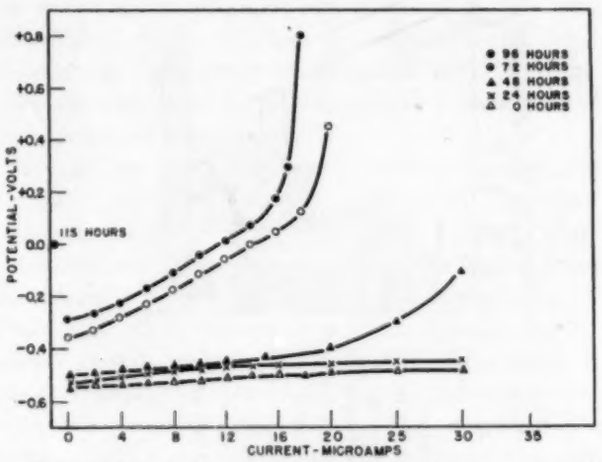

FIG. 13. Effect of repeated redetermination on the anodic polarization curve of iron on deaerated 0.1*N* sodium tungstate solution.

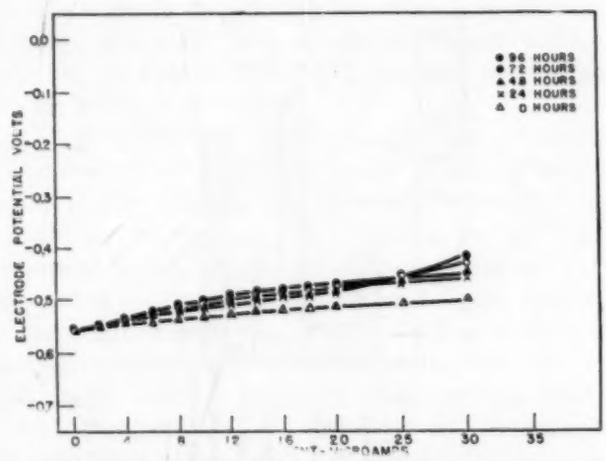

FIG. 14. Effect of repeated redetermination on the anodic polarization curve of iron in deaerated 0.1*N* disodium phosphate solution.

polarization curve was little affected by repeated redetermination (Fig. 14).

Effect of Chloride Ions on Inhibition

A series of experiments was carried out in order to determine the concentration of chloride ions, added as potassium chloride, required to break down the

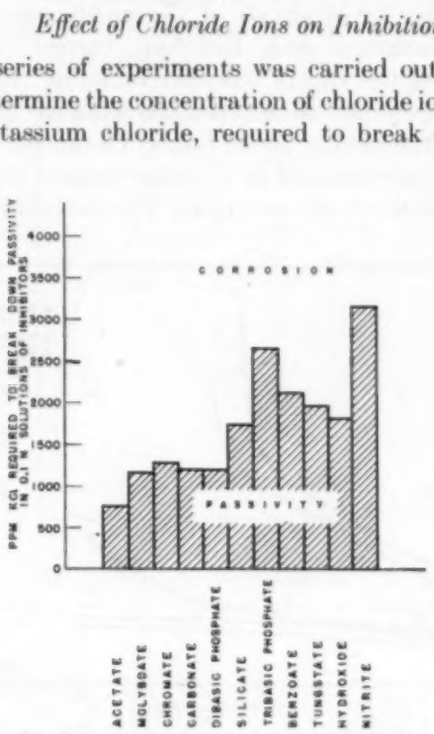

FIG. 15. Diagram showing the concentration of potassium chloride required to initiate corrosion in 0.1*N* inhibitor solutions in the presence of air.

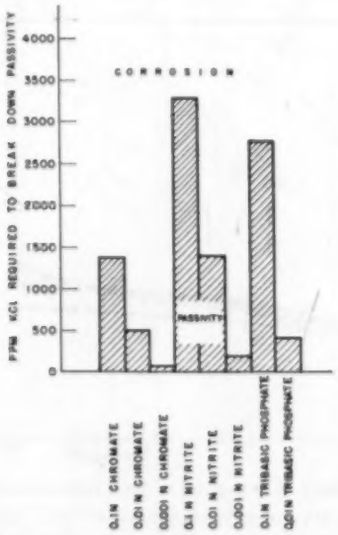

FIG. 16. Diagram showing the concentration of potassium chloride required to initiate corrosion in more dilute inhibitor solutions in the presence of air.

passivity resulting from immersion in 0.1*N* inhibitor solutions.

The specimens were in the form of sheet measuring 10.0 x 2.5 cm and were partially immersed in 200 ml of solution contained in open 250 ml beakers. Experiments were carried out for periods of up to one week, but it was generally found that, if a specimen was going to corrode, the corrosion would become evident within the first 24 hours. The results are shown in Fig. 15.

Several experiments were carried out in a similar manner to determine the effect of dilution on the concentration of chloride required to initiate corrosion. The inhibitors investigated in this manner were sodium chromate, nitrite, and tribasic phosphate. The results are shown in Fig. 16.

Effect of Carbon Dioxide on the Rate of Corrosion of Iron

The deaeration technique described above removed all dissolved gases from solutions. The weight losses were, therefore, determined not only in the absence of oxygen but also in the absence of carbon dioxide which has an appreciable effect on the *p*H

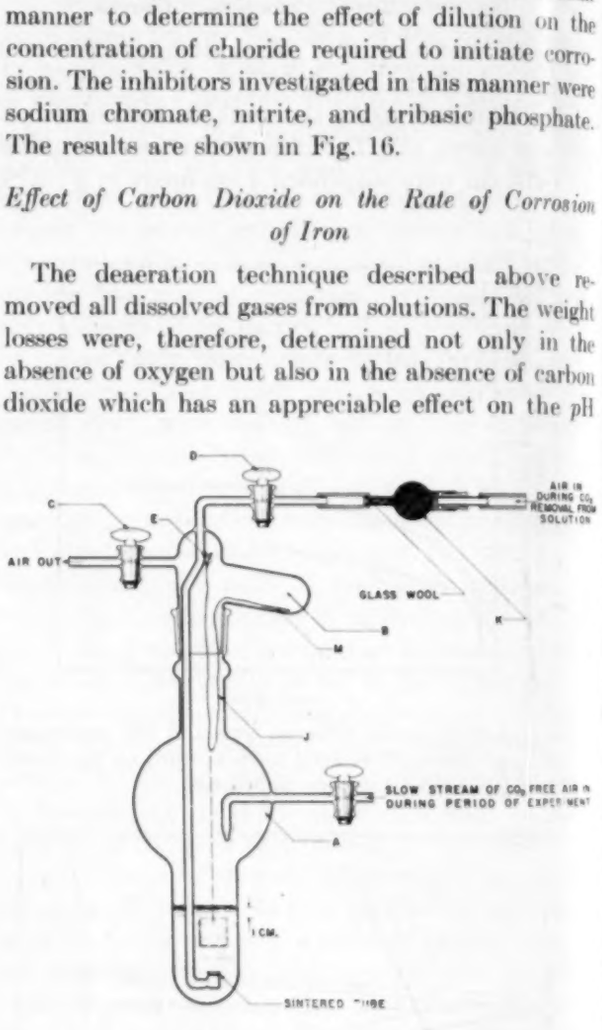

FIG. 17. Apparatus for determining weight loss in the presence of air freed from carbon dioxide.

value of unbuffered solutions. As a result, the experiments are not strictly comparable with the weight losses determined in the open beaker experiments (Fig. 1) where the solutions did contain carbon dioxide. A series of experiments was therefore carried out to determine the weight losses in solutions saturated with dissolved air but freed from carbon dioxide.

The apparatus used is shown in Fig. 17. The carbon dioxide present in solution was removed by bubbling for two hours with air freed from CO_2 by passing through the tube K filled with ascarite. The air left the apparatus through C. During this period the specimen M was situated in the side-arm B. After the solution and apparatus had been freed from carbon dioxide the stopcock D was closed and air freed from CO_2 passed in through F and out

through C, at constant pressure, for the period of the experiment. The apparatus was tilted so that the specimen, which was attached by the thread J to the glass hook E, fell 1 cm below the waterline of the solution. Banks of six similar apparatuses were placed in a constant temperature enclosure operating at 25° ± 0.5°C. Blank experiments were carried out in which a similar procedure was employed, except that the air was not freed from CO_2.

The specimens were in the form of sheet 2.5 x 2.5 cm with a small hole located at the center of the upper edge. They were degreased, abraded, and weighed as described above. At the end of the experiments, which lasted 5 days, the corrosion products were removed by treatment with inhibited 1:1 HCl and the specimens washed, dried, and reweighed. Two hundred ml of solution were used in all experiments. The inhibitor investigated by this method was disodium phosphate. The results, together with the blank experiments in which CO_2 was not removed, are shown in Fig. 18.

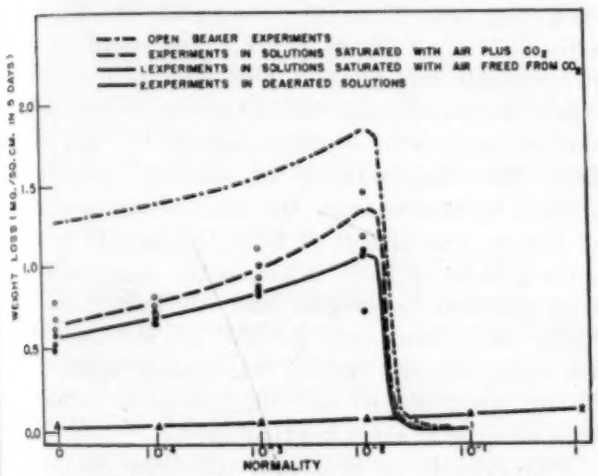

FIG. 18. Relationship between weight loss/cm² in 5 days and concentration in solutions of disodium phosphate in the presence of air freed from carbon dioxide.

DISCUSSION

All inhibitor solutions described above are capable of behaving as oxidizing agents toward iron when they contain dissolved oxygen. However solutions with nonoxidizing anions, e.g., sodium hydroxide, carbonate, silicate, acetate, benzoate, dibasic and tribasic phosphate, lose this property when deaerated. The remaining solutions, sodium chromate, nitrite, tungstate, and molybdate, which contain oxidizing anions of various degrees of effectiveness, do not completely lose their oxidizing powers on deaeration, although it has been shown (Fig. 11) that, in deaerated, neutral solutions, tungstate and molybdate are only very mild oxidizing agents. These two classes of inhibitors show rather different properties and will, therefore, be considered separately in the following discussion.

Inhibitors Having Nonoxidizing Anions

These inhibitors behave very similarly to that described previously for sodium hydroxide (3) and orthophosphates (4, 5) in that passivity is only obtained when the solutions contain dissolved air (Fig. 1 and 2, Table II). In deaerated solutions, iron corrodes very slowly, the rate of corrosion decreasing with a rise in *p*H, with the exception of disodium phosphate which exhibits an anomalously high weight loss; this point is discussed later. At high *p*H values the rate of corrosion is very slow and of little practical consequence.

The curves of Fig. 2 are not strictly comparable to the equivalent results obtained in the open beaker experiments (Fig. 1) since the solutions then contained carbon dioxide in addition to air, whereas the deaeration removed both air and carbon dioxide. From Fig. 18 it can be seen that although the removal of CO_2 reduces the weight losses slightly it does not affect the form of the curves. By comparison with the curves in Fig. 2 it can be seen that the removal of dissolved air greatly reduces the rate of corrosion at low inhibitor concentrations since the cathodic reaction is no longer depolarized by dissolved oxygen. At higher concentrations the weight losses in the presence of air begin to decrease rapidly and reach zero as the specimens become passive, whereas in deaerated solutions the weight losses continue to increase.

The potential/time curves of passivated specimens (Fig. 4–6) all fall largely within the range 0 to +0.35 volt. If the solutions are deaerated, however, the potentials of specimens in solutions having nonoxidizing anions become much more negative (Fig. 8) and either remain constant or become slightly more negative with time; the final value of the potential also becomes more negative with rise in pH, with the exception of disodium phosphate which exhibits an anomalously low potential. Weight loss determinations (Table II) indicate that the specimens are corroding very slowly and the form of the potential/time curves suggests that this corrosion is under cathodic control. This is confirmed by polarization curves[5] in deaerated solutions (Fig. 12) which show that, at the low current densities operative during this slow corrosion, the anodic polarization curves are practically flat whereas the cathodic polarization curves have a much greater slope which increases with rise in *p*H.

In a corroding system of low resistance the com-

[5] It should be noted that these polarization curves are the continuation of the curves representing a corroding specimen.

promise potential of the specimen and the corrosion current are given by the potential and current intercepts at the junction of the anodic and cathodic polarization curves (Fig. 19a). At the low current densities operative during the cathodically controlled slow corrosion in deaerated solutions, the compromise potential of the specimen is very close to that of the anodic reaction and is given approximately by the Nernst equation:

$$E = E_0 + \frac{RT}{2F} \log_e [Fe^{++}] \qquad (I)$$

where $E_0 = -0.44$ volt.

At the steady state in solutions of relatively high pH the ferrous ion concentration is that in equilibrium with ferrous hydroxide, except in solutions of disodium phosphate where the corrosion product is ferrous phosphate (5). The ferrous hydroxide corrosion product in deaerated solution is a whitish gelatinous product and is difficult to observe in very small amounts. However, conditions of pH and the rate at which iron passes into solution necessitate its formation. The concentration of ferrous ions, once ferrous hydroxide is formed as a corrosion product, is given by

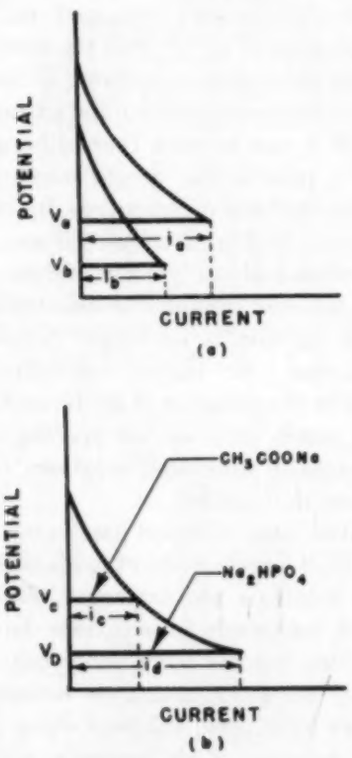

FIG. 19. Potential/current diagrams showing the effect of (*a*) pH and (*b*) ferrous ion concentration on the corrosion current and potential.

$$Fe^{++} = \frac{S_{Fe(OH)_2}}{[OH']^2} \qquad (II)$$

where $S_{Fe(OH)_2}$ is the solubility product of ferrous hydroxide.

The open-circuit potential of the cathodic reaction

$$2H^+ + 2e' = H_2 \qquad (III)$$

varies with hydroxyl ion concentration in a similar manner, at constant pressure of hydrogen, so that the open-circuit potential difference between anodic and cathodic reactions should remain constant despite the fact that a rise in pH results in a shift of both potentials in the negative direction. When current is drawn from this corrosion cell the cathodic reaction polarizes much more than the anodic reaction and this polarization increases with a rise in pH (Fig. 12). Thus, as the pH of the solution is raised, the compromise potential of the specimen shifts in the negative direction, e.g., from V_a to V_b, while the corrosion current falls, e.g., from i_a to i_b (Fig. 19a). If the Nernst equation is accurately obeyed, a unit increase in pH should result in a 59 mv decrease in potential. This appears to be true when the equilibrium concentration of Fe^{++} does not exceed a value of approximately 10^{-5} gm ions/liter. Thus calculation of the solubility product of ferrous hydroxide from the equilibrium potential of iron in deaerated 0.1N CH_3COONa (pH = 8.5) gives a value of $10^{-14.5}$ which is the same value as that obtained by Shipley and McHaffie (16). At higher pH values, when the $[Fe^{++}]$ is less than 10^{-5} gm ions/liter, the Nernst relationship appears to be no longer obeyed and the change in potential for a unit rise in pH is less than 59 mv.

Iron exposed to deaerated disodium phosphate exhibits an anomalously low potential and high weight loss. At pH 8.5, however, the corrosion product in deaerated 0.1N disodium phosphate is not ferrous hydroxide but ferrous phosphate, and consequently the ferrous ion concentration in equilibrium with ferrous phosphate must be lower than that in equilibrium with ferrous hydroxide. The potential of the anodic reaction will, thus, be lower in deaerated disodium phosphate than in a deaerated solution of similar pH in which the corrosion product is ferrous hydroxide, e.g., 0.1N sodium acetate. The cathodic polarization curve will be the same in both cases with the result that the compromise potential in disodium phosphate (V_D) will be lower than in acetate (V_C) (Fig. 19b), while the corrosion current (i_d) will be greater than acetate (i_c). At pH values above 10, ferrous hydroxide should be more insoluble than ferrous phosphate and it is interesting to note that crystalline ferrous phosphate is not observed as a corrosion product in deaerated solutions above this pH value. Presumably the potential of iron in deaerated tri-

sodium phosphate is controlled by the precipitation of ferrous hydroxide, despite the fact that ferric phosphate is found in the passivity films formed on iron immersed in trisodium phosphate containing dissolved air (9, 6). Calculation from potential data, the *p*H value of the solution, and dissociation constants of the orthophosphate ions (17), leads to an approximate value of 10^{-25} for the solubility product of ferrous phosphate.

It appears that inhibitors having nonoxidizing anions behave in a similar manner and that the mechanism of inhibition is like that put forward for orthophosphates (4, 5). Inhibition is due primarily to oxygen, dissolved in solution, which has been shown to be a powerful oxidizing agent in neutral solution (Fig. 9). The oxygen, dissolved in solution, is believed to adsorb on the surface of the iron and react with surface iron atoms forming a thin, invisible film of γ-Fe_2O_3, of the order of 200 Å thick, in a manner similar to that by which oxide films are formed in air. Film formation is, however, not instantaneous and very slow corrosion, leading to the production of inclusions of corrosion product, accompanies the early stages of passivation. A more detailed account of the mechanism will be given later.

Inhibitors Having Oxidizing Anions

Sodium chromate and sodium nitrite are well-known oxidizing agents and Fig. 11 shows that tungstate and molybdate ions have mild oxidizing powers in neutral solutions. These inhibitors show many points of similarity to the inhibitors having nonoxidizing anions; for instance the films formed by passivation of initially film-free iron specimens in chromate and nitrite are composed mainly of γ-Fe_2O_3 (2, 8) and films formed by nitrite also contain small quantities of lepidocrocite (8), although its distribution throughout the film was not determined. It is probable that the films formed by chromate also contain small quantities of lepidocrocite in addition to small amounts of chromium compounds (18, 19, 20). The method of electron diffraction previously used to examine these films (2) was, however, not sufficiently sensitive to detect very small amounts of other compounds.

The possibility of oxidizing inhibitors contributing to the formation of the oxide film cannot be dismissed. It was found previously (3), as well as during this research (Table II), that 0.1*N* sodium chromate passivates iron in deaerated solutions. Also 0.1*N* sodium nitrite, a milder oxidizing agent, behaves similarly (Table II) except that the potential of an iron specimen in deaerated solutions (Fig. 8) takes longer to reach the passive range. Sodium tungstate and sodium molybdate are much weaker oxidizing agents toward ferrous solutions (Fig. 11), although these experiments do not necessarily represent their oxidizing powers with respect to an iron surface. However, tungstate and molybdate are not sufficiently powerful oxidants to build up a protective oxide film in deaerated solution, at least during the period of the experiments, and so appreciable quantities of iron pass into solution (Table II). Fig. 8, however, provides definite evidence of increasing anodic polarization with time—which is quite different behavior to that shown by deaerated inhibitors with nonoxidizing anions. Presumably some oxide is being formed by adsorption of the tungstate (or molybdate) ion followed by oxidation of the iron and reduction of the inhibitor anion, but the rate of formation is not sufficiently high to form a protective film. Similar behavior is exhibited by tungstate during determinations of the polarization curves in deaerated solution (Fig. 12) where it is observed that the gradient of the anodic polarization curve is slightly greater than that of nonoxidizing agents at similar *p*H values.

Despite the fact that tungstate and molybdate are such weak oxidizing agents, they passivate iron in solutions containing dissolved air at similar concentrations to chromate and nitrite (Fig. 1), an effect previously noticed by Robertson (11). In order to explain this, the significance of Fig. 13 must first be considered. Successive redetermination of the anodic polarization curve in deaerated 0.1*N* sodium tungstate solution results in passivation of the anode in a comparatively short time, whereas similar treatment of an iron anode in a deaerated inhibitor with nonoxidizing anions, such as disodium phosphate, results in very little change in the anodic polarization curve (Fig. 14) and the potential of the anode always returns to the equilibrium value. The fact that the potential of the cathode remains at the equilibrium value in both experiments indicates that oxygen was not evolved at the anode. Apparently the tungstate ions are more effective oxidizing agents when discharged at the anode under conditions of high current density. In the later redeterminations the anode is probably so largely covered by oxide that the local current density is very high at the anodic areas.

When an abraded specimen is immersed in a passivating solution, the surface is initially largely covered with oxide formed by exposure to the atmosphere. Under these conditions the already small areas available for anodic reaction become even smaller due to the progressive growth of oxide in solution. It was previously suggested (5) that under such conditions a high local current density was developed at the anodic areas. If this is the case, the anions of such a weak oxidizing agent as sodium

tungstate would be discharged at high current density and would then prove a relatively rapid and efficient oxidizing agent. This may explain the great similarity between the four oxidizing inhibitors of unequal oxidizing powers.

Thus the mechanism of inhibition for these four inhibitors is essentially the same as described in the previous section. Inhibition is primarily due to a thin film of γ-Fe_2O_3 probably formed mainly by oxygen dissolved in solution. The importance of the oxidizing inhibitor seems to be confined mainly to the reactions taking place at discontinuities in the oxide film where slow corrosion is occurring. In the absence of air, oxidizing anions react with the iron surface to form iron oxide, the rate of this reaction being sufficiently high with chromate and nitrite to form a protective film. A more detailed account of the mechanism of inhibition will be given later in the discussion.

Effect of Chloride on Passivity

It can be seen from Fig. 1 and 15 that those inhibitors which passivate iron at low concentrations are not necessarily more effective in the presence of chloride. For instance, the concentration of chloride required to make 0.1N sodium carbonate and disodium phosphate corrosive is very similar to that required to make 0.1N sodium chromate and molybdate corrosive despite the fact that, in the absence of chloride, the former do not inhibit the corrosion of iron until their concentration is of the order of $10^{-1}N$ whereas the latter inhibit at $10^{-3}N$. It is probable that film breakdown initially starts at inclusions of corrosion product in the passivity films and that the concentration of chloride that can be tolerated is related in a complex manner to the pH changes at the anodic areas.

Nature of the Passive Potentials

One of the surprising features of Fig. 4, 5, and 6 is that specimens exhibit more positive potentials in more dilute inhibitive solutions despite the fact that these solutions are poorer inhibitors, in that a much lower concentration of chloride is required to make them corrosive (Fig. 16). Furthermore, with the exception of sodium silicate and the phosphates, the steady value of the passive potential becomes more negative with rise in pH (Fig. 7). It is believed that the potential of a passive specimen is the potential of the very slow corrosion occurring at discontinuities in the oxide film.

Mechanism of Inhibition

It appears that a mechanism, based on the concept of protective films of γ-Fe_2O_3 maintained in constant repair, can be put forward to explain inhibition by anodic inhibitors. The oxide film is believed to be formed entirely by dissolved oxygen in inhibitors which do not contain oxidizing anions and mainly by dissolved oxygen even when the inhibitor contains oxidizing anions. The film is believed to be formed by adsorption of oxygen, followed by heterogeneous reaction and thickening until it reaches an equilibrium thickness of approximately 200 Å when it is sufficiently thick to prevent the outward diffusion of iron ions. The mechanism of formation of the oxide film is considered to be similar to that by which oxide films are formed in dry air. However, this film must be maintained in constant repair, usually by dissolved oxygen, in order to stop iron ions entering the solution.

The formation of a protective oxide film is not instantaneous and very slow corrosion accompanies the initial formation of oxide. The oxygen dissolved in solution exhibits a dual role, since it is not only largely responsible for the formation of the passivity film, but also acts as a cathodic depolarizer for the accompanying corrosion reaction. The rate of this corrosion is controlled by high anodic polarization brought about by the very small size of the anodic areas resulting from the progressive growth of the oxide film in solution. It was previously suggested (5) that a high current density was developed at these anodic areas.

Small inclusions of lepidocrocite (γ-FeO·OH), the natural corrosion product, of the order of 1 to 2μ in diameter have been detected in the passivity films formed in sodium hydroxide (3). Inclusions of strengite ($FePO_4 \cdot 2H_2O$), of the order of 1μ in diameter have also been found in passivity films formed on iron by disodium phosphate (9). It is probable that, in the remaining inhibitors which have nonoxidizing anions, inclusions of lepidocrocite are present in the passivity films; the lepidocrocite may also contain some α-FeO·OH and Fe_3O_4 which are also oxidation products of $Fe(OH)_2$ (Table I). The precipitation of corrosion product over the small anodic areas probably retards the further lateral growth of oxide; additional anodic polarization will, however, result from thickening and consequent increase of resistance of the corrosion product. The initial corrosion is believed to become very slow after about one day when the duplex film is apparently sufficiently thick and continuous to practically prevent the further outward diffusion of iron ions. The nonoxidizing inhibitor anions do not participate directly in the formation of the oxide film; their function seems to be confined to the initial discontinuities in the oxide film where slow corrosion is occurring. The rate of corrosion must be sufficiently slow to prevent undermining of the film and the inhibitor probably ensures this condition by controlling the pH of the solution so that the anodic areas do not become too acidic.

The same general mechanism is applicable to

inhibitors which contain oxidizing anions. In deaerated solutions, chromate and nitrite form an oxide film sufficiently rapidly to give inhibition while tungstate and molybdate do not form oxide sufficiently rapidly to prevent corrosion. In solutions containing dissolved air, however, the main part of the oxide film is still formed by dissolved oxygen with slow corrosion, under anodic control, accompanying the early stages of film formation. It was suggested in an earlier paper (5) that a high current density was operative at the small anodes. Even such a mild oxidizing anion as the tungstate ion when discharged anodically at high current density proves to be a relatively efficient oxidizing agent, comparable, in fact, to chromate and nitrite. This is suggested as the reason for the great similarity of behavior, in the presence of air, of the four oxidizing anions of vastly different oxidizing power. The discharge of oxidizing anions at small anodes at high current density is considered to result in the additional formation of oxide with the result that inhibition is achieved at lower concentrations than in inhibitors having nonoxidizing anions. The inclusions, which are probably thicker than the surrounding oxide film, are believed to consist of a mixture of oxide, corrosion product, and the reduction product of the inhibitor anion if this is insoluble.

It should be emphasized, however, that even after the film has become protective it must be kept in a state of constant repair either by dissolved oxygen or by an oxidizing anion or both. Under conditions leading to inhibition any local breakdown is repaired by the formation of fresh film by the inhibitor.

The formation of γ-Fe_2O_3 by dissolved oxygen should be independent of the *p*H of the solution. The simultaneous corrosion process is, however, dependent on conditions existing in solution and on the surface condition of the metal (6). In general, factors tending to increase this rate of corrosion will militate against passivity since it is believed that the inclusions in duplex films are points of weakness from which film breakdown may begin.

Summary

Decinormal solutions of sodium acetate, benzoate, carbonate, hydroxide, orthophosphate, and silicate passivate iron only in the presence of dissolved air. If the solutions are deaerated, they attack iron slowly, potential/time and polarization curves showing that the attack is under cathodic control.

Powerful oxidizing inhibitors such as decinormal solutions of sodium chromate and nitrite can passivate iron even in deaerated solutions. Inhibitors of weaker oxidizing power such as sodium tungstate and molybdate behave similarly to chromate and nitrite in the presence of air, in that inhibition sets in at the same minimum concentration, but are unable to prevent corrosion in deaerated solution. Potential/time and polarization curves show that in deaerated solution of tungstate and molybdate some film formation is taking place, but that it is too slow to prevent iron passing into solution. However, tungstate and probably molybdate ions when discharged anodically at high current density are effective oxidizing agents toward iron.

The view is put forward that oxygen dissolved in solution is mainly responsible for passivity by virtue of its heterogeneous reaction with surface iron atoms to form a thin, self-repairing film of γ-Fe_2O_3, of the order of 200 Å thick, in a manner similar to that by which oxide films are formed in air. Oxidizing inhibitors assist in the formation of the passivity films by acting as film repairing agents at discontinuities present during the early stages of film formation.

Acknowledgments

The authors are indebted to Dr. W. H. Barnes and Mrs. H. Shepard for carrying out the x-ray examination of the corrosion products and to Mr. P. Marier for assistance with some of the experimental work.

Any discussion of this paper will appear in a Discussion Section, to be published in the December 1953 issue of the Journal.

REFERENCES

1. R. Pyke and M. Cohen, *J. Electrochem. Soc.*, **93**, 63 (1948).
2. J. E. O. Mayne and M. J. Pryor, *J. Chem. Soc.*, **1949**, 1831.
3. J. E. O. Mayne, J. W. Menter, and M. J. Pryor, *J. Chem. Soc.*, **1950**, 3229.
4. M. J. Pryor and M. Cohen, *Nature*, **167**, 157 (1951).
5. M. J. Pryor and M. Cohen, *J. Electrochem. Soc.*, **98**, 263 (1951).
6. M. J. Pryor, F. Brown, and M. Cohen, *J. Electrochem. Soc.*, **99**, 542 (1952).
7. M. Cohen, R. Pyke, and P. Marier, *J.* (*and Trans.*) *Electrochem. Soc.*, **96**, 254 (1949).
8. M. Cohen, *J. Phys. Chem.*, **56**, 451 (1952).
9. J. W. Menter, "Comptes rendus du Premier Congrès International de Microscopie Electronique," Paris 1950. Editions de la Revue d'Optique, Paris (1952).
10. H. L. Lochte and R. E. Paul, *Trans. Electrochem. Soc.*, **64**, 164 (1933).
11. W. D. Robertson, *J. Electrochem. Soc.*, **98**, 94 (1951).
12. M. J. Pryor and M. Cohen, *J. Electrochem. Soc.*, **98**, 513 (1951).
13. G. Schikorr, *Z. Elektrochem.*, **35**, 65 (1929).
14. G. Schikorr. *Z. anorg. u. allgem. Chem.*, **212**, 33 (1933).
15. U. R. Evans and J. N. Wanklyn, *Nature*, **162**, 27 (1948).
16. J. W. Shipley and I. R. McHaffie, *Can. Chem. Met.*, **8**, 5, 121 (1924).
17. G. A. Abbott and W. C. Bray, *J. Am. Chem. Soc.*, **31**, 729 (1909).
18. T. P. Hoar and U. R. Evans, *J. Chem. Soc.*, **1932**, 2476.
19. M. T. Simnad, *Rev. met.*, **48**, 522 (1951).
20. D. M. Brasher and E. R. Stove, *Chemistry & Industry*, **1952**, 171.

Amount of Oxygen on the Surface of Passive Stainless Steel[1]

HERBERT H. UHLIG AND SAMUEL S. LORD, JR.

Corrosion Laboratory, Department of Metallurgy, Massachusetts Institute of Technology, Cambridge, Massachusetts

ABSTRACT

The amount of oxygen on the surface of 18-8 stainless steel was obtained by pickling the alloy with HCl-H_2SO_4, washing with nitrogen-saturated water, then exposing the metal to water of known dissolved oxygen content. The decrease in dissolved oxygen for a definite period of exposure was a measure of the oxygen taken up by the 18-8 surface.

The take-up of oxygen was rapid the first few minutes, then proceeded slowly, reaching a maximum, after 6 hr, of 1.1 microgram/apparent cm^2 of metal surface. No further oxygen was consumed up to a maximum exposure of 48 hr. The alloy attained maximum passivity after about 3 hr in aerated water, as shown by potential measurements. When 18-8 was pickled with HNO_3-HF, the oxygen consumed was only 0.33 μg/apparent cm^2 of surface. This smaller value is related to the decreased true surface area of 18-8 so pickled (roughness factor = 1.2) compared with the HCl-H_2SO_4 pickle (roughness factor = 4.0).

The maximum amount of oxygen on passive 18-8 based on so-called true surface area is 0.27 $\mu g/cm^2$. This value is equivalent to a supposed Cr_2O_3 film only 17 Å thick. On the other hand, an equivalent adsorbed oxygen film consists approximately of 1 layer of atoms over which a close-packed layer of oxygen molecules is adsorbed. The data are not inconsistent, therefore, with the adsorbed film theory of passivity, and, accordingly, the mechanism of passivation by oxygen need not be considered different from that produced by carbon monoxide in hydrochloric acid saturated with this gas, where the adsorption theory heretofore has provided the only plausible explanation.

The point of view is proposed that oxide films previously isolated from stainless steels by several investigators were produced by reaction of the adsorbed film with the metal, the reaction being induced by polishing and abrading, presence of halogen ions and water in the stripping solution, or by high temperatures. Such oxide films, however, are considered to be of secondary importance in accounting for passivity as measured by corrosion resistance and by a noble potential.

INTRODUCTION

Stainless steels are defined as iron-base alloys containing at least 12 per cent chromium. The most widely used composition is the 17–19 per cent chromium, 8–10 per cent nickel, remainder iron alloy called 18-8. All these alloys are phenomenally corrosion resistant despite their high iron content, and because of this property, plus a noble galvanic potential in the order of silver or platinum, are called passive.

The property of passivity resides in certain films on the surface, the nature of which depends on properties of the base metal. According to one viewpoint, the passive film on stainless steels is composed of metal oxides, predominantly chromic oxide, acting as a diffusion barrier layer between the metal and its environment and kept in repair by an oxidizing environment. This film is supposedly thick enough to allow its isolation by chemical means (1–3), accomplished, for example, by immersing the metal into iodine or bromine dissolved in methyl alcohol. This reagent reacts preferentially with the metal directly beneath any oxide film allowing the oxide to "float" to the surface of the liquid, after which it can be examined optically or analyzed chemically.

A second viewpoint (4–6) ascribes passivity to a chemisorbed film on the alloy surface, which satisfies residual affinities of the metal for its environment, and which makes up a dipole layer with negative charge on the outer surface. The satisfaction of chemical valence forces plus the dipole layer account for diminished reactivity of the alloy, in addition to a noble galvanic potential.[2] The important source of passivity, by this viewpoint, is a film in the order of a monolayer in thickness, and, therefore, too thin to be seen and handled. Thicker oxide films which may form subsequent to formation of the adsorbed film are considered to be of secondary importance in the passivation mechanism, and are not necessary to the observed corrosion resistance.

It has been difficult to distinguish experimentally

[1] Manuscript received May 6, 1952. This paper was prepared for delivery before the Montreal Meeting, October 26 to 30, 1952.

[2] To a first approximation, the change of potential in the noble direction by such a dipole layer is given by the expression $4\pi n\rho$, where $n\rho$ is the electric moment per unit area of metal surface.

between these two viewpoints, especially since a thick oxide film under certain conditions may be present on a stainless steel and, by circumstantial evidence, would seem to accompany its corrosion resistance, in the same sense as the thick oxide film on aluminum appears to accompany its corrosion resistance. One distinguishing experiment is possible, however, which depends on the fact that an adsorbed film is appreciably thinner than a diffusion barrier oxide film and, hence, contains less oxygen. Therefore, a measure of the minimum amount of oxygen on the surface of a stainless steel necessary to make it corrosion resistant, and to impart to it a noble potential, may serve as a critical experiment. It is the results of this experiment that are described herewith.

Procedure

The procedure consisted in pickling a stainless steel sheet out of contact with air to remove all films from the surface. The pickled sheet was then washed with nitrogen-saturated water, followed by contact with aerated water for a definite time. The drop in oxygen content of the water was a measure of the amount of gas taken up by the metal surface. The procedure is similar to that described previously by Forrest, Roetheli, and Brown (7), with the refinement of an all-glass vessel to minimize contamination by air, and with greater emphasis on general quantitative features of the experiment. The "true" surface area of the stainless steel on which oxygen was taken up was also measured, since without this a calculation of film thickness cannot be made.

Commercial 18-8 sheet, (0.045% C, 18.50% Cr, 9.43% Ni) supplied by courtesy of Armco Steel Corporation, measuring 0.010 in. thick and 1744 cm² in area (both sides) was formed into a 3½- by 2½-in.-diameter coil. This was placed inside a 565 ml glass vessel. A glass cover with ground glass surface fitted over the bottom portion of the vessel and was held in place by a clamp (Fig. 1). A magnetic stirrer insured renewed contact of liquid with all portions of the alloy sheet.

An acid pickle from a separatory funnel entered the vessel by way of inlet B. This consisted of 25 vol per cent commercial concentrated HCl and 25 vol per cent commercial concentrated H_2SO_4 at 35°C in contact with the alloy for 10 min. Hydrogen bubbles escaping from all portions of the metal surface indicated uniform attack and removal of surface films. The metal coil and glass vessel were then washed with nitrogen-saturated water by filling the vessel successively 3 times through B, each time using purified nitrogen supplied through inlet A to force the water out through efflux E. The nitrogen-saturated water was prepared by bubbling the gas through a large volume of distilled water for 5 hr or longer, using a sintered glass bubbler, and gave a negative Winkler test for oxygen. The nitrogen used for this purpose was purified by passing it over copper turnings at 400°C, the path of which was 3 ft long. Distilled water of known oxygen content was then admitted to the cell through D (about 30 sec for filling), and allowed to remain, with continuous stirring, in contact with the stainless steel for a definite time. Finally, a sample of water was removed from the vessel and analyzed for oxygen by the standard Winkler method.

Because a small amount of oxygen from the aerated water was lost to the nitrogen atmosphere above it during filling of the vessel, a blank correction was necessary, obtained by following the procedure described above for the empty vessel. The

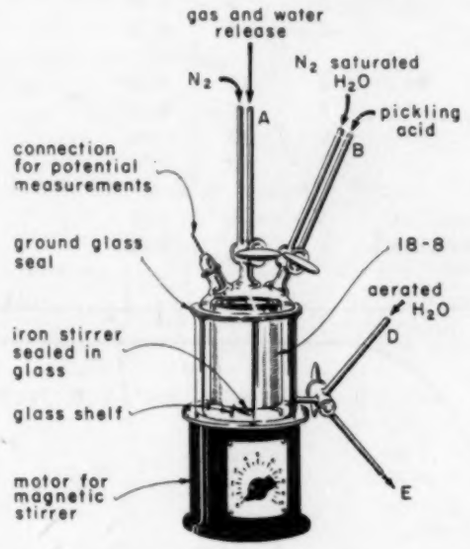

Fig. 1. Glass vessel for measuring oxygen take-up by pickled 18-8 stainless steel.

blank, averaged for 8 separate determinations, was 0.12 ± 0.04 ppm oxygen, and was independent of the length of time, ranging from 15 min to 25 hr, that the aerated water remained in the glass vessel. This value is 3.5 per cent of the maximum oxygen taken up by the pickled stainless steel surface after contact with aerated water and, hence, was not critical.

Potential measurements were made by connecting the coil to a tungsten wire sealed in a glass stopper at the top of the vessel which, in turn, made connection to a vacuum-tube potentiometer. The second electrode was a miniature calomel cell immersed in the water above partially opened stopcock A.

Effect of Varying Pickle and Washing Time

There is always the possibility that nitrogen-saturated water may have carried some small amount

of dissolved oxygen, or the water itself may have reacted directly with the alloy to form an oxide. To check this, the pickled sheet and glass vessel were washed 3 times with nitrogen-saturated water as usual, and compared with a run employing 6 washes, and with runs when nitrogen-saturated water remained in contact with the metal as long as 1 hr. Also, the time of pickle was varied from the usual 10 min to double this time to insure that the surface was free of films. Differences in oxygen take-up were largely within the experimental error, as shown by data of Table I. The low value for 6 washes may be evidence of some residual oxygen in the water, indicating that oxygen take-up values, if anything, are slightly low.

TABLE I. *Effect of variation in pickling and washing time, and phosphorus addition to pickle, on oxygen take-up of 18-8.* HCl-H_2SO_4 *pickle, 15-min contact with aerated water*

Pickling time (min)	Washes	Washing time (min)	O_2 Take-up ($\mu g/cm^2$)
10	3	5	0.69 (normal proced.)
20	3	5	0.68
20	3	5	0.73
10	3	15	0.65
10	3	15	0.64
10	6	10	0.60
10	3	60	0.70
10, P addition	3	5	0.71
10, P addition	3	5	0.65

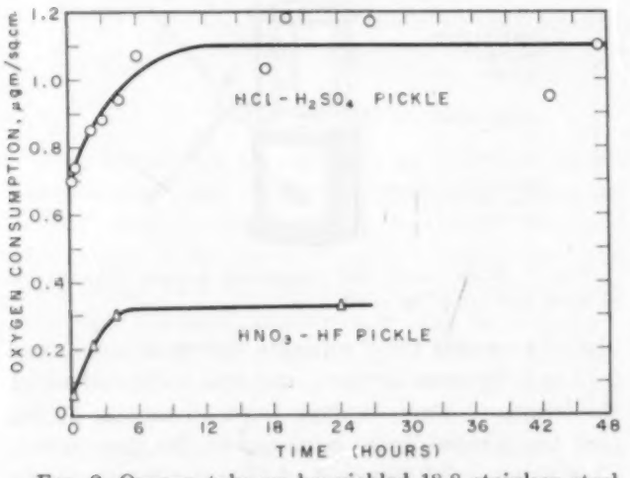

FIG. 2. Oxygen take-up by pickled 18-8 stainless steel after various times of exposure to aerated water.

RESULTS

Data showing take-up of oxygen by the pickled 18-8 stainless steel are plotted in Fig. 2. Oxygen is consumed rapidly the first few minutes of contact with aerated water, then more slowly for about 6 hr. After this, no further change occurs within the limit of reproducibility for the longest period of exposure equal to 48 hr. The maximum consumption is equal to 1.1 ± 0.1 μg oxygen/cm^2 of apparent metal surface. The true surface of stainless steel is appreciably greater than the apparent surface, as discussed later, and, hence, the variation of the true surface with each pickling operation probably accounts for the observed scattering of data over long periods of exposure. For shorter periods, and before the surface takes up maximum oxygen, the effect of true area is less important and in this region, therefore, the data scatter less.

Data are included in Table I for addition to the pickle of yellow phosphorus dissolved in CS_2. This pickle before use was filtered through a sintered glass funnel to remove any particles of phosphorus. The phosphorus addition markedly increases absorption of hydrogen by iron and alloys of iron during pickling (8, 9) and, hence, is expected to increase hydrogen absorption by 18-8.[3] Any hydrogen so absorbed would increase oxygen consumption because of its reaction with dissolved oxygen to form water. However, using this pickle did not increase oxygen consumption, so that presumably, very little hydrogen was absorbed by the alloy in a 10-min pickle.

The pickle was next replaced by one in which hydrogen is apparently not a reaction product and, hence, no hydrogen is expected to enter the stainless steel lattice during the pickling operation. This pickle was 15 vol per cent HNO_3, 10 vol per cent HF, based on the commercial concentrated acids, used at 90°C for 10 min. Oxygen consumption was now much less than in the case of the HCl-H_2SO_4 pickle. Data are included in Fig. 2 showing that maximum oxygen consumption amounts to about 0.33 $\mu g/cm^2$ of apparent surface. The lower oxygen consumption, however, was not due to less hydrogen absorbed by the alloy, as further investigation proved.

Forrest, Roetheli, and Brown (7) reported that maximum consumption of oxygen by an 18-8 stainless steel occurred within 3 min of pickling, instead of 6 hr as found here. The cause for this difference is not clear. It is possible that their use of a hot water wash to remove hydrogen from the pickled alloy allowed a more rapid access of oxygen to the metal surface, although this seems improbable. The difference is not a function of dissolved oxygen content of the water, because a single run using oxygen-saturated water gave an oxygen take-up, corrected by an appropriate blank, of 0.86 $\mu g/cm^2$ for 20-min

[3] Less so than in the case of iron, because the rate of diffusion of H_2 into the face-centered cubic 18-8 lattice is much less than into the body-centered cubic iron lattice.

exposure, compared with the interpolated value of 0.71 $\mu g/cm^2$ for air-saturated water (Fig. 2), both values being less than the maximum oxygen that can exist on the surface. Significantly, potential measurements of the pickled coil during exposure to aerated water showed a slow, rather than a rapid trend toward a passive noble potential, the maximum occurring at about 3 hr after pickling. Previous potential measurements by one of us also showed that maximum passivity of pickled 18-8 exposed to aerated water required several hours (10). The rate of consumption of oxygen, therefore, illustrated by Fig. 2, is approximately in line with potential-time measurements.

True Surface Area of Pickled 18-8

In order to convert oxygen consumption in $\mu g/cm^2$ to thickness of an oxygen or oxide film, it is necessary to know the true surface area of the pickled stainless steel. Measurements of this kind were obtained by O'Connor of this laboratory using the Brunauer-Emmett-Teller method (11–13). Ethane was adsorbed on 40.5 cm^2 of 18-8 cut from the same sheet as used in the above experiments and pickled identically. The adsorption isotherm was obtained at liquid oxygen temperatures (−183°C). Helium, after passing through a charcoal trap at −196°C, was used to calibrate the volume of the adsorption system. The area of the ethane molecule was taken as 21.5 $Å^2$ derived from x-ray data. This is in good agreement with a separate calibration made in this laboratory using glass beads of known diameter, for which the roughness factor is assumed to be unity. It is apparent from results given in Table II that the true surface area of stainless steel pickled with HNO_3-HF is only ⅓ that of 18-8 pickled with HCl-H_2SO_4.

Additional experiments showed that a pickling time of 20 min decreased the true area of the stainless sheet by 3 per cent compared with a 10-min pickle, and a 50-min pickle decreased the total area 9.5 per cent. The same sheet of stainless steel could be used, therefore, for several runs without large change in the true surface area.

Thickness of Oxygen Layer or Oxide Layer on 18-8

From the true surface area, the thickness of an adsorbed oxygen or of an oxide layer on the alloy surface equivalent to the measured oxygen take-up was calculated. Calculations assumed a chemisorbed close-packed oxygen atom layer of covalent atomic radius 0.7 Å, with the area per atom equal to $(\text{diam}^2)\sqrt{3}/2$. The oxide composition, on the other hand, was assumed to be Cr_2O_3 with density 5.2. The results are given in Table III.

Whatever the assumed composition of the oxide, this has only minor effect on the calculated thickness. The gas film is reported as atom layers, because of the fact that oxygen on tungsten appears to adsorb atomically (14), and the affinities of tungsten and chromium for oxygen are similar (heat of formation for WO_3 = 196 Cal/mol; for CrO_3 = 140 Cal/mol). On this basis, the calculated second layer of atoms over the first is not entirely complete or, alternatively, the atoms in pairs can be assumed to have greater than close-packed atomic spacing. The structure can also be considered to be a close-packed atomic layer over which molecular oxygen is adsorbed. If molecular oxygen is assumed to have a radius of 1.2 Å, and atomic oxygen 0.7 Å, both in close-packed layers, the weight of total oxygen/cm^2 corresponds exactly to the observed 0.27 microgram/cm^2. This structure, therefore, is in good agreement with the facts, in addition to being a plausible structure based on present knowledge of chemisorbed and physically adsorbed gas films.

TABLE II. *True surface area of pickled 18-8 stainless steel sheet*

Pickle	Roughness factor (true area/apparent area)
HCl-H_2SO_4, 35°C, 10 min	4.10
HCl-H_2SO_4, " "	3.90
HNO_3-HF, 90°C, 10 min	1.21

TABLE III. *Thickness of oxygen or oxide films on 18-8 stainless steel*

Pickle	Roughness factor	Oxygen take-up $\mu g/cm$		Equiv. thickness of	
		Apparent surface	True surface	Close-packed oxygen layer	Oxide as Cr_2O_3
HCl-H_2SO_4	4.0	1.1	0.27	1.8 atom layers (or 1 atom layer + 1 molecule layer)	17 Å
HNO_3-HF	1.2	0.33	0.27	1.8 atom layers	17 Å

It is of interest to note that the amount of oxygen adsorbed from the gas phase by iron is very close to that reported here for 18-8. Values obtained from gas adsorption determinations by several investigators (15–17) are within the range 0.2–0.4 μg oxygen/cm^2 of apparent surface, including measurements using the microbalance (18). These measurements are largely for hydrogen-reduced iron surfaces for which the apparent surface and the so-called true surface are not greatly different. Another

similarity is found in the rapid initial adsorption of oxygen by both iron and 18-8 followed by a slower rate of oxygen consumption. The slow rate is a logarithmic function of time for iron (16) and appears also logarithmic for 18-8. Data of Fig. 2 transferred to a semilogarithmic plot in Fig. 3 follow the equation:

$$\mu g\ O_2/cm^2 = 0.188 \log \left(\frac{t}{\tau} + 1\right)$$

where τ is equal to 0.19 sec. This equation indicates that half the total oxygen adsorbed by 18-8 (0.55 $\mu g/cm^2$) occurs within about 2.7 min, which is in qualitative agreement with our observation that a large fraction of gas is adsorbed before measurements are possible.

The logarithmic relation is sometimes interpreted as evidence of oxide growth in accord with the similar equation expressing oxidation of several metals at elevated temperatures. However, the

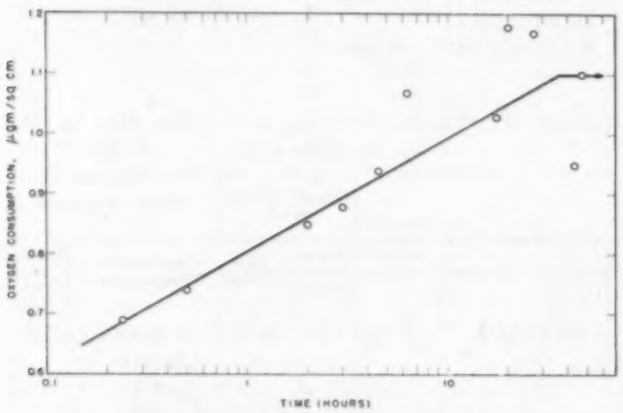

FIG. 3. Oxygen take-up by HCl-H_2SO_4 pickled 18-8 vs. time of exposure to aerated water.

logarithmic relation may also apply to rate of chemisorption, where the first layer of gas molecules is rapidly adsorbed physically, followed by slow conversion to dissociated atoms which are chemisorbed. As chemisorption proceeds, more gas, less tightly bound than the first layer, is adsorbed at a rate dependent upon the rate of chemisorption.

DISCUSSION OF DATA

It appears that most of the hydrogen from the HCl-H_2SO_4 pickle is washed off the 18-8 surface by the nitrogen-saturated water, since the HNO_3-HF pickled surface consumes as much oxygen per true unit area as does the HCl-H_2SO_4 pickled surface. The fact that phosphorus added to the HCl-H_2SO_4 pickle gave about the same consumption of oxygen per unit area of metal surface is further evidence along these lines. Had considerable adsorbed hydrogen been present and later oxidized, this might, presumably, have given rise to small quantities of H_2O_2 in the aerated water. A check was made for hydrogen peroxide after contact of pickled 18-8 with aerated water for 1, 2, 4, 6, and 15 min using the yellow color reaction occurring with $TiOSO_4$ in dilute H_2SO_4. Although a very faint yellow first appeared and then quickly faded, comparative tests showed that any hydrogen peroxide must have been present in quantity less than 0.3 $\mu g/ml$ and, hence, was insignificant.

The amount of oxygen in the order of 0.27 $\mu g/cm^2$ of true surface, as reported herewith, is adequate to impart full passivity to 18-8. This was proved by potential measurements of the 18-8 coil and absence of visible rusting. The potential after 23 hr exposure was 0.15 volt more noble than the saturated calomel half cell. On the other hand, 5 min after exposure to aerated water, the coil was more active in potential than the saturated calomel half cell by 0.03 volt. Potentials of similar 18-8 specimens immediately after pickling in HCl-H_2SO_4 and washing indicated a value 0.5 to 0.6 volt more active than the calomel half cell, leaving no doubt that passivity is destroyed by the acid. The potential of 18-8 is similarly shifted in the active direction several tenths volt by the HNO_3-HF pickle, and again becomes noble as oxygen is taken up by the surface.

The potential data removed the possibility that a major passive film could have been built up during the nitrogen-saturated water wash by direct reaction of the metal with water to form oxide plus hydrogen. Had such an oxide formed, a noble potential might have been expected after the water wash instead of an active potential.

Since the alloy is fully passive after a few hours' exposure to aerated water, the small amount of oxygen on the surface, even after 48 hr, is consistent with a thin so-called passive film, in accord with ideas expressed by previous investigators. The maximum thickness of a supposed oxide film is about half that of the thinnest film (30 Å) isolated by Vernon *et al.* for polished 18-8. It should be noted in this connection, however, that it is not at all certain that isolated oxide films have any relation to those of concern here, because the oxide films were obtained from polished specimens, whereas our specimens were pickled. Polishing and abrading operations produce high local temperatures sometimes reaching the melting point of the metal (19) and, hence, can easily produce an oxide where none existed before. In this connection, it is pertinent that, so far, an oxide film has not with certainty been isolated from a pickled 18-8 surface, where the techniques employed have clearly avoided formation of oxides by the stripping solution itself. Vernon *et al.* (2) showed that the halogen methyl

alcohol solution must be free of water and oxygen. Fontana presented similar evidence (20).

It seems reasonable to conclude that if an oxide film is present on pickled 18-8, it is extremely thin and not more than a few molecules thick. There is some question how thin a film can be and still act as a reliable diffusion barrier of the kind that matches the observed corrosion resistance of the stainless steels. On the other hand, the measured oxygen on an 18-8 surface, treated as an adsorbed film, is in the order of a monolayer. Therefore, the present data can be interpreted as being consistent with the adsorbed film theory of passivity, where the primary passive film is made up of a monolayer of oxygen atoms over which a layer of molecular oxygen is adsorbed. A structure of this kind is in quantitative agreement with the measured amount of oxygen on the surface whether the steel is pickled in HCl-H_2SO_4 or in HNO_3-HF and, hence, is probably true generally.

If this conclusion is valid, it indicates that the mechanism of passivity in stainless steels by oxygen is no different than that by carbon monoxide, where the adsorption theory heretofore (21) has been the only reasonable explanation for the passivity of 18-8 in hydrochloric acid saturated with this gas. It also indicates that the thin or thick oxide films, sometimes observed on stainless steels, are produced by reaction of the adsorbed oxygen film with the metal, stimulated by polishing and abrading, by presence of halogen ions and water, or by high temperatures. These oxide films, however, are of secondary importance in accounting for passivity, as measured by corrosion resistance or by a noble potential.

Acknowledgment

The authors are pleased to acknowledge joint support of this research by the Office of Naval Research on Contract N5-ori-07815 and by the Shell Fellowship Committee of the Shell Companies in the United States. They also wish to acknowledge the assistance of Henry Paige and James Forstner in obtaining preliminary data.

Any discussion of this paper will appear in a Discussion Section, to be published in the December 1953 issue of the Journal.

References

1. U. R. Evans, "Metallic Corrosion, Passivity and Protection," p. 26, Ed. Arnold and Co., London (1946).
2. W. Vernon, F. Wormwell, and T. Nurse, *J. Iron Steel Inst. (London)*, **150**, 81P (1944).
3. E. Mahla and N. Nielsen, *J. (and Trans.) Electrochem. Soc.*, **93**, 1 (1948).
4. I. Langmuir, *Trans. Electrochem. Soc.*, **29**, 260 (1916); *J. Chem. Soc. (London)*, **1940**, 518.
5. G. Tammann, *Stahl u. Eisen*, **42**, 577 (1922).
6. H. H. Uhlig, *Chem. Eng. News*, **24**, 3154 (1946); "Corrosion Handbook," p. 20, John Wiley & Sons, Inc. New York (1948); *J. Electrochem. Soc.*, **97**, 215C (1950).
7. H. O. Forrest, B. E. Roetheli, and R. H. Brown, *Ind. Eng. Chem.*, **22**, 1197 (1930).
8. F. Körber and H. Ploum, *Mitt. Kaiser Wilhelm Inst. Eisenforsch. Düsseldorf*, **14**, 229 (1932).
9. H. H. Uhlig, *Trans. Am. Inst. Mining Met. Engrs.*, **158**, 183 (1944).
10. H. H. Uhlig, *Trans. Am. Inst. Mining Met. Engrs.*, **140**, 387 (1940).
11. S. Brunauer, P. Emmett, and E. Teller, *J. Am. Chem. Soc.*, **59**, 2682 (1937).
12. L. Wooten and C. Brown, *J. Am. Chem. Soc.*, **65**, 113 (1943).
13. C. Brown and H. H. Uhlig, *J. Am. Chem. Soc.*, **69**, 462 (1947).
14. I. Langmuir, *J. Am. Chem. Soc.*, **38**, 2267 (1916).
15. I. Langmuir, *J. Am. Chem. Soc.*, **39**, 1380 (1918).
16. M. Armbruster and J. Austin, *J. Am. Chem. Soc.*, **68**, 1347 (1946).
17. R. Burstein, N. Shumilova, and K. Golbert, *Acta Physicochim. U.R.S.S.*, **21**, 785 (1946).
18. E. Gulbransen, *Trans. Electrochem. Soc.*, **81**, 327 (1942).
19. F. Bowden and D. Tabor, "Friction and Lubrication of Solids," pp. 33–57, Oxford University Press, Oxford, England (1950).
20. M. G. Fontana, *Trans. Electrochem. Soc.*, **93**, 335 (1948).
21. "Corrosion Handbook," p. 25, edited by H. H. Uhlig, John Wiley & Sons, Inc., New York (1948).

Distribution of Conductivity within Dielectric Films on Aluminum[1]

J. E. Lilienfeld and Charles Miller

Power Condsener and Electronics Corporation Laboratory, Washington, D. C.

ABSTRACT

The characteristics of the dielectric film itself are substantially linear to alternating current within the limits listed. Since these characteristics are linear, the electrolytic capacitor appears equivalent to the characteristic of: (*a*) the conventional model of an electrolytic condenser film consisting of a capacity, which is determined by formation voltage, together with a high "leakage" resistance in parallel with that capacity; and (*b*) another capacity which is not so determined, with a relatively lower resistance in parallel, and in series with the conventional model indicated in (*a*).

It is concluded that conductivity within the film is not homogeneously distributed through it; assumption of an interface stratum is needed to render an adequate electrodynamic picture justifiable by a physicochemical concept.

Introduction

The purpose of this communication is to present an outline of some studies made to determine the electrical performance of the condenser film on anodized aluminum, (*a*) by constructing a model circuit which would reproduce the electrical characteristics of the actual electrolytic condenser; and (*b*) by drawing a correlation between the physical components of the condenser and the electrical elements of the model circuit. Regarding the first point, it should be noted that the simple model of a resistance in series with a parallel resistance-capacity combination is still being used (1), but more elaborate models have been presented in various publications over the last 15 years (2, 3).

General Experimental Procedure

In order to have a well-defined electric field between anode and cathode of the electrolytic condenser, the construction of Fig. 1 was used. The specimen consists of a thin filmed aluminum anode 3 in. x 4 in. inserted between two interconnected nonfilmed cathodes held ¼ in. apart. Separators were used to keep the anode centered without hindering the passage of current. Each such assembly was put in a sealed Pyrex jar containing the electrolyte made up of boric acid and borates.

In every case referred to here the rule was followed that at all times the anode be kept at a positive potential with respect to the electrolyte. This condition is met by biasing the anode as in the circuit (4) of Fig. 2, which is made symmetrical either by using two identical electrolytic condensers or by combining the electrolytic condenser with a paper oil condenser decade adjusted to give equal a-c voltages across the decade and the electrolytic condenser. Nearly all films studied were formed to 180 v DC and operated as in Fig. 3 on 55 volts RMS AC with a 90-volt d-c bias, corresponding to the operation of a complete condenser on 110 v AC.

The d-c leakage current on our test condenser was usually of the order of 50–300 μa.[2] This current was measured on a microammeter inserted in the center branch, while the power dissipation was measured by a wattmeter, as shown in Fig. 3. To confine the alternating current to the outside branches, a resistor of 3000 ohms was inserted in the center branch with the effect that a 1 per cent unbalance in the impedances of the condensers allows less than 0.1 per cent of the alternating current to flow in the center branch, while lowering the effective bias voltage less than 1.5 v. The "excess" bias of more than 5 v fulfills the indicated condition that the anode be kept positive with respect to the electrolyte. Since the leakage current depends, among other things, on small local imperfections in the filmed anode, it may only with due caution be considered significant in discussing the basic nature of the film.

The purposes of the present investigation called for the knowledge of the performance of the condenser as a function of frequency, as part of its experimental foundation. Observations were made within the range from 20–10,000 cps.[3] The test

[1] Manuscript received June 24, 1952. This paper was prepared for delivery before the Philadelphia Meeting, May 4 to 8, 1952.

[2] Much smaller leaks are obtainable in other types of electrolytic condensers which, however, are less suitable for the present experiments.

[3] Measurements of this kind are to be found in a paper by C. Wachenhusen (3). Although Wachenhusen's point of view was different from ours, some of his observations make it highly probable that the conclusions reached by us would hold true over the extended frequency range he used.

equipment included an audio oscillator, audio amplifier, a-c bridge, and a cathode ray oscilloscope high gain detector. The bridge was a General Radio 740-B, modified to be operated with an external generator and detector. The amplifier driving the bridge was a single-ended push-pull amplifier similar to that designed by Petersen (5). This in turn was fed from an audio oscillator built in our laboratory and calibrated against the 60-cycle line frequency by the Lissajou figure method. The condenser to be tested was thus operated with a ripple voltage of about 3 v RMS. When the condenser is thus operated at 60 cps the bridge measurements check the wattmeter measurements of Fig. 3. For all frequencies other than 60 cps the bridge measurements

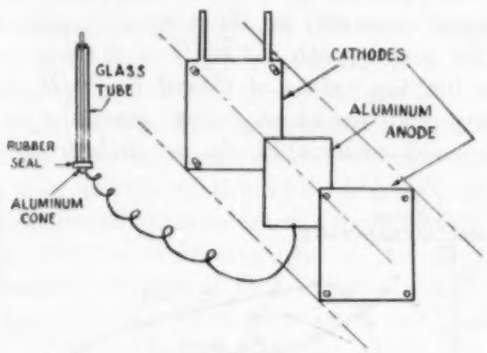

FIG. 1. Construction of typical condenser

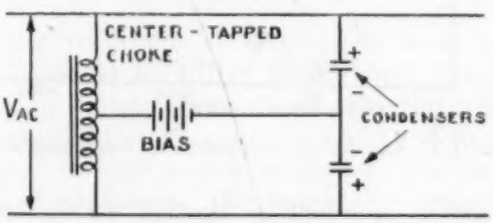

FIG. 2. Test circuit

were used exclusively, because operation as shown in Fig. 3 was not feasible at the higher frequencies.

OBSERVATIONS AS FUNCTION OF FREQUENCY

A typical set of measurements is shown in the plot of Fig. 4. In every case, the bridge unbalance was less than 0.7 per cent residual harmonics. Most of the harmonics were undoubtedly caused by amplifier mismatch, particularly at the higher frequencies. Therefore, we may consider the loss due to dielectric hysteresis as negligible and thus the electrolytic condenser may be represented as a combination of linear circuit elements.[4] These conclusions are corroborated by observations of a different kind presented below.

[4] This statement is to define the relation between voltage and current, in each individual element, as linear.

Electrolyte Resistance Independent of Frequency

The equivalent series resistance and capacity of a typical electrolytic condenser were measured as functions of frequency. The results are shown in Fig. 5. The effective series resistance is seen to be asymptotic to a value R_e (resistance of the electrolyte) at high frequencies. To determine the nature of R_e two tests were made. First, a geometrical substitute of the electrolytic condenser cell was

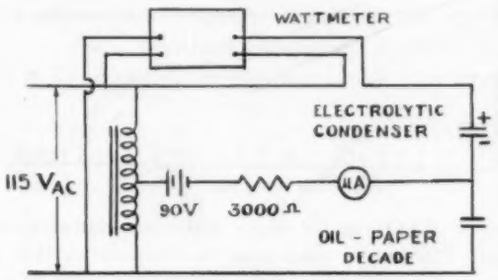

FIG. 3. Test circuit

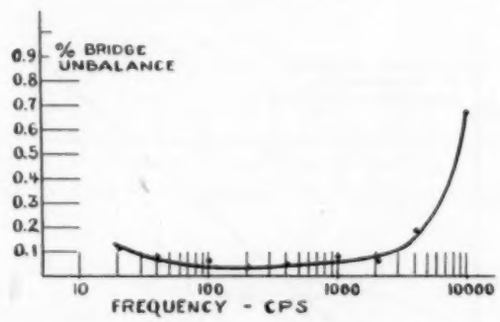

FIG. 4. Per cent bridge unbalance vs. frequency

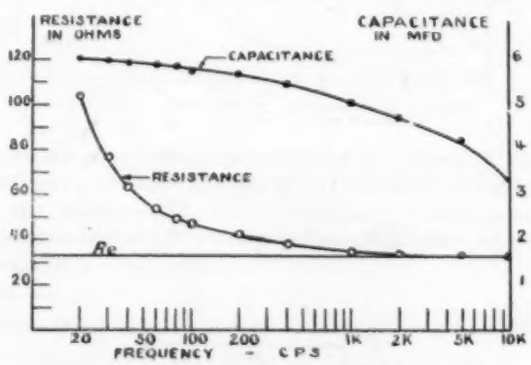

FIG. 5. Measurements on condenser #161

made, in which the filmed aluminum anode was replaced by a geometrically identical silver foil. When this cell is operated with the same electrolyte as the condenser, the effective series resistance vs. frequency is observed as seen in Fig. 6. The second set of tests was made on an electrolytic condenser starting in pure boric acid; and then adding sodium borate in stages. After each such addition, the condenser was operated for 24 hours to insure uniform concentration in the electrolyte. The specific resistance of the electrolyte was then determined by

a bridge measurement between platinum electrodes of a dip cell, while R_e was determined by the high frequency method. When the corresponding sets of these two values are plotted against each other the straight line of Fig. 7 results. Consequently, the value R_e represents within the limits of measurement the effective series component of resistance due to the condenser electrolyte, and as such R_e ought to be independent of frequency. This is confirmed by our observations inasmuch as the straight line of Fig. 7 passes through the origin. Obviously if R_e depended on frequency then the graph would intersect the axis of abscissae at some positive value $R_e - n$. Conversely, inasmuch as the electrolyte resistance is known to be frequency independent, a finite value n would correspond to dielectric losses *in the film*, and the fact that $n = 0$ does not contradict an earlier conclusion that the dielectric loss in the film is negligible.

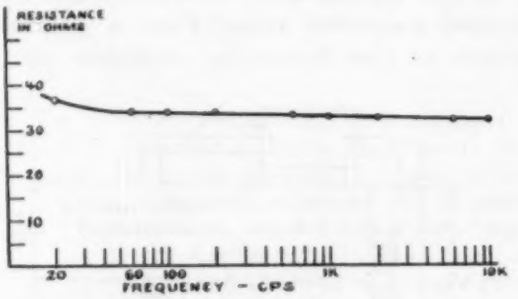

FIG. 6. Resistance of silver duplicate sandwich vs. frequency. Electrolyte resistance vs. frequency-silver anode sandwich copper end plates. Electrolyte tested 43 K in L. & N. conductivity cell.

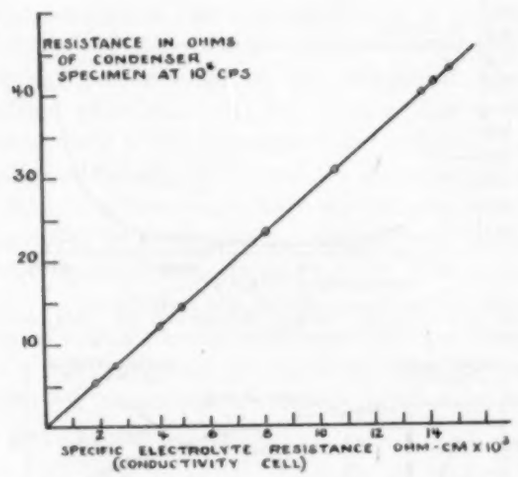

FIG. 7. Resistance of condenser specimen as determined by bridge at 10,000 cps vs. the specific electrolyte resistance as determined by conductivity cell. The function was obtained by varying the concentration of the electrolyte.

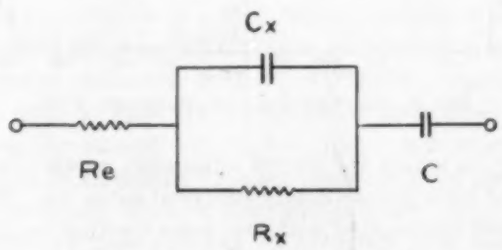

FIG. 8. Equivalent circuit diagram

Equivalent Circuit of Electrolytic Condenser

The preceding observations may be correlated by means of the equivalent circuit of Fig. 8, which will reproduce the electrical characteristic of the electrolytic condenser. It is not the only possible model, but it is the simplest one accounting for the measurements shown in Fig. 5. This may be seen by considering the behavior of the circuit of Fig. 11 at the frequency extremes; as the frequency approaches zero, the current path will be through C, R_e and R_x giving limiting values of C and $R_e + R_x$ as the capacity and resistance values measured on the bridge; and correspondingly, at high frequencies, the current path will be through R_e, C_x, and C, giving respectively R_e and $C_x\ C/C_x + C$ as the limiting values.

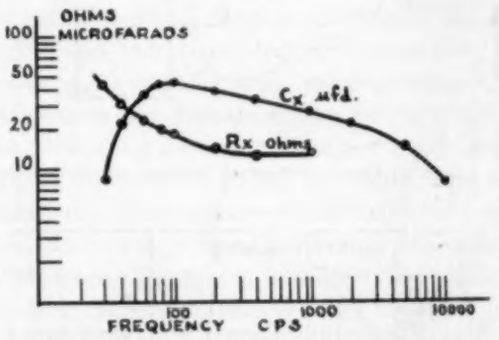

FIG. 9. C_x and R_x vs. frequency for condenser #161

Considering the circuit of Fig. 8 and postponing the consideration of a possible correlation between this circuit and the physical condenser, we can calculate these values from the above presented actual bridge measurements in which the electrolytic condenser as a unit is balanced at various frequencies against a resistance in series with a capacity. From these quantities can be calculated the elements C, C_x, and R_x of Fig. 8. The problem, however, is indeterminate unless one of the elements C, C_x, or R_x is postulated as being independent of frequency. We choose C as such an element.

The resultant value of C_x and R_x for a typical condenser are plotted in Fig. 9. The physical justification of the assumption that C is frequency independent is based on the observation that leakage current and dielectric hysteresis losses are negligible for the entire electrolytic condenser. Thus the physi-

cal counterpart of C contains a dielectric free of such losses (compare above), and as such is not likely to be frequency dependent.

Physicochemical Interpretation

Now it is possible to propose a hypothetical picture of the physical counterparts of the elements composing the circuit of Fig. 8. The quantities measured are not due to polarization effects, as such polarization capacities are relatively enormous compared to those due to the anodized film. Thus the film may be thought of as consisting of two strata. The first stratum, best thought of as adjacent to the metal surface, contains a good dielectric relatively free of conductivity and dielectric hysteresis losses. The second stratum consists of a compound with a rather high conductivity and it is best thought of as superimposed on the first stratum. It is referred to hereafter as the "interface stratum."

This picture would be more appealing if it could be shown that the first, good, dielectric stratum grows in proportion to the peak formation voltage, while the second stratum is not determined by that voltage. Conclusive observations to this effect are not available yet except that comparative tests on films formed to 180 v and 360 v make this probable.

Observations as Function of Formation Voltage

In this connection, reference can be made to plots like those shown by Deely (6) of formation voltage vs. elastance, which is the reciprocal of capacity, (in Deely's case in.^{2}/mfd vs. formation voltage). Such plots were made with one of our specimen condensers. The formation voltage was varied in steps, and in each step formation was carried to completion. Then the effective capacity was measured at 60 cps with the bridge setup mentioned before. The plot is shown in Fig. 10. With the conventional model of the electrolytic condenser, this plot would consist of a straight line through the origin. However, from both our plot and that of Deely, there is[5] a finite value of capacity at zero voltage, of the order of magnitude of 50 μf. An obvious interpretation is that the film consists of two strata; one, of the first kind, determined by the formation voltage; and the other one, of the second kind, not so determined. The graph of Fig. 10 does not, however, produce any evidence for the hypothetical interface stratum to be part or all of the stratum of the second kind. In order to ascertain this, it has been shown that the interface phenomenon can be produced on a nonanodized surface.

This simple experiment was performed by using one of the specimen condenser cells in which, however, the aluminum foil was neither preformed on d-c nor at any other time positively biased with respect to the electrolyte. In series with this cell was connected a 6 μf paper-oil condenser. Then the usual measurements were taken within the full range of frequencies. The plot of Fig. 11 reproduces measurements which appear typically the same as in Fig. 5. The "interface" capacity at 200 cps in Fig. 11 is 37 μf, while in Fig. 5 it is 40 μf. Thus the

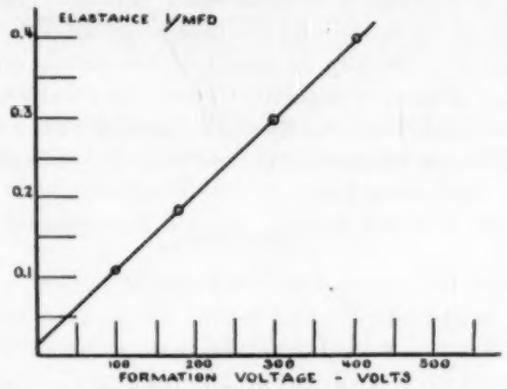

Fig. 10. Inverse microfarads vs. formation voltage

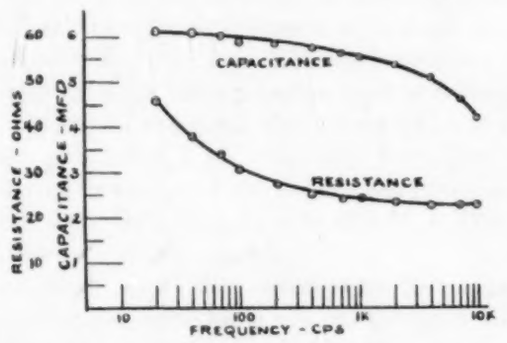

Fig. 11. Impedance of nonformed aluminum anode in series with 6-μf oil condenser.

hypothetical interface stratum may be regarded as the "stratum of the second kind."[6]

The latter experiment not only corroborates our interface hypothesis but also, by substituting a paper-oil condenser in place of the dielectric C of the film, it supports the previous assumption that the physical counterpart of C exhibits a capacity substantially independent of frequency.

Experiments of the latter kind are scheduled to be extended more widely over a variety of conditions

[5] This is estimated by extending the rectilinear part of the plot to its intersection with the $\frac{1}{C}$ axis. A precise determination of the point of intersection presents serious experimental difficulties.

[6] Strictly speaking the question remains open as to whether or not the interface stratum is all or part of the stratum of the "second kind." The answer to this question can, of course, be found by experiment, for instance, by a more elaborate determination of such graphs as Fig. 10.

and we expect that they will contribute substantially to our knowledge of anodized films.

Summary

1. It is concluded, on the basis of experimental observations, that an electrodynamic model of the film is feasible containing a finite number of linear elements.

2. The simplest such model to reproduce the observed frequency dependent characteristic is proposed (Fig. 11) and it is shown that one of the elementary capacities,—the main capacity C—does not depend appreciably on frequency.

3. A correlation is established between the elements of the model and the here-proposed structure of the film: the film to consist of two strata, one of a good dielectric, capacity C; and the other one of a poor dielectric, capacity C_x, in parallel with a relatively small resistance R_x, and with a correspondingly high power loss.

4. It is shown that C_x, R_x are functions of frequency, but are not determined by peak formation voltage. Indeed they may be reproduced on a non-anodized surface, substituting for stratum C a paper-oil condenser.

5. While the above, No. 1 to 4, refer to relations observed with frequency as variable, the conclusions arrived at are corroborated by measurements, at a constant frequency, of the specific capacity of the film while varying the peak formation voltage.

Any discussion of this paper will appear in a Discussion Section, to be published in the December 1953 issue of the Journal.

REFERENCES

1. M. Whitehead, *Bell Labs. Record*, **28**, 448 (1950).
2. G. Raoult, *Rev. gen. élec.*, **54**, 145 (1945).
3. C. Von Wachenhusen, *Hochfrequenztechnik und Elektroakustik*, **57**, No. 5, 125 (1941).
4. S. Moscicki, U. S. Pat. #926128, June 29, 1909.
5. A. Peterson, *Proc. I. R. E.*, **40**, No. 1, 7 (1952).
6. P. Deely, "Electrolytic Capacitors," p. 117, Recorder Press, Plainfield, N. J., (1938).

Electrodeposition of Copper from the Monoethanolamine Bath[1]

T. L. Rama Char and N. B. Shivaraman[2]

Electrochemistry Laboratory, Indian Institute of Science, Bangalore, India

ABSTRACT

Copper has been electrodeposited on steel by using a complex copper-monoethanolamine solution. This does not deposit copper on steel by immersion. The deposits are smooth, fine grained, bright, and adherent, and the bath is comparable to the cyanide bath. The inclusion of rochelle salt considerably improves its performance. The optimum conditions are: copper oxalate 60 g/l, monoethanolamine 60 ml/l, rochelle salt 60 g/l, 2.4–4.8 amp/dm² (22.3–44.6 amp/ft²), *p*H 9.5, and 24°C. The addition of nitrates has some beneficial effect.

Introduction

Some attempts have been made to evolve a substitute for the commercial cyanide bath used in the electrodeposition of copper in view of its poisonous nature, instability, and low current efficiencies. Work has been done on solutions like thiosulfate, iodide, thiocyanate, amine, oxalate, tartrate, sulfammate, pyrophosphate, thiourea, fluoborate.

The electrodeposition of copper from complex solutions containing mono-, di-, and triethanolamines has been studied by Brockman and coworkers (1, 2, 3), Schweig (4), and Levin (5). The present investigation formed part of the general program on the electrodeposition of metals and alloys from cyanide-free baths. In a previous communication from this laboratory (6), it has been shown that the silver iodide bath gives satisfactory deposits of silver. The electrodeposition of copper and brass from the ethanolamine baths has been briefly reported in preliminary notes by Rama Char and coworkers (7–9). This paper describes in detail the work on the deposition of copper from monoethanolamine solutions. Electrodeposition from di- and triethanolamine baths will be reported in subsequent papers.

The Plating Bath

When 1 ml of monoethanolamine was added to 1 g of copper oxalate suspended in water, a clear blue solution was obtained indicating the formation of a complex. The salt:amine ratio remained the same at all concentrations. The concentration of copper oxalate in the bath was in the range 15–120 g/l (6–48 g/l of copper). These solutions are simpler than those attempted before.

Experimental

The monoethanolamine (technical) and copper oxalate were of the British Drug House make. The other chemicals were made by British Drug House or Merck. The amine had a specific gravity of 1.019 at 24°C. It had a strong smell of ammonia and its *p*H was 13.75. It distilled off completely at 170°C.

The cathodes were cut from a mild steel sheet of $\frac{1}{32}$ in. (0.08 cm) thickness. Each cathode was 1 in. x 3 in. (2.5 cm x 7.5 cm) and submerged to a depth of 2 in. (5 cm) in the bath, the submerged electrode surface area being 4 in.² (25 cm²). Two Canning's rolled copper anodes of the same dimensions as the cathode were used, at a distance of 0.75 in. (1.9 cm) on either side of the cathode.

Rust, scale, and other oxides were best removed by pickling the cathodes in hot (60°C) dilute hydrochloric acid (1:1). The cathodes were dried after cleaning with water, and then rubbed with smooth emery. They were further cleaned by cathodic treatment for about 1 min in a hot alkaline bath containing: trisodium phosphate 100 g/l, sodium carbonate 80 g/l, and sodium hydroxide 20 g/l, at 6 amp/dm² and 6–8 volts. The cathodes were finally rinsed in water and alcohol, dried, and kept in a desiccator for use.

The experiments were carried out in 100 ml beakers. The plating time was 2.5 min and the temperature 24°C. The rest of the experimental procedure was the same as described before (6).

Experimental Results

Copper Ion Concentration

The copper (cupric) ion concentration in the plating solutions was determined by the emf method

[1] Manuscript received April 10, 1952. This paper was prepared for delivery before the Montreal Meeting, October 26 to 30, 1952. This paper is based on part of the thesis submitted by N. B. Shivaraman for the Associateship of the Indian Institute of Science in partial fulfillment of the requirements for the Diploma of the Indian Institute of Science in Chemical Engineering.

[2] Present address: Tata Chemicals Ltd., Mithapur, India.

and was of the order of 10^{-11} to $10^{-13}N$. The addition of 60 g/l rochelle salt decreased the metal ion concentration of the bath 60 g/l copper oxalate, 60 ml/l amine from 1.90×10^{-11} to $3.16 \times 10^{-13}N$, indicating that further complexes are formed. In the cuprocyanide bath the cuprous ion concentration is of the order of $10^{-30}N$. The ethanolamine solutions did not deposit copper on steel by chemical displacement due to the low metal ion concentration.

TABLE I

*p*H: 9.15–9.20

Copper oxalate g/l	Amine ml/l	C.D. amp/dm²	Bath tension volts	Cathode efficiency %	Appearance of electrodeposit
15	15	0.4	2.5	96	Bright
		0.6	3.8	93	Bright
30	30	0.8	8.1	96	Nonuniform
		1.2	5.2	100	Fairly bright
		1.6	6.7	93	Bright
		2.0	9.6	93	Partly burnt
45	45	0.8	2.5	90	Nonuniform and dull
		1.6	5.3	93	Dull
		2.0	7.5	94	Fairly bright
		2.4	8.4	98	Partly burnt
60	60	2.4	4.3	90	Dull
		3.2	5.5	95	Fairly bright
		4.0	6.9	91	Bright
		4.8	9.2	90	Bright
75	75	2.4	4.5	95	Dull
		3.2	5.2	93	Fairly bright
		4.0	8.5	91	Bright
		4.8	10.2	90	Bright
90	90	2.4	4.0	90	Dull
		3.2	4.8	98	Dull
		4.0	5.7	100	Fairly bright
		4.8	6.7	94	Fairly bright
		5.6	9.0	93	Bright
		7.2	10.0	90	Burnt
120	120	4.8	5.2	86	Dull
		6.4	7.2	90	Fairly bright
		8.0	10.0	90	Bright

Electrodeposition

Variation of concentration.—Electroplating was carried out over a wide range of concentration and current density and the results obtained are given in Table I.

The cathode efficiency ranged from 86 to 100 per cent and was 90 per cent and above in the bright C.D. range. The plating range for good deposits was from 0.4–8.0 amp/dm². Increase in the concentration of metal (complex) increased the limiting C.D. for bright deposits. But, at concentrations above 90 g/l of copper oxalate the bath tended to crystallize out and the anode corrosion was not good at high C.D. In view of the dragout losses and the fact that a decrease in the metal ion concentration causes finer grained deposits, it was not advisable to raise the copper concentration above 24 g/l. The optimum concentration was that of the bath containing copper oxalate 60 g/l and amine 60 ml/l (60:60). The bath voltage, ranging from 2.5–10.2 volts, was rather high as compared with the cyanide bath. The deposits were treed at high C.D. The adherence of the electrodeposits to the base metal, as found from bending and breaking tests, was good. Addition of 10, 30, and 60 ml/l of excess amine to the optimum concentration bath did not improve the quality of the deposit.

Rochelle salt bath.—It was found that the addition of rochelle salt as one of the constituents of the bath considerably improved its performance. Rochelle salt facilitated anode corrosion by preventing blackening of the anodes at high C.D.; reduced the bath voltage and minimized the fluctuations in voltage and current; increased the C.D. range, conductivity, cathode polarization, and throwing power; and yielded better quality deposits by eliminating treeing and increasing the brightness. It also reduced the copper ion concentration. Table II gives the results with the rochelle salt bath.

Even at high concentrations, copper oxalate 120 g/l, amine 120 ml/l, rochelle salt 120 g/l (120:120:120), the bath did not crystallize out at room temperature. The optimum concentration was 60:60:60. The deposits were brighter than those obtained from the rochelle salt-cyanide bath. There was no change in the bath performance on allowing the bath to age for a period of 4 months. It was possible to go up to 10.0 amp/dm².

Temperature.—Higher temperatures were not conducive to the good working of the bath with and without rochelle salt.

Addition agents.—In order to see whether the rochelle salt-amine bath could be further improved, some inorganic salts were added to the optimum concentration bath 60:60:60. Ammonium, potassium, and sodium nitrates (5 g/l) increased the brightness of the deposits and raised the limiting C.D. from 4.8 to 6.0 amp/dm² but considerably decreased the cathode efficiency to 58–80 per cent (2.4–6.0 amp/dm²). Ammonia (5–40 ml/l) eliminated the brittleness of the deposits but the bright C.D. range decreased and the anodes tended to blacken. Ammonium sulfate, chloride, and carbonate (5–15 g/l) decreased the C.D. range. The deposits were unsatisfactory with ammonium carbonate. Sodium chloride (5–15 g/l) decreased the C.D. range considerably and the anode corrosion was poor at higher C.D.

Conductivity, cathode polarization, and throwing power.—Table III gives the conductivity, cathode polarization (range), and throwing power of the bath, with and without additions. The polarization

values give a general idea of the variations but should not be considered as very accurate in view of the difficulties in reproducibility. The throwing power of the bath was fairly good. Satisfactory deposits were obtained on the reverse side of the cathode when only one anode was used and the plating solution threw well into the recesses of irregularly shaped cathodes. The values given below were calculated according to the equation of Schlotter-Korpiun (10).

TABLE II

*p*H: 9.4–9.7

Copper oxalate g/l	Amine ml/l	Rochelle salt g/l	C.D. amp/dm²	Bath tension volts	Cathode efficiency %	Appearance of electrodeposit
30	30	30	0.8	2.2	100	Dull
			1.2	2.7	97	Bright
			1.6	3.4	90	Bright
			2.0	4.1	88	Bright
30	30	60	0.8	1.8	96	Dull
			1.2	2.6	97	Bright
			1.6	2.6	92	Edges rough
60	60	30	2.4	3.2	96	Dull
			3.2	4.0	93	Bright
			4.0	4.6	90	Bright
			4.8	5.0	88	Bright
60	60	60	1.6	2.2	94	Dull
			2.4	2.9	94	Brighter
			3.2	3.6	92	Brighter
			4.0	3.9	90	Brighter
			4.8	4.3	90	Brighter
			5.6	4.6	87	Burnt
60	60	120	1.6	2.2	92	Bright
			2.0	2.4	91	Brighter
			3.2	3.0	90	Brighter
			4.0	3.6	90	Edges burnt
			4.8	4.0	87	Burnt
90	90	90	1.6	1.9	90	Dull
			3.2	3.0	96	Bright
			4.0	3.6	100	Brighter
			7.2	4.4	86	Brighter
			8.0	4.9	94	Bright
			10.0	6.5	90	Burnt
90	90	180	1.6	1.6	95	Dull
			2.4	2.4	93	Brighter
			3.2	2.6	90	Brighter
			4.0	2.9	90	Brighter
			6.0	3.8	89	Bright
120	120	120	2.0	2.2	60	Dull
			3.2	2.8	83	Bright
			4.0	3.2	90	Bright
			5.6	4.0	91	Bright
			7.2	4.4	100	Bright
			8.0	4.8	100	Bright
			8.8	5.0	95	Bright
			10.0	5.3	92	Bright

An increase in the metal concentration increased the conductivity and decreased the polarization and throwing power. Excess of amine decreased the polarization. Rochelle salt increased the conductivity, cathode polarization, and throwing power. Addition of nitrates had little effect on the conductivity but in some cases slightly increased the polarization and throwing power at higher C.D. The cathode polarization at which burning occurred was of the order of 0.9 volt.

TABLE III

*p*H: 9.15–9.50

Copper oxalate g/l	Amine ml/l	Rochelle salt g/l	Addition agents g/l	Sp. conductivity mhos/cm³	Cathode polarization range volts (C.D. 1.6–4.0 amp/dm²)	Throwing power at 3.2×10^{-2} amp/cm²
30	30	—	—	0.0090	—	—
60	60	—	—	0.0141	0.38–0.72	1.28
60	120	—	—	—	0.26–0.60	—
90	90	—	—	0.0183	0.20–0.36	1.17
60	60	30	—	0.0299	—	—
60	60	45	—	0.0347	(C. D. 1.6–4.8 amp/dm²)	
60	60	60	—	0.0398	0.71–0.82	2.01
60	60	75	—	0.0430	—	—
60	60	60	KNO_3 5	0.0394	0.26 –0.89	2.03
60	60	60	NH_4NO_3 5	0.0417	0.49–0.98	2.11
60	60	60	$NaNO_3$ 5	0.0392	0.39–0.83	1.95

TABLE IV

Composition	*Ethanolamine* Copper oxalate, 60 g/l Mono amine, 60 ml/l Rochelle salt, 60 g/l	*Cyanide* Copper cyanide, 40 g/l Sodium cyanide, 50 g/l Sodium carbonate, 30 g/l Rochelle salt, 60 g/l
*p*H	9.5	11.4
Temp, °C.	24.0	60.0
(Cu) g/l	24.0	28.4
(Copper ion) g ion/l	3.16×10^{-13} (Cu^{++})	2.29×10^{-20} (Cu^{+})
Sp. conductivity, mhos/cm³	0.0398	0.0987
Bright C. D. range amp/dm²	2.4–4.8	2.0–2.5
Cathode polarization, volts (0.8–5.6 amp/dm²)	0.24–0.82	0.65–1.11
Bath voltage volts	2.9–4.3	0.9–4.0
Cathode efficiency, %	90–94	70–76
Throwing power	Fairly good	Good
Quality of deposit	Brighter	Bright

The throwing power was less than that of the cyanide bath where it is of the order of 4. In the amine bath, it can be improved to a value of 3 under certain conditions. It was also calculated from the equation of Gardam (11) by substituting, as an approximation, the interelectrode distance for l_2 in the equation. At a C.D. of 2.0×10^{-2} amp/cm²

(where the cathode polarization—log C.D. relationship was roughly linear) the throwing power for the ethanolamine bath with and without additions was in the range 7–30 per cent, as against the normal value of 30–40 per cent for the cyanide bath.

Comparison between ethanolamine and cyanide baths.—Table IV will give an idea of the relative performance of the rochelle salt-copper oxalate-monoethanolamine and rochelle salt-copper cyanide baths. The values for the cyanide bath were experimentally determined under the conditions recommended by Bakhvalov (12).

The advantages of the amine bath over the cyanide are: (*a*) wider C.D. range; (*b*) higher cathode efficiency; (*c*) brighter deposits; (*d*) ability for good working at the room temperature; (*e*) satisfactory performance without the use of special additions; and (*f*) stability. On the other hand, the cyanide bath has a higher conductivity and cathode polarization, and superior throwing power.

The rate of deposition of copper from the rochelle salt-amine bath was compared with that from the "low concentration" cyanide bath (13) and "high efficiency" cyanide bath without brightener (14), at a C.D. of 2.4 amp/dm^2. It was in between the rates for the cyanide baths.

Discussion

The electrodeposition of copper from the complex monoethanolamine bath yields smooth, fine-grained, and bright deposits on steel. There is no immersion deposition due to the low copper ion concentration. The high cathode efficiency, which is very near 100 per cent, is a definite advantage. Brockman and Tebeau (3) used the plating composition: copper sulfate, sodium oxalate, and monoethanolamine at cathode efficiencies from 93–111 per cent and concluded that, so far as the throwing power is concerned, the monoethanolamine bath is the least suitable of the ethanolamine baths (mono-, di-, and tri-) for copper plating. In the present work the throwing power of the monoethanolamine bath has been found to be fairly good and of the same order as that of the di- and triethanolamine baths (15).

The inclusion of rochelle salt in the amine bath improves its performance to a great extent and the beneficial effects are on the lines observed in the rochelle salt-copper cyanide bath (13). The action of this salt is probably due to its reducing nature and tendency to form further complexes. A decrease in the metal ion concentration on addition of rochelle salt is accompanied by the formation of brighter deposits. The addition of nitrates to the rochelle salt-amine bath increases the brightness and the C.D. range but reduces the cathode efficiency. This can be attributed to the inhibiting action of the nitrate ion (16, 17). It is preferentially reduced to ammonia before the hydrogen ion, preventing the formation of spongy deposits and enabling higher C.D. to be used. The effect of the addition of other ions is of a specific character. Small variations in *p*H are not of much significance.

Complex salt plating baths generally give fine-grained and bright deposits due to the low metal ion concentration. The cathode polarization and throwing power in such solutions is high. In the ethanolamine bath the copper ion concentration is low and fine-grained; bright deposits are obtained. The cathode polarization is high. But the conductivity is lower, the cathode efficiency higher, and the throwing power less than that of the cyanide bath. The polarization is increased by the addition of rochelle salt and by some nitrates (to a little extent) which act as brighteners. It is likely that cathode polarization has some significance in the electrodeposition of copper from the ethanolamine baths.

Summary

1. The copper oxalate-monoethanolamine-rochelle salt bath gives smooth, fine-grained, and bright electrodeposits of copper directly on steel. The optimum conditions are: copper oxalate 60 g/l, monoethanolamine 60 ml/l, rochelle salt 60 g/l, C.D. 2.4–4.8 amp/dm^2, *p*H 9.5, and temp 24°C.

2. The beneficial effects of rochelle salt are of the same nature as in the rochelle salt-copper cyanide bath.

3. The advantages of the amine bath over the cyanide are: (*a*) higher cathode efficiency, (*b*) brighter deposits, (*c*) comparative stability, (*d*) nonpoisonous nature.

4. The bath is not suitable for plating at higher temperatures. Its conductivity and throwing power are lower than that of the cyanide bath. The bright C.D. range is of the same order.

5. The addition of nitrates increases the brightness and the limiting C.D. but reduces the cathode efficiency for deposition.

Any discussion of this paper will appear in a Discussion Section, to be published in the December 1953 issue of the Journal.

REFERENCES

1. C. J. Brockman and A. L. Brewer, *Trans. Electrochem. Soc.*, **69**, 535 (1936).
2. C. J. Brockman and J. B. Whitley, *Trans. Electrochem. Soc.*, **71**, 251 (1937).
3. C. J. Brockman and C. P. Tebeau, *Trans. Electrochem. Soc.*, **73**, 365 (1938).
4. B. F. Schweig, Brit. Pat. 503,095, March 31, 1939.

5. V. I. Levin, *J. Appl. Chem. U.S.S.R.*, **14**, 74 (1941).
6. T. L. Rama Char and R. Sadagopachari, *Current Sci., India*, **19**, 284 (1950).
7. T. L. Rama Char and N. B. Shivaraman, *Current Sci., India*, **19**, 311 (1950).
8. N. B. Shivaraman and T. L. Rama Char, Proc. 37th Indian Science Congress, Part 3, 179 (1950).
9. R. Sadagopachari, N. B. Shivaraman, and T. L. Rama Char, *Current Sci., India*, **20**, 154 (1951).
10. M. Schlotter and J. Korpiun, *Trans. Electrochem. Soc.*, **62**, 129 (1932).
11. G. E. Gardam, *Trans. Faraday Soc.*, **34**, 698 (1938).
12. G. T. Bakhvalov, *J. Appl. Chem.* U.S.S.R., **14**, 270 (1941).
13. A. K. Graham and H. J. Read, *Trans. Electrochem. Soc.*, **80**, 341 (1941).
14. H. L. Benner and C. J. Wernlund, *Trans. Electrochem. Soc.*, **80**, 355 (1941).
15. Unpublished work.
16. *Electroplating*, **1**, 523 (1948).
17. R. Taft, *Trans. Electrochem. Soc.*, **63**, 75 (1933).

Electrodeposition of Cadmium from Fluoborate Solutions[1]

T. R. Anantharaman[2] and J. Balachandra

Department of Metallurgy, Indian Institute of Science, Bangalore, India

ABSTRACT

The optimum conditions for electroplating cadmium from its fluoborate solution have been arrived at by a systematic study of the effects of all types of variables on its plating characteristics. The best deposits of cadmium are obtained from a bath containing 210 g/l of cadium fluoborate, 25 g/l of sodium fluoborate, 25 g/l of boric acid, and 1 g/l of sodium-beta-naphthalene sulfonate at a *p*H of 3.2–3.6 and temperatures of 20°–30°C, and at current densities of 2.2–6.5 amp/dm² (20–60 amp/ft²). The deposits which are obtained on steel, brass, or copper are uniform, bright, fine grained, adherent, and of pleasing appearance. The current efficiency of the process is 98–100 per cent cathodic and 102–104 per cent anodic. The bath is nonpoisonous, stable, and easily controlled. The new bath is slightly inferior to the cadmium cyanide bath in the throwing power and resistivity, but vastly superior in all other respects.

Introduction

In commercial electroplating practice, cadmium is almost invariably plated from a complex cyanide bath containing sodium cadmicyanide, sodium cyanide, sodium hydroxide, and some inorganic addition agents (1). This bath has proved satisfactory from many points of view, but it is not a very efficient plating medium. Its current efficiency is only 85–90 per cent and its plating range is only 1.6–3.2 amp/dm² (15–30 amp/ft²). The control of the bath is not easy as the anode produces a cadmium sludge at very low current densities, and behaves as an oxygen electrode at current densities of more than 2.2 amp/dm² (20 amp/ft²). The deposits obtained from this bath become brittle on certain occasions and have to be heated to a high temperature before use (2). The cadmium fluoborate solution has two definite advantages as a plating medium; it is nonpoisonous and is very stable. If some other advantages like very high current efficiency and wide plating range which are claimed for some fluoborate solutions (3) are also realized, in this case it can replace the cyanide solution in the commercial field.

In the present investigations, the effects of all types of variables on the plating characteristics of the cadmium fluoborate solutions have been studied to deduce the optimum conditions for electroplating cadmium from a fluoborate bath. As far as the authors are aware such a systematic study has not so far been attempted by workers in this field (3, 4).

[1] Manuscript received April 10, 1952. This paper was prepared for delivery before the Montreal Meeting, October 26 to 30, 1952. Part of a dissertation submitted by T. R. Anantharaman and accepted for the award of the degree of Master of Science by the University of Madras.

[2] Present address: Trinity College, Oxford, England.

Experimental Procedure

After preliminary studies on the range of electrolyte concentration and current density giving satisfactory deposits, a detailed study was undertaken of the influence separately of (*a*) electrolyte concentration; (*b*) hydrogen ion concentration; (*c*) temperature; and (*d*) agitation, on the following factors: 1. nature of the deposit (brightness, texture, adherence, distribution, and treeing tendency); 2. anodic and cathodic efficiency; 3. limiting cathodic current density, i.e., the current density where the deposition of the metal practically ceases; 4. resistivity; and 5. throwing power of the solution.

The influence of some inorganic salts and a number of selected addition agents on the plating characteristics of the solution was studied before arriving at the best conditions for plating the metal.

Experimental Details

The plating experiments were conducted on a small scale in 200 ml beakers placed in a thermostat. Anodes of uniform size 7.62 cm x 1.27 cm x 0.32 cm (3 in. x ½ in. x ⅛ in.) were employed together with standard rectifiers, rheostats, ammeters, voltmeters, etc., which generally make up a plating circuit. Special wooden stands were made to suspend the electrodes freely and immerse them in the plating solutions to any desired mark. The immersed anode area was equal to the immersed cathode area and the interelectrode distance was exactly 2.54 cm (1.0 in.) in all the experiments.

Plating Solutions

Cadmium fluoborate solutions of varying concentrations were prepared by the method utilized for lead fluoborate solutions by Blum and collaborators

(5). A stock solution of fluoboric acid (approx. 5*N*) was prepared from powdered boric acid and concentrated hydrofluoric acid (48–50%). The fluoborate solutions were made up whenever required by saturating this acid with cadmium carbonate powder, filtering through glass wool and diluting the filtrate to the desired extent. Analytical reagents were employed to ensure the highest purity in the plating solutions. The cadmium content of the solutions was determined whenever necessary by the electrolytic method with the aid of the Fisher electroanalyzer.

Electrodes

The anodes were rolled cadmium specimens of very high purity and required no preparation before plating, save washing in water, rinsing, wiping, and drying.

Cathodes of brass, copper, and steel were used in the preliminary investigations. It was found that equally good deposits are obtained on any of the cathodes with suitable preliminary treatments. Brass cathodes were thereafter used, as they could be polished comparatively easily and stored for a long time without becoming tarnished.

The brass cathodes were prepared for the plating experiments as follows: (*a*) polishing up to 00 grade emery papers; (*b*) an "alkaline dip" for 30 sec in a hot solution (6) containing 15 g/l of sodium hydroxide and 60 g/l of sodium carbonate; (*c*) a wash with distilled water; (*d*) a "brightening dip" for 10 sec in an acid solution containing 435 g/l of sulfuric acid, 72 g/l of nitric acid, and 2 g/l of hydrochloric acid; and (*e*) a final wash with distilled water.

Hydrogen Ion Concentration

A *p*H meter could not be used in these studies as the fluoborate solutions attack the delicate glass electrode used in the meter. The *p*H of the plating solutions had to be measured roughly with the aid of suitable indicators and British Drug House narrow range test papers, and a Lovibond comparator. The Universal Indicator was first used to get a rough idea of the *p*H within the range 3.0 to 11.0. The *p*H of the solution was then adjusted to any value required within the range 3.0 to 6.6 with an accuracy of ±0.2 with the aid of bromophenol blue (*p*H range 3.0 to 4.6) and methyl red (*p*H range 4.4 to 6.6) and using fluoboric acid or ammonia.

Temperature and Agitation

The temperature of the plating solutions was controlled to ±1°C with the aid of an immersion thermostat. Agitation was secured by means of a variable speed electric motor rotating a glass stirrer immersed in the plating solution, at speeds up to 200 rpm. The effects of agitation were studied in detail at speeds of 100 and 200 rpm—the two types of agitation being designated "mild" and "vigorous," respectively.

Current Efficiency

The anodic and cathodic current efficiencies were determined by carefully weighing the anodes and cathodes before and after the passage of definite known currents for exactly 30 minutes. It was possible to calculate the current efficiencies fairly accurately from the ammeter reading as the current was fairly steady throughout the period of deposition. To ensure a greater degree of accuracy, however, a copper coulometer was also utilized in all the experiments.

Limiting Current Density

The limiting cathodic current density, i.e., the cathodic current density at which the deposition of the metal practically ceases, was measured by following the changes in cathodic potential with increasing current density, plotting them on a graph, and noting down the current density where the curve undergoes a sudden change. This stage was always marked by copious evolution of hydrogen at the cathode and a considerable blackening of the deposit. The cathode potential was measured at various current densities with a calomel half cell and a Tinsley General utility potentiometer.

Resistivity and Throwing Power

As the current density–cathodic potential relation was linear and as the current efficiency was very high in the cadmium fluoborate solutions, the following equation due to Gardam (7) was employed to calculate the throwing power:

$$T\,\% = \frac{1}{1 + \dfrac{2l_2}{N_1}} \times 100$$

where T is throwing power expressed as a fraction; l_2 is the interelectrode distance in cm and N_1 the throwing number $= m/\rho$, where m = the slope of the current density–cathode potential curve expressed in volts per amp/cm^2 and ρ = the resistivity of the plating solution in ohms/cm^3.

The cathode potential–current density curves were not strictly reproducible in these investigations, but they were made as representative as possible by taking into account a number of sets of readings (at least three) for a particular solution, using different electrodes of the same type and shape but keeping the interelectrode distance constant. The Kohlrausch method was employed to measure resistivity of the plating solutions.

It should be mentioned in passing that even very low values of throwing power (e.g., 2.5%) obtained by the Gardam equation indicate reasonably good throwing power in practice.

TABLE I. *Influence of electrolyte concentration on the plating characteristics of cadmium fluoborate solutions*

(Temp: 27°C; pH: 3.2–3.4; other conditions as in the paper)

Concentration		Current effy. % at 3.2 amp/dm² (30 amp/ft²)		Limiting current density (cathodic)		Resistivity ohm/cm²	Throwing power %
Normality	g/l	Anodic	Cathodic	amp/dm²	amp/ft²		
4*N*	572	104.9	97.7	14.7	136	5.2	4.3
3*N*	429	104.1	98.1	12.2	113	5.7	4.6
2*N*	286	105.0	98.9	10.0	93	7.1	4.8
N	143	103.9	98.3	6.5	60	12.2	4.4

TABLE II. *Influence of pH on the plating characteristics of cadmium fluoborate solutions*

(Temp: 27°C; concentration of the electrolyte: 1*N* (i.e., 143 g/l of cadmium fluoborate)

pH range	Current efficiency (% at 3.24 amp/dm²) 30 amp/ft²		Limiting cathodic current density		Resistivity ohm/dm²	Throwing power %
	Anodic	Cathodic	amp/dm²	amp/ft²		
3.4–3.6	104.2	99.1	6.5	60	12.2	3.8
4.0–4.2	103.6	99.7	6.8	63	12.2	3.6
4.6–4.8	103.8	100.1	7.2	66	12.2	3.4
5.2–5.4	104.1	99.9	7.6	70	12.2	2.8

TABLE III. *Influence of temperature on the plating characteristics of cadmium fluoborate bath*

(pH: 3.2–3.4; concentration of solution: 1*N*, i.e., 143 g/l; other conditions as before)

Temp °C	Current efficiency (% at 3.24 amp/dm²) 30 amp/ft²		Limiting cathodic current density		Resistivity ohm/dm²	Throwing power %
	Anodic	Cathodic	amp/dm²	amp/ft²		
30	104.2	99.2	6.7	62	12.2	3.0
50	104.4	98.9	7.2	67	9.2	2.8
70	104.7	96.1	8.2	76	7.3	2.0

TABLE IV. *Influence of agitation on the plating characteristics of cadmium fluoborate bath*

(Temp: 30°C; pH: 3.2–3.4; concentration of electrolyte: 1*N*, i.e., 143 g/l; other conditions as before)

Condition	Current efficiency (% at 3.24 amp/dm²) 30 amp/ft²		Limiting cathodic current density		Resistivity ohm/cm²	Throwing power %
	Anodic	Cathodic	amp/dm²	amp/ft²		
Still	104.2	99.2	6.7	62	12.2	3.0
Mildly agitated	106.4	98.0	7.7	72	12.2	1.6
Vigorously agitated	106.7	98.0	12.7	118	12.2	1.1

Experimental Results

The more important results obtained in these investigations are given in the Tables I to VI.

Summary of Results

(*a*) *The quality of the deposit.*—Highly satisfactory white cadmium deposits can be obtained on steel, brass, or copper from cadmium fluoborate solutions under a wide range of plating conditions. A *p*H of more than 4.0 makes the deposit dull and grayish, while an increase in temperature or agitation makes it coarser. The addition of 1.0 g/l of sodium beta naphthalene sulfonate or 1.0 ml/l of methyl ethyl ketone improves the brightness and texture of the deposit considerably.

(*b*) *Current efficiency.*—Under practically all conditions, the cathodic current efficiency of the cadmium fluoborate solutions is 95–100 per cent and the anodic current efficiency is 100–105 per cent.

TABLE V. *Influence of some inorganic salts on the performance of a cadmium fluoborate bath*

No marked influence on current efficiency

(Temp: 30°C; *p*H: 3.2–3.4; concentration of electrolyte: 1*N*; other conditions as before)

Salt added	Amount g/l	Limiting cathodic current density		Resistivity ohm/cm²	Throwing power %
		amp/dm²	amp/ft²		
None	—	6.7	62	12.2	3.2
NH_4BF_4	20	5.0	46	10.3	3.5
NH_4BF_4	40	4.9	45	9.8	3.6
$NaBF_4$	20	5.4	50	11.0	3.4
$NaBF_4$	40	5.2	48	10.5	3.9
CdF_2	20	7.1	66	11.3	3.4
CdF_2	40	7.7	71	10.8	3.5
NaF	20	5.2	48	11.7	3.4
NH_4F	20	4.5	42	11.6	3.2

These values are altered but little by the changes in concentration, *p*H, temperature, etc.

(*c*) *Throwing power.*—The calculated values for throwing power are not satisfactory in cadmium fluoborate solutions, but the throwing power is reasonably satisfactory in practice. It reaches a maximum value, according to calculations at a concentration of 1.5*N* (i.e., 210 g/l of cadmium fluoborate). It decreases in value with increase in *p*H, temperature, and agitation. Additions of up to 40 g/l of sodium or ammonium fluoborate generally improve the throwing power.

(*d*) *Limiting cathodic current density.*—This is fairly high in cadmium fluoborate solutions. It increases phenomenally with increase in concentration, temperature, and agitation, and very slightly with increase in *p*H. At a concentration of 1.5*N* and at a temperature of about 30°C, the value is about 8.2 amp/dm² (75 amp/ft²).

TABLE VI. *Influence of addition agents on the cadmium fluoborate bath; physical characteristics of deposits*

(Temp: 27°C; pH: 3.4–3.6; concentration of electrolyte: 1*N*, i.e., 143 g/l; current density: 3.2 amp/dm² (30 amp/ft²); other conditions as before)

(A: Marked improvement; B: slight improvement; C: no improvement; D: slight deterioration; E: marked deterioration)

Addition agent	Amount added	Effect on			
		Brightness	Texture	Adherence	Distribution
Gelatin	0.2 g/l	B	D	D	D
	0.5 g/l	B	D	D	C
Dextrine	0.5–2.0 g/l	C	B	C	C
Ammonium alum	0.5 g/l	C	C	C	D
	2.0 g/l	B	C	C	D
Citric acid	0.2 g/l	C	C	D	C
	0.5 g/l	C	C	D	E
Thiourea	0.5 g/l	B	B	C	C
	2.0 g/l	B	B	C	D
Beta naphthol	0.5 g/l	B	B	C	C
	1.0 g/l	D	B	C	C
Sodium beta naphthalene sulfonate	1.0 g/l	A	B	C	B
	2.0 g/l	A	B	C	D
Glycerine	0.5 ml/l	B	B	C	C
	1.0 ml/l	B	C	D	C

(*e*) *Control and maintenance.*—Cadmium fluoborate solutions can be maintained and controlled very easily as there are no complications like anode sludge formation, anode passivity, etc., during electrodeposition. Composition changes occur only very slowly in these solutions as the anodic efficiency of the process is a little more than the cathodic efficiency and this makes up for dragout losses. These solutions can be used conveniently for barrel plating at higher current densities.

Optimum Plating Conditions

From the above results, it is possible to arrive at the following composition and plating conditions for obtaining excellent deposits.

Bath composition (pH: 3.2 to 3.6)	g/l	Operating conditions
Cadmium fluoborate (Cadmium content)	210 84	Temperature: 20°–30°C Cathodic current density: 2.2–6.5 amp/dm² (20–60 amp/ft²)
Sodium fluoborate	25	
Boric acid	25	
Sodium beta naphthalene sulfonate	1.0	Anode area = cathode area Anodic current effy. = 102–104% Cathodic current effy. = 98 – 100%

Anode: rolled cadmium; cathode: steel, brass or copper.

TABLE VII. *Comparison between the cyanide and the fluoborate baths for cadmium plating*

Particulars	Fluoborate bath		Cyanide bath	
Composition g/l	$Cd(BF_4)_2$	210	CdO	40
	$NaBF_4$	25	NaCN	130
	H_2BO_3	25		
	HBF_4	Slight excess		
Metal content g/l	84		35	
Metal content geq/l	1.5		0.6	
pH	3.2–3.6		Not specified	
Resistivity (ohms/cm³)	About 9.0		About 6.0	
Plating range (amp/dm²)	2.2–6.5		2.2–4.3	
Still plating (amp/ft²)	20–60		20–40	
Max. cathodic current density				
amp/dm²	About 8.1		About 5.4	
amp/ft²	About 75		About 50	
Max. anodic current density				
amp/dm²	More than 8.1		About 2.2	
amp/ft²	More than 75		About 20	
Cathodic current efficiency	98–100%		85–95%	
Anodic current efficiency	100–104%		95–100%	
Throwing power	5–6% (calculated)		20–30% (measured)	
Stability of the bath	Good		Poor	
Nature of the bath	Nonpoisonous		Poisonous	
Deposit				
brightness	Good		Good	
texture	Fine		Very fine	
adherence	Very good		Good	
distribution	Satisfactory		Very good	
Control and maintenance	Easy		Difficult	

Comparison with the Cyanide Bath

A study of the salient features of the newly developed cadmium fluoborate bath and the standard cyanide given in Table VII shows that the former is superior to the latter in the following respects: (*a*) plating range; (*b*) cathodic current efficiency; (*c*) rate of deposition; (*d*) general finish of the deposit; (*e*) stability; (*f*) nonpoisonous nature; and (*g*) ease of control and maintenance.

The fluoborate bath is inferior to the cyanide bath in the throwing power and resistivity. The difference in throwing power is not, however, so marked as the values denote because the value for the fluoborate bath is calculated unlike in the other case.

Considering all aspects the fluoborate bath appears to be more efficient than the cyanide bath for deposition of cadmium.

Acknowledgments

The authors wish to thank the Head of the Department of Metallurgy and Dr. E. G. Ramachandran, Assistant Professor of Metallurgy, for their interest and encouragement in the course of the investigations.

Any discussion of this paper will appear in a Discussion Section, to be published in the December 1953 issue of the Journal.

REFERENCES

1. G. Soderberg and L. R. Westbrook, *Trans. Electrochem. Soc.*, **80**, 525 (1941).
2. W. Blum and G. B. Hogaboom, "Principles of Electroplating and Electroforming," p. 278, McGraw-Hill Book Co., New York, (1924).
3. H. Narcus, *Metal Finishing*, **43**, 188, 199, 242 (1945).
4. F. C. Mathers and H. M. Marble, *Trans. Electrochem. Soc.*, **25**, 319 (1914).
5. W. Blum, F. J. Liscomb, Z. Jenicks, and W. E. Bailey, *Trans. Electrochem. Soc.*, **36**, 243 (1919).
6. A. K. Graham, *Trans. Electrochem. Soc.*, **52**, 289 (1927).
7. G. E. Gardam, *Trans. Faraday Soc.*, **34**, 698 (1938).

Electrogalvanizing from Fluoborate Solutions[1]

T. R. Anantharaman[2] and J. Balachandra

Department of Metallurgy, Indian Institute of Science, Bangalore, India

ABSTRACT

The optimum conditions for electroplating zinc from its fluoborate solution have been deduced by a systematic study of the effects of all types of variables on its plating characteristics. The best deposits of zinc are obtained from a bath containing 180 g/l of zinc fluoborate, 30 g/l of ammonium fluoborate, 25 g/l of boric acid, and 1.0 g/l of beta naphthol at a *p*H of 5.0 to 5.4 and temperatures of 20°–30°C, and at current densities of 4.3 to 9.7 amp/dm² (40 to 90 amp/ft²). The deposits which are obtained on steel, brass, or copper are uniform, fine grained, adherent, and of pleasing appearance. The current efficiency of the process approximates 98 to 100 per cent cathodic and 102 to 105 per cent anodic. The bath is nonpoisonous, stable, and easily controlled. The new bath is comparable to the zinc cyanide bath, and is vastly superior to the zinc sulfate bath.

Introduction

The only solutions used for commercial zinc plating are the acid sulfate solution and the alkaline cyanide solution. Satisfactory deposits can be obtained from either of these solutions, but the latter is preferred by platers for its excellent throwing power and wide plating range. From the commercial standpoint both solutions are highly efficient and it is difficult to imagine a better substitute for them. Previous work on zinc fluoborates has shown, however, that a fluoborate solution may have advantages of both solutions, i.e., it will be stable and nonpoisonous like the sulfate bath and will also have the good throwing power and plating range of the cyanide bath. The investigations were made to determine optimum conditions for electroplating zinc from its fluoborate solution and compare the best fluoborate bath with baths in vogue for electrogalvanizing.

Experimental Procedure

The procedure adopted by the authors in their investigations of the cadmium fluoborate bath[3] was also followed in the present studies.

Experimental Results

Experimental results are given in Tables I to VI on page 238.

Summary of Results

(*a*) *Quality of deposit.*—The quality of zinc deposits on steel, brass, or copper is of a very high order under a wide range of plating conditions. The addition of 0.5 to 1.0 g/l of beta naphthol leads to a very fine and bright deposit while higher temperatures and agitation make the deposits slightly coarser and rougher.

(*b*) *Current efficiency.*—The current efficiency of the zinc fluoborate solution is very satisfactory over a wide range of plating conditions. The cathode efficiency is very near 100 per cent and the anodic efficiency usually varies from 100 to 110 per cent. The latter is influenced appreciably by the *p*H of the solution, an increase in *p*H bringing the value to nearer 100 per cent.

(*c*) *Throwing power.*—The throwing power is higher than in the case of the corresponding cadmium fluoborate bath, but still not very satisfactory when the calculated values are considered. It reaches a maximum as in the case of cadmium bath at a concentration of 1.5*N* (i.e., 180 g/l of zinc fluoborate). It decreases slightly with increase in *p*H, temperature, and agitation. Additions up to 40 g/l of ammonium and sodium fluoborate, especially the former, improve the throwing power.

(*d*) *The limiting cathodic current density.*—The limiting current density is generally quite high in zinc fluoborate solutions. It increases phenomenally with increase in concentration, temperature, and agitation. An increase in *p*H also increases, although slightly, the limiting current density. At a concentration of 1.5*N* (i.e., 180 g/l of zinc fluoborate) and at a temperature of 30°C, the limiting current density for a still solution is about 10.3 amp/dm² (95 amp/ft²).

(*e*) *Control and maintenance.*—As in the case of the cadmium fluoborate bath the control and maintenance is very easy. The zinc fluoborate solu-

[1] Manuscript received April 10, 1952. This paper was prepared for delivery before the Montreal Meeting, October 26 to 30, 1952. Part of the dissertation submitted by T. R. Anantharaman and accepted for the degree of Master of Science by the University of Madras, Madras, India.

[2] Present address: Trinity College, Oxford, England.

[3] Published elsewhere in this issue.

TABLE I. *Influence of electrolyte concentration on the plating characteristics of zinc fluoborate solutions*

(Temp: 26°C; *p*H: 3.5; other conditions as mentioned in the paper on cadmium fluoborate)

Concentration		Current effy. % at 3.2 amp/dm² (30 amp/ft²)		Limiting cathodic current density		Resistivity ohms/cm³	Throwing power %
Normality	g/l	Anodic	Cathodic	amp/dm²	amp/ft²		
4*N*	480	111.2	97.8	18.8	174	5.859	4.85
3*N*	360	112.5	99.3	15.0	139	6.246	4.90
2*N*	240	110.7	99.5	12.5	116	7.235	5.51
N	120	109.7	99.7	8.50	79	11.060	5.48

TABLE II. *Influence of* p*H on the plating characteristics of zinc fluoborate solutions*

(Temp: 25°C; concentration of electrolyte: 1*N* [120 g/l of zinc fluoborate])

*p*H range	Current efficiency % at 3.2 amp/dm² (30 amp/ft²)		Limiting cathodic current density		Resistivity ohms/cm³	Throwing power %
	Anodic	Cathodic	amp/dm²	amp/ft²		
3.5	109.7	99.3	8.50	79	11.06	4.58
4.5	106.7	99.5	9.80	91	11.06	4.33
5.5	102.3	99.7	12.30	114	11.06	4.01

TABLE III. *Influence of temperature on the plating characteristics of the zinc fluoborate solutions*

(*p*H: 5.0; concentration of electrolyte: 1*N* [120 g/l of zinc fluoborate])

Temp, °C	Current effy. % at 3.2 amp/dm² (30 amp/ft²)		Limiting cathodic C.D.		Resistivity ohms/cm³	Throwing power %
	Anodic	Cathodic	amp/dm²	amp/ft²		
30	103.7	99.8	10.60	98	11.07	5.03
50	103.4	99.2	12.10	112	8.33	5.45
70	104.1	99.0	14.70	136	6.52	5.58

TABLE IV. *Influence of agitation on the plating characteristics of zinc fluoborate solutions*

(Temp: 30°C; *p*H: 5.0; concentration of electrolyte: 1*N*, i.e., 120 g/l of zinc fluoborate)

Condition	Current effy. % at 3.2 amp/dm² (30 amp/ft²)		Limiting cathodic C.D.		Resistivity ohms/cm³	Throwing power %
	Anodic	Cathodic	amp/dm²	amp/ft²		
Still	103.7	99.8	8.5	79	11.07	3.98
Mildly agitated	105.4	99.2	10.5	97	11.07	2.20
Vigorously agitated	105.8	99.0	14.3	123	11.07	1.97

TABLE V. *Influence of some inorganic salts on the performance of a zinc fluoborate bath*

(No marked influence on current efficiency)

(Temp: 30°C; *p*H: 5.0; concentration of electrolyte: 1*N*, i.e., 120 g/l of zinc fluoborate)

Salt added	Amount g/l	Limiting C.D.		Resistivity ohms/cm³	Throwing power %
		amp/dm²	amp/ft²		
None	—	8.4	78	11.07	5.00
NH_4BF_4	20	7.3	68	9.19	7.49
NH_4BF_4	40	6.4	59	8.86	8.47
$NaBF_4$	20	7.2	67	9.88	5.86
$NaBF_4$	40	5.8	54	9.49	6.99
ZnF_2	20	9.3	86	10.21	5.68

TABLE VI. *Influence of addition agents on the physical characteristics of deposits from zinc fluoborate solutions*

(Temp: 27°C; *p*H: 5.0; C.D. (50 amp/ft²) 5.4 amp/dm²; concentration of electrolyte: 1*N*, i.e., 120 g/l of zinc fluoborate)

(A—Marked improvement; B—Slight improvement; C—No effect; D—Slight deterioration; E—Marked deterioration)

Addition agent	Amount added	Effect on			
		Brightness	Texture	Adherence	Distribution
Gelatin	0.2 g/l	B	B	D	C
	0.5 g/l	B	B	D	C
	1.0 g/l	E	E	D	C
Dextrine	0.5 g/l	C	B	C	C
	1.0 g/l	D	B	C	C
Ammonium alum	0.5 g/l	B	C	C	C
	1.0 g/l	B	C	C	D
Citric acid	0.2 g/l	C	C	D	D
	0.5 g/l	D	C	D	E
Thiourea	0.5 g/l	B	B	C	C
	2.0 g/l	B	B	C	C
Beta naphthol	0.5 g/l	A	B	C	C
	1.0 g/l	A	B	C	C
Sodium beta naphthalene sulfonate	0.5 g/l	B	B	C	C
	1.0 g/l	B	B	C	C
Glycerine	0.5 ml/l	B	B	C	C
	1.0 ml/l	B	B	C	C
Methyl ethyl ketone	0.5 ml/l	B	B	C	C
	1.0 ml/l	B	C	D	C
Carbon bisulfide	0.01 ml/l	A	B	C	C
	0.02 ml/l	B	B	D	D
	0.03 ml/l	B	B	D	E

tions are ideally suited for barrel plating, at higher current densities.

Optimum conditions and composition

Bath composition:	zinc fluoborate	180 g/l
	(zinc content)	49 g/l
	ammonium fluoborate	30 g/l
	boric acid	25 g/l
	beta naphthol	1.0 g/l
Operating conditions:	*p*H: 5.0 to 5.4	
	Temperature, 20°–30°C	
	Cathodic current density, 4.3–9.7 amp/dm² (40–90 amp/ft²)	
	Anodic current effy., 102–105%	
	Cathodic current effy., 98–100%	
	Anode area is the same as cathode area	
	Anode: pure zinc	
	Cathode: steel, brass, or copper	

ACKNOWLEDGMENT

The authors wish to thank the head of the department of metallurgy and Dr. E. G. Ramachandran, Assistant Professor, for their interest and encouragement in the course of the investigations.

Any discussion of this paper will appear in a Discussion Section to be published in the December 1953 issue of the JOURNAL.

GENERAL REFERENCES

1. E. H. LYONS, *Trans. Electrochem. Soc.*, **80,** 585 (1941).
2. R. O. HULL AND C. J. WERNLUND, *Trans. Electrochem. Soc.*, **80,** 601 (1941).
3. W. G. HORSCH, AND T. FUWA, *Trans. Electrochem. Soc.*, **41,** 363 (1922).
4. A. E. CARLSON AND M. J. KRANE, *Monthly Rev. Am. Electroplaters' Soc.*, **32,** 1022 (1945).
5. H. NARCUS, *Metal Finishing*, **43,** 138, 199, 242 (1945).

Factors Controlling the Combustion of Zirconium Powders[1]

HOLGER C. ANDERSEN AND LAWRENCE H. BELZ

Research and Development Laboratories, Foote Mineral Company, Berwyn, Pennsylvania

ABSTRACT

The activity of zirconium metal powders was studied by measurements of ignition temperature, burning time, and ignition energy on subsieve powders prepared by calcium reduction of ZrO_2 and on coarse powders made by grinding fused zirconium. Particle diameter of 10 microns represents approximately the dividing line between hazardous and nonhazardous powder, using 0.01–0.04 joule spark ignition energy as a criterion. Thermal ignition appears to occur by spontaneous combustion, and a theory was developed which accounts qualitatively for the dependence of ignition temperature on a number of variables. The burning time of Zr powders is related to, but not uniquely determined by, the surface area. Ignition sensitivity of Zr powders was not successfully decreased by alloying with Ti, Ni, Cu, Fe, Co, or H_2. Hazards are discussed briefly, and details of evaluation methods reported.

INTRODUCTION

Zirconium metal has increased greatly in technological importance during the past decade, and a large body of literature has consequently evolved which describes its preparation, properties, and applications. The largest proportion of scientific effort has been devoted to the metal in its massive form. The preparation of pure crystal bar by the deBoer method (1), as first represented commercially by installations at the Foote Mineral Company, and of high purity sponge by the Kroll method, as practiced by the U. S. Bureau of Mines (2), are the major developments in this field. The principal properties of pure massive zirconium which have accelerated this development are its resistance to corrosion in various media (3), its ductility (4), and its low neutron-capturing tendency (5).

In powdered form, zirconium retains to a remarkable degree its resistance to corrosion, and is, in contrast with other metal powders of commerce, stable for long periods of time under all normal conditions of storage. Coupled with this stability is a high degree of chemical reactivity at slightly elevated temperature. Absorption of gases such as O_2, N_2, and H_2 accounts for vacuum tube gettering applications (6, 7). Combustion in air or oxygen is rapid, and is accompanied by evolution of considerable heat and light. Such behavior makes zirconium powder of great use in photoflash bulbs (8) and of interest as a fuel in ammunition elements (9–11). It is the purpose of this paper to report the results of recent investigations of the combustion properties of zirconium powder.

PREPARATION OF ZIRCONIUM POWDERS

Among the objectives of this research were two essential extremes: the preparation of zirconium powders of the highest possible burning speed, and the preparation of zirconium powder of the lowest possible sensitivity to ignition by static electricity or heat. These objectives dictated preparation, on the one hand, of powder with minimum particle size, and, on the other, of powder of maximum particle size consistent with other desired qualities.

Powder of high burning speed was made by the calcium reduction of ZrO_2:

$$ZrO_2 + 2Ca = Zr + 2CaO. \quad (I)$$

Several other reactions were considered:

$$ZrO_2 + 2Mg = Zr + 2MgO \quad (II)$$

$$ZrO_2 + 4Na = Zr + 2Na_2O \quad (III)$$

$$ZrO_2 + 2Na = Zr + Na_2O_2$$

$$ZrO_2 + 4H = Zr + 2H_2O \quad (IV)$$

$$ZrO_2 + 2CaH_2 = ZrH_2 + 2CaO + H_2 \quad (V)$$

$$ZrH_2 + \text{heat} = Zr + H_2$$

$$ZrX_4 + 2M = Zr + 2MX_2 \text{ (where X is Cl or F, and M is Ca, Mg, or 2Na).} \quad (VI)$$

Magnesium reduction of the oxide was incomplete, yielding powder of great sensitivity to ignition, but with low free metal content. Reaction (III) did not proceed, as predicted by thermodynamics.[2] Reac-

[1] Manuscript received April 28, 1952. This paper was prepared for delivery before the Philadelphia Meeting, May 4 to 8, 1952. Part of the research in this paper was made possible through Philadelphia Ordnance District Contracts DA-36-034-ORD-88—388 and 389, sponsored by the Pitman-Dunn Laboratories of the Frankford Arsenal.

[2] The literature (12, 13) indicates, however, that sodium reduction occurs, possibly through intermediate zirconium halide formation, when an alkaline earth halide is included with the charge.

tion (IV) was studied by generating atomic hydrogen on a hot filament and passing it over ZrO_2, but no reduction was observed. Reaction (V), which may be written in several different ways, yields a metal powder containing more or less hydrogen depending upon conditions in the reduction cycle. It is shown later that hydrogen decreases the burning speed of the powder without appreciably diminishing its sensitivity to ignition. The reaction therefore did not appear useful for our purposes. Reductions of the type shown in reaction (VI) are sufficiently exothermic to yield sponges or fused metal, rather than powders.

Powder of maximum particle size and low ignition sensitivity was prepared by grinding fused zirconium metal resulting from the reaction

$$ZrCl_4 + 2Ca \rightarrow Zr + 2CaCl_2. \qquad \text{(VII)}$$

Grinding of fused metal, rather than sponge metal, was favored because the sponges might yield agglomerates composed of small particles. Such agglomerate powders would be expected to have the ignition characteristics of the smaller units, rather than of the larger particles of measured size. Calculation of peak temperatures reached during the reactions of equation (VI), in a manner analogous to the calculation of flame temperatures, showed that the melting point of zirconium (1830°C) might theoretically be exceeded in the sodium reduction of $ZrCl_4$, and in the calcium reductions of $ZrCl_4$ and ZrF_4. Experience in the sodium reduction of $ZrCl_4$ indicated that sponges were obtained, whereas calcium reduction yielded well-fused metal; ZrF_4 was not used because of its cost and the solubility of Zr in acidic fluoride solutions which would necessarily be present during acid-washing of the raw product.

Preparation of Subsieve Zirconium Powder by Reduction of ZrO_2 with Calcium

The calcium reduction process was studied by charging mixtures of C.P. ZrO_2[3] (-200 mesh) and granulated calcium, in measured excess, to a steel reduction bomb (approximately 3½ in. diameter × 7 in. high), igniting the mixture by placing the bomb in an electric furnace at 900°C, and, after cooling, removing the contents and washing the product with water and HCl. Typical yields of metal powder were in the range of 83–92 per cent. Determination of dissolved Zr showed that a loss of 5–6 per cent was incurred in the hot acid treatment used to minimize acid-soluble impurities. Small samples of powder were taken for analysis and other tests by filtering through a Büchner funnel, washing with acetone, and allowing the filter cake to air-dry at room temperature. Chemical properties of such powder have been reported previously (4).

The procedure differed from that of Rentschler and Lilliendahl (14) in that an evacuated bomb was used and cooled as rapidly as possible after reaction, instead of maintaining the reacted mass at high temperature, and under argon atmosphere, for a protracted period. The deleterious effect of extended heating on powder activity is shown in a separate series of experiments summarized in Table I.

The combustion properties of the metal powder were not a function of the purity or fineness of the calcium employed, but it was found that reaction was difficult to initiate when calcium coarser than 10 mesh was used. The Ca:ZrO_2 molar ratio was varied over the range of 1.8 to 4, corresponding respectively to 10 per cent deficiency and 100 per cent excess. The free metal content of the powder made with a deficiency of reductant was lower than that of other powders, as anticipated, but there was no significant dependence of the combustion properties (ignition temperature and burning time) on the Ca:ZrO_2 ratio. For a given oxide type,[4] the metal powder qualities appeared to be relatively independent of the state of subdivision of the oxide (Table II).

TABLE I. *Effect of extended heating of* Ca-ZrO_2 *mixtures on zirconium powder activity*

(In these experiments, Ca-ZrO_2 mixtures were ignited in graphite crucibles under argon atmosphere, and maintained at 1200°C for indicated times after completion of reaction.)

Time, min	Properties of zirconium powder, after acid-washing and drying			
	Particle size, microns, air permeability method	Burning time, sec/10 in.	Ignition temp, °C	Ignition energy, joules
0	2.05	1.6	196	0.000045
5	2.61	6.7	201	0.000045
10	2.75	3.5	203	0.000045*
20	3.22	14.2	200	0.000045*

* Static ignition tests were performed by the Pitman-Dunn Laboratory of the Frankford Arsenal. Asterisk indicates that ignition was not followed by sustained combustion.

Preparation of Coarse Zirconium Powder

Fused zirconium was obtained by bomb reduction of $ZrCl_4$ with Ca under suitable conditions. The Zr

[3] All Zr and its compounds mentioned in this work contained Hf(Hf/Zr = approximately 0.01).

[4] Oxides which were predominantly monoclinic yielded "fast" metal powders, whereas the tetragonal modification produced powders of long burning time. Unfortunately, there are no data on the heat of transition to indicate whether the difference is attributable to differences in the exothermic heat of reaction.

content of such fused metal varied from 96 to 98.6 per cent, the principal impurities being oxygen, calcium, minor metallic impurities present in the $ZrCl_4$, and included salt. The salt and calcium contents were sharply reduced by acid-washing the ground metal. Average oxygen content was of the order of 1–2 per cent, rendering the material sufficiently brittle for grinding.

The fused metal was crushed in a small jaw crusher equipped with a special housing permitting maintenance of an argon atmosphere. By repeated recycling of crushed metal, and "choke-feeding," it was possible to obtain metal finer than 100 mesh. The possibility of crushing to a coarser size (4 to 60 mesh), and further reducing such material to size in a high-speed hammer mill (Mikropulverizer) was also explored briefly. With extreme care in the matter of inert gas atmosphere, and using only a few hundred grams, it was possible to obtain appreciable quantities of powder finer than 100 mesh, with a minimum occurrence of fires. Crushed metal finer than 100 mesh was washed with HCl and water, and wet-sieved to produce the 100/325 cut desired as a part of this research. Subsieve portions of the ground metal were studied for various properties, as described later, in an attempt at over-all correlation of the properties of zirconium with particle size. Microscopic examination showed the crushed metal to consist of discrete particles of irregular, angular shape.

TABLE II. *Dependence of zirconium powder properties on particle size of oxide*

(ZrO_2—Commercial C.P. product, predominantly monoclinic. Ca—10 mesh, 10% stoichiometric excess.)

Experiment no.	Oxide treatment	Average ZrO_2 particle size, hydrometer method, microns	Free Zr (a) %	Avg part. size, hydrometer method, microns	Ignition temp, °C	Burning time, sec/10 in.	Photoflash bulb peak time, m. sec (b)
1	Sieved through 200 mesh	7.7	91.3	6.6	181	1.3	6.1
2	Sieved through 200 mesh	7.7	90.8	6.8	186	1.2	6.3
3	None	6.9	88.0	5.8	192	1.6	6.0
4	Air-milled	1.1	91.0	5.9	181	1.3	5.4
5	Ball-milled	<1.	91.3	6.1	181	12.2	8.8

(a) Determined by weight gain on ignition.

(b) Peak time is the time taken for the light emitted from the photoflash bulb to reach maximum intensity. Typical light emission curves are shown in reference (19). Values cited were provided through the courtesy of Dr. W. C. Fink, Sylvania Electric Products Company.

Combustion Properties of Zirconium Powders

Combustion of zirconium powders was studied by measuring the following properties.

Burning time.—Burning time was measured on a 10-in. powder train prepared in a steel mold (12 in. x 1/8 in. x 1/16 in.). No attempt was made to pack the dry powder. The train was transferred to a transite board, ignited at one end, and the time interval measured either visually with a stopwatch, or electronically by two Cetron CE2P phototubes spaced 10 in. apart. Reproducibility was approximately ±20 per cent or ±1/2 sec, whichever was the greater.

Ignition energy.—Ignition energies were measured by subjecting a small sample of metal powder to an electric spark from a charged condenser. The energy of the spark ($W = \frac{1}{2} Ce^2$, where C is the capacitance and e the instantaneous voltage) was increased stepwise until actual burning occurred. The limits of the equipment used (Pitman-Dunn Laboratory Electrostatic Discharge Tester No. 307-141) were 0.000045 to 21.9 joules. These tests were performed by the Pitman-Dunn Laboratories of the Frankford Arsenal.

Ignition temperature.—Ignition temperatures were measured by heating one-gram samples in a massive copper block (3 in. diameter x 3 in. high) with a blind 3/4-in. hole for the sample and a blind 5/16-in. hole for a thermometer. The block was set on a hot plate producing a temperature rise of 15°C per minute at the anticipated ignition temperature. Ignition was seen as a glow in the dark sample cavity, and the thermometer reading was recorded as ignition temperature. In some of the early work, ignition temperatures were determined by placing samples, in porcelain crucibles, in an oven. The rising oven temperature was read by thermometer. This method was discarded because better conditions for uniform heat transfer existed in the massive copper block. Duplicate readings generally agreed within 2°C.

Particle size.—Particle sizes were measured by three techniques: gas elutriation with a Roller particle size analyzer (15); settling in water by the hydrometer method (16); and air permeability, read

on a Fisher subsieve sizer (Fisher Scientific Company, Catalog No. 14-312). As a safety precaution, argon instead of air was used as a fractionating medium in the Roller analyzer.

Ignition Energy and Particle Size

Zirconium powder can be ignited in two ways: by elevating its temperature, or by adding to it a minute amount of electrical energy. From the industrial standpoint, the ignition energy, which is the minimum energy required to ignite the powder, is probably the more important property. Hartmann (17) states that electrostatic spark energies of the order of 10 millijoules might be built up and discantation after times computed from Stoke's Law (18). Ignition energy, burning time, and ignition temperature for these three fractions, and also for a commercial ground magnesium sample, were measured as described above, with the results shown in Table III. It is worth noting that the finest sample of this series had a higher order of spark energy than that characteristic of metal powder made by oxide reduction (Table I). The ignition energy data, plotted in Fig. 1, show that particle diameter of 10 microns represents approximately the borderline between safe and hazardous zirconium powder, on the basis of the criteria previously cited. The practical significance of this conclusion, that zirconium in the sieve range (44 microns and greater in effective particle diameter) can be handled dry without danger of ignition by static discharge, requires one important qualification: the size limit refers only to discrete particles, and not necessarily to particles which are essentially agglomerates of finer units. Ground sponges nominally coarser than 325 mesh may be static-sensitive, if they consist of agglomerates of particles smaller than 10 microns.

TABLE III. *Combustion properties of ground fused zirconium powders and commercial magnesium powder*

	Zirconium (GZ) 200/325 mesh, by sieving	Zirconium (GZ) 10 to 44 μ, by decantation	Zirconium (GZ) 2 to 10 μ, by decantation	Commercial ground magnesium
Particle size range, μ, estimated	44–74	10–44	2–10	Screen analysis:
				100/200 mesh 37%
				200/325 30%
				through 325 33%
Average particle size, μ, air permeability method	33	18.3	3.15	12.4
Free Zr, %	86.4	84.5	72.5	—
Ignition temp, °C	378	312	199	412–490
Burning time, sec/10 in.	414, 397	127, 165	21.5, 23.5	54, 46
Ignition energy, joules	12.5*	0.0200–0.0378*	0.000125–0.000225	0.045–0.046

* Ignition not sustained.

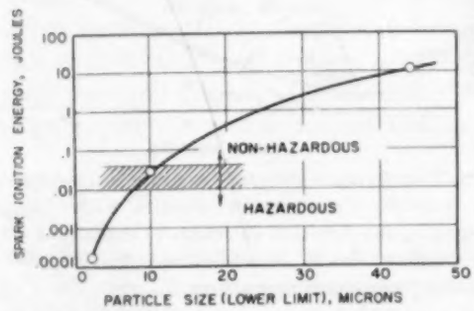

Fig. 1. Spark ignition energy as a function of particle size (ground fused Zr).

charged from a human body under some conditions. By this criterion, any metal powder which can be ignited by a spark less energetic than 0.01 joule would present serious hazards in dry handling. Corresponding approximately with this statement is the fact that commercial magnesium powder, having a spark sensitivity of 0.045 joule, can be handled with relative safety. Fine zirconium powder, on the other hand, having a spark sensitivity of 0.00004 joule, must generally be handled wet to obviate danger of inadvertent combustion.

The crushed, fused zirconium was split into three fractions by screening between the limits of 200 and 325 mesh (Tyler sieve series), and treating the subsieve portion to repeated suspension and de-

Ignition Temperature

When zirconium powder is heated, it is found that sudden ignition occurs at some reproducible external temperature, here defined as the ignition temperature. The literature indicates that zirconium has the lowest ignition temperature of the commercially available metal powders.

Certain interesting regularities were observed in the determination of ignition temperatures (Fig. 2). The increase of ignition point with water content (Fig. 2B) is ascribed to a slight oxidation of the zirconium by water near the boiling point. Physical dilution of the zirconium powder raises the ignition temperature (Fig. 2C), but the trend is not carried over into metal powders "internally diluted," that is, incompletely reduced metal powders. No correlation has been found between the free metal content

and the ignition temperature. Indeed, some of the lowest ignition temperatures were recorded for incompletely reduced powders, such as those made by the magnesium reduction of ZrO_2.

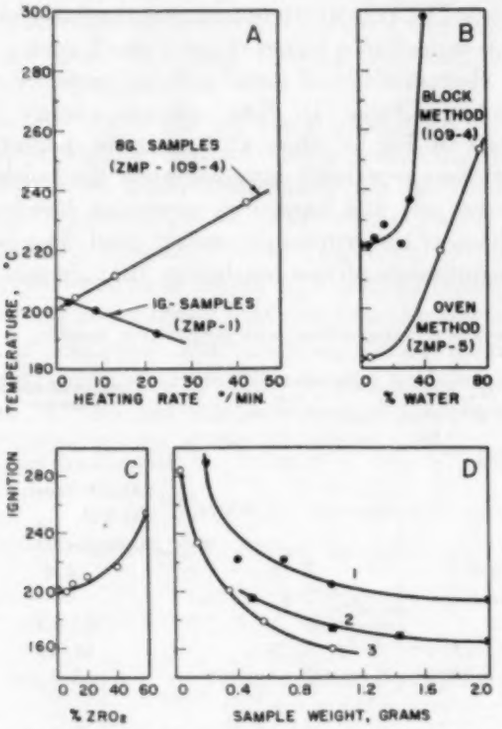

FIG. 2. Influence of several variables on ignition temperature of zirconium powder made by Ca-reduction of ZrO_2. A, heating rate. B, water content at room temperature (1-gram Zr samples). C, dilution with ZrO_2 (1-gram total weight). D, sample weight: 1—ZMP-7, copper block method; 2—ZMP-5, compacted at 14,000 psi, oven method; 3—ZMP-5 oven method.

TABLE IV. *Effect of high-temperature pumping on the ignition temperature of zirconium powder*

(Metal powder—ZMP made by calcium reduction of ZrO_2. Sample pumped at high vacuum for one hour at indicated temperature.)

Temp, °C	(No treatment)	420	900*
Ignition temp, °C	187	158	160
Burning time, sec/10 in.	8.4	7.3	8.4
Average particle size, air permeability method, μ	2.5	2.6	4.2*
Ignition energy, joules	0.000045	0.000045	0.000045

* To permit measurements on this sample, it was necessary to grind the sintered cake in a mortar and pestle.

In all cases where ignition point determinations were repeated on a given powder sample after a prolonged period, it was found that the ignition temperature had risen. The only rational explanation of this fact is that an oxide film forms which hinders subsequent oxidation. The effect can be accelerated by maintaining the powder a few degrees below the nominal ignition point for several minutes. Conversely, it was found that powders pumped at high temperatures show a decrease in ignition temperature (Table IV), because of inward migration of the surface oxide film (20).

Perhaps the most revealing variation of the ignition temperature is its dependence on the sample weight (Fig. 2D). The observed variation is consistent with a spontaneous combustion mechanism, wherein the heat of reaction within the powder mass increases the oxidation rate continuously, limited only by the rate at which the heat can be dissipated to the container. Burning from the inside of the sample to the outside was evidenced in several experiments during which internal temperature was compared with the external. The internal temperature lagged behind that of the container throughout most of the heating period. Shortly after the internal temperature exceeded the external, visible ignition occurred (Fig. 3).

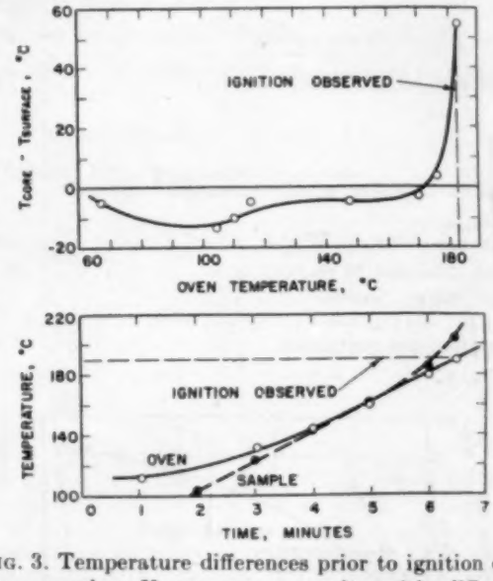

FIG. 3. Temperature differences prior to ignition of zirconium powder. Upper curve—results with differential thermocouple, one junction in center of sample, other near exposed surface; lower curve—comparison of oven and metal powder sample temperatures.

A semiquantitative explanation of these facts follows. Assume a spherical mass of zirconium powder of radius, r, in perfect thermal contact at its periphery with an infinite heat reservoir at a controlled temperature, T_1. Assume further that the mass consists of small perfect spheres, each of diameter d. At ordinary temperatures, oxidation occurs so slowly that the infinitesimal amount of heat developed is easily dissipated to the surroundings. As the temperature is raised, and the oxidation rate increases, the exothermic heat becomes appreciable and causes further temperature increase of a segment of the powder which is thermally isolated. If the rate

of heat development at the center of the mass is greater than the rate at which the heat can be transported to the container, ignition eventually occurs. Then the following condition is necessary to ignition: rate of exothermic heat development > rate of heat loss.

Gulbransen (21) has shown that zirconium reacts with oxygen in the temperature range of 200°–425°C according to a modified parabolic law:

$$W^2 = Kt + C$$

where W is the weight gain of a sample of known geometric area, t is the time, and K a reaction rate constant with Arrhenius temperature dependence. The constant C expresses a slight deviation from the simple parabolic law in the initial stages of reaction, and can be omitted as negligibly small for reactions in advanced stages or metal with appreciable oxide film thickness. The reaction rate per unit area is then

$$\frac{dW}{dt} = \frac{K^{\frac{1}{2}}}{2t^{\frac{1}{2}}} = \frac{K' e^{-E/2RT}}{t^{\frac{1}{2}}}$$

where E is the activation energy, reported to have a value of 18.2 kcal.

For a small mass of fixed weight at the center of the hypothetical spherical sample, the rate of heat development is obtained by multiplying the reaction rate per unit area by the total surface area and the heat of reaction ΔH. The total area per gram of a system of uniformly sized spheres is $6/\rho d$,[5] where ρ is the density and d the sphere diameter. The rate of heat generation by center element is thus

$$K'' \frac{\Delta H e^{-E/2RT_2}}{t^{\frac{1}{2}} d}$$

where T_2 is the temperature of the central mass, and K'' includes all previous constants. Assuming that the rate of heat transport from the center element to the reservoir is of the form $k'''(T_2 - T_1)/r$, the fundamental condition for ignition becomes

$$K'' \frac{\Delta H e^{-E/2RT_2}}{t^{\frac{1}{2}} d} > \frac{k'''(T_2 - T_1)}{r}.$$

The expression cannot be solved for T_1, the ignition temperature, in terms independent of T_2, the internal temperature. On the assumption that ignition is possible when T_2 exceeds T_1 by some small constant value, two simplifications are possible: $(T_2 - T_1)$ in the heat loss term can be taken as constant, and T_2 can be taken as roughly equal to T_1 in the exponential. The inequality then simplifies to

$$e^{-E/2RT_1} > \frac{Kt^{\frac{1}{2}} d}{r}$$

or eventually,

$$T_1 > \frac{E}{2R \ln\left(\frac{r}{Kt^{\frac{1}{2}} d}\right)}; \qquad T_1 > \frac{E}{2R \ln\left(\frac{m^{\frac{1}{3}}}{Kt^{\frac{1}{2}} d}\right)},$$

where m is the sample mass.

Various interpretations of the time factor in this expression are possible. If it is interpreted as an inverse function of the external heating rate, then the expression predicts a decrease in ignition temperature with heating rate. This is the experimental case for small samples (Fig. 2A). In the case of larger samples, the increase of ignition temperature with heating rate is attributed to increased lag of internal temperature with respect to external temperature.

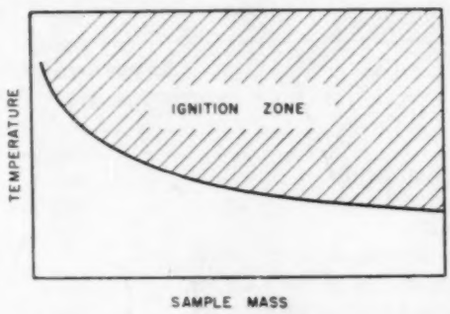

FIG. 4. Theoretical curve of ignition temperature vs. mass, for any given powder (heating rate constant).

The predicted increase of ignition temperature with time is in qualitative agreement with the observations that the ignition temperature can be greatly raised by keeping powder below the usual ignition point for some time. For a system of fixed particle size and shape distribution, and constant time, i.e., heating rate, the expression indicates a relationship between sample mass and ignition temperature as shown in Fig. 4. The form of this theoretical curve is very similar to those found experimentally (Fig. 2D). Likewise, the expression is in qualitative agreement with the data of Table III, as regards particle size.

A similar theoretical treatment for massive magnesium, developed by Eyring and Zwolinski (22), and based in part on the data of Leontis and Rhines (23), has recently been tested by Fassell, Gulbransen, Lewis, and Hamilton (24). An interesting demonstration of the dependence of ignition temperature on sample mass is cited by Hartmann (25), who found that one gram of uranium hydride ignited at 110°C, whereas 5 grams ignited after a few minutes' exposure to room temperature.

[5] A general treatment would include a roughness factor to account for the fact that the measured surface area is greater than that calculated for smooth spheres. For a given powder lot, however, the necessity for this refinement disappears.

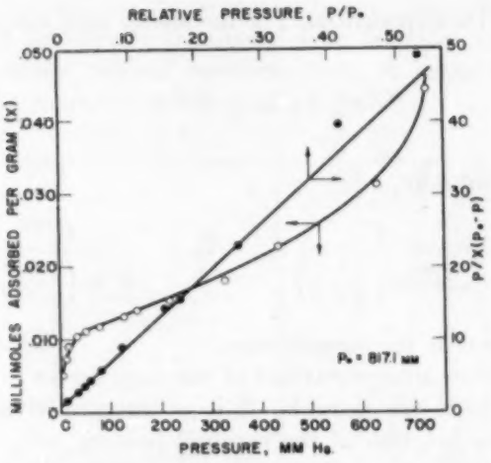

FIG. 5. Adsorption of N_2 on Zr powder (made by calcium-reduction of ZrO_2) at 77°K. Open circles—x vs. pressure; closed circles—$P/x(P_0 - P)$ vs. P/P_0.

tion, rather than chemical combination, occurred at liquid nitrogen temperature. Degassing temperatures of 200°–400°C yielded reproducible areas (Table V, experiments on ZMP 110-5).

In Table V are summarized surface area results on the three categories of material studied, in the order of decreasing area. It is apparent that the magnitude of the surface area does not uniquely determine the burning speed. It seems reasonable to ascribe the failure of correlation to variations in the oxide film thickness, just as certain variations in the ignition temperature were ascribed to such films, through the time factor in the ignition temperature equation. As noted in the following section, burning time is also affected by hydrogen content. Judging from the substantial increase in area (and accompanying increase in activity[6]) on wet ball-

TABLE V. *Surface areas of* Zr *and* ZrO_2 *powders and combustion properties of* Zr *powders*
(Area of N_2 molecule taken as 16.2 Å²)

Powder	Area, m²/g	Equivalent particle diameter, μ*	Ignition temp, °C	Burning time, sec/10 in.
Zr powders made by calcium reduction of ZrO_2 (ZMP)				
ZMP-41	2.90	0.32	214	1.75
ZMP-5	2.85	0.32	160	1.8
103 G-3, ball-milled	2.85	0.32	171	10.3
ZMP-19	1.10	0.85	135	2.6
ZMP 110-5				
degassed 1 hr at 20°C 0.85	1.08	0.86	222	2.3
degassed 1 hr at 200°C 1.08				
degassed 1 hr at 400°C 1.08				
degassed 1 hr at 600°C 0.41				
degassed 1 hr at 750°C 0.25				
103 G-3	0.83	1.1	281	25.5
ZMP 106-1	0.52	1.8	222	10.0
Ground fused zirconium (GZ)				
5 to 10μ fraction, by separation in Roller analyzer	1.07	0.87	200	22
10 to 44μ fraction, by separation in Roller analyzer	0.25	3.7	240	122
100/325 mesh, by screening (44 to 149μ)	0.13	7.2	>500	∞
Zirconium oxide	3.08–7.0	0.30–0.13	—	—

*$d = \frac{6}{\rho S} = \frac{0.93}{S}$.

Surface Areas of Zirconium Powders

Surface areas of various zirconium powder samples were measured by the Brunauer-Emmett-Teller nitrogen adsorption method (26). The ultimate objective of these measurements was to correlate the surface area with the burning time of zirconium powder. Although this objective was not achieved, certain other information of interest was developed. It was found that the adsorption was reversible, which, together with the S-shape of the isotherm (Fig. 5), was taken to prove that physical adsorp-

milling zirconium powder, it would appear that porosity contributes negligibly to the surface area.

[6] In addition to the increase in activity (decreased burning time and ignition temperature) caused by ball-milling, slight chemical change is also effected. The free metal content decreases and hydrogen pressure develops in the mill, which consequently requires periodic venting. All the changes are consistent with reduction in particle size, as is also indicated by air permeability measurements, and reaction of the freshly exposed Zr surfaces with water:

$$Zr + 2H_2O = ZrO_2 + 2H_2.$$

and that grinding results in actual particle rupture. The reduced metal surface area approaches but does not equal or exceed that of the parent oxide. This is consistent with a reduction mechanism in which the zirconium metal would have a particle size corresponding to the ZrO_2 grain size, but for a tendency to increase in size because of sintering effects at the high reaction temperature.

The surface areas of all the metal powders were substantially greater than would be inferred from the particle sizes as determined independently. The particle sizes calculated from the surface areas, on the assumption of smooth, uniform spheres, are smaller, by factors of 7 to 18, than the particle sizes as determined by sieve limits or hydrometer settling. These factors, which are due to the irregular shape of the Zr particles, are of the same order of magnitude as that calculated from the data of Guldner and Wooten (27), who compared the B-E-T particle size with microscopic measurements.

Zirconium Alloys

Attempts were made to decrease the extreme ignition sensitivity of zirconium powder by preparing binary alloys with other elements. The results of addition of Ti, Ni, Cu, Fe, Co, and H_2 (Table VI) show that very large additions of these elements are required to reduce the ignitability materially. Furthermore, in every case for which the ignition energy was increased to values near the nonhazardous limit (of the order of 0.01 joule), the ignition temperature was high and the burning rate low. Emission of heat and light during burning was, under these circumstances, much less than that desired.

The titanium-zirconium mixtures were prepared by calcium-reducing intimate mixtures of TiO_2 and ZrO_2 in a small bomb, as described previously for the preparation of Zr powder. Prior to the preparation of these mixed metal powders, a few experiments were made in the reduction of TiO_2 with calcium.

TABLE VI. *Effect of alloying constituents on zirconium powder*

Alloying Constituent (A)	% Zr	% A	Particle size or range microns	Ignition temp, °C	Burning time, sec/10 in.	Ignition energy, joules
Ti	44.7	40.0	2–8 (*a*)	228	7	0.000125
Ti	21.8	66	2–8 (*a*)	279	9.9	0.000045
Ti	11.8	73.5	2–8 (*a*)	>400	30.5	0.00045*
Ti	8.1	75.2	2–8 (*a*)	>500	45.2	0.0025*
Ti	0	86.0	2–8 (*a*)	>500	81	>21.9
Ni	87.2	6.2	<44	176	9.4	0.00016
Ni	79.1	13.8	<44	250	60	0.00036
Ni	64.5	29.9	<44	>400	202	12.5*
Ni	54.9	38.9	<44	>400	324	21.9*
Ni	34.7	54.3	<44	Would not burn		
Cu	85.3	7.7	<44	210	21.2	0.000625
Cu	72.1	15.1	<44	194	25.8	0.00125
Cu	64.0	31.4	<44	200	18.2	0.00144
Cu	49.2	46.0	<44	210	47.5	0.0025*
Fe	86.7	6.1	<44	132	31.0	0.000625
Fe	81.6	11.9	<44	162	23.4	0.000625
Co	89.0	13.5	<44	188	32.6	0.00025
H_2 (*b*)	90.0 (*c*)	0	3.77 (*a*)	218	11.8	0.00009
H_2 (*d*)	89.9	0.07	3.77 (*a*)	200	6	0.000045
H_2	89.9	0.08	3.77 (*a*)	204	11.5	0.000045
H_2	89.9	0.13	3.77 (*a*)	208	8	0.000045
H_2	89.4	0.55	3.77 (*a*)	230	42.5	0.000080
H_2	88.9	1.1	3.77 (*a*)	224	51	0.000125
H_2	88.6	1.5	3.77 (*a*)	260	73.1	0.00050*
H_2	88.5	1.8	3.77 (*a*)	>400	81	0.0225*

* Ignition not sustained.

(*a*) By air permeability method. (*b*) Degassed at 1100°C. (*c*) Free Zr, as determined by gain on ignition. (*d*) Degassed at 700°C.

The resulting metal powders had Ti contents varying from 86 to 91 per cent, burning times from 24 to 81 seconds, and ignition temperature over 500°C. The reaction rate constant for oxidation of Zr is some 23 times as great at 350°C as for Ti (28), and the corresponding activation energies are 18.2 and 26 kcal. The ignition temperature of Ti is thus different from that of Zr in the direction indicated by the theoretical expression developed earlier.

The other metallic alloys were prepared by vacuum melting, in graphite crucibles, appropriate mixtures of fused zirconium and powdered metal, crushing the resultant ingots, and grinding them to pass 325 mesh. No attempt was made to obtain a specific particle size, but the results are sufficient to show that the static sensitivity of Zr cannot be appreciably decreased except by use of very large proportions of the alloying metal.

The hydrided zirconium samples were prepared from metal powder made by calcium reduction of ZrO_2. A quartz tube containing a weighed amount of the powder was sealed to a glass vacuum system, and heated under high vacuum to expel hydrogen already contained. Hydrogen was then admitted to the system, and in turn admitted to the sample. Amount of hydrogen consumed was calculated from pressure decrease and the known volume of the system. After degassing at 1100°C, the sample absorbed H_2 very slowly; after degassing at 700°C, the hydrogen absorption started readily at room temperature. The absorption was exothermic and increased in rate as the sample temperature rose. A portion of the sample richest in hydrogen (corresponding to $ZrH_{1.8}$) was degassed at 1100°C, and the sintered cake ground lightly to permit burning measurements. The burning time was 9.2 sec, and the ignition temperature 216°C, essentially duplicating the values found for the original Zr powder simply degassed at 1100°C. The effect of hydriding on powder properties is, therefore, reversible. Inspection of the data indicates a slight break in burning time and ignition temperature near 0.5 atom H/atom Zr. Not until the sample had been almost completely converted to ZrH_2, however, was there a significant increase in ignition energy. Such results are in accord with the findings of Hartmann (25), who reported ignition energies of 64–320 microjoules for ZrH_2 dust layers; although slightly greater than most of the values reported for Zr powder, these spark energies still place the hydrides in the hazardous category.

Hazards

The hazards incident to handling subsieve zirconium powders arise because of their sensitivity to ignition by static electricity or heat. Suggestions for safe handling of such material have been published by the National Safety Council (29) and by Fink (30).

As shown in this paper, zirconium powder intrinsically coarser than 10 microns is relatively insensitive to ignition, and such powder can be safely handled dry. The statement does not apply to powders nominally coarser than 10 microns but consisting of agglomerates of particles smaller than 10 microns. Powders containing an unknown proportion of fines (particles smaller than 10 microns) should be handled with the same care as recommended by the National Safety Council, until extensive testing and experience have shown that extreme precautions are unnecessary.

Conclusions

Subsieve zirconium powder made by calcium reduction of ZrO_2 has maximum activity when the high-temperature exposure of the reacted mass is kept to a minimum. The combustion properties (ignition temperature and burning time) are not a critical function of the calcium purity, size, nor molar excess, but depend upon the type of oxide used. Magnesium reduction of ZrO_2 yielded powders of high activity but low free metal content. Fused zirconium prepared by bomb reduction of $ZrCl_4$ with calcium can be ground to discrete particles in the sieve range. Ignition energy determinations on fractions of such ground Zr showed that particle diameter of 10 microns represents approximately the dividing line between hazardous and nonhazardous powder, using 0.01–0.04 joule as a criterion of critical ignition energy. Thermal ignition appears to occur by spontaneous combustion, and the dependence of ignition temperature on several variables follows qualitatively the expression:

$$\text{ignition temperature} > \frac{E}{2R \ln (m^{\frac{1}{2}}/Kt^{\frac{1}{2}} d)},$$

where E is the activation energy for zirconium oxidation, m the sample mass, d the particle diameter, and t a time factor related to the oxide film thickness. Because of variations in this film thickness, the burning time of Zr powders is not uniquely determined by the surface area, as measured by low-temperature nitrogen adsorption. The adsorption experiments showed that the metal particle size approaches, as a lower limit, that of the oxide, and also that the metal particles are not appreciably porous. The ignition sensitivity of Zr could not be decreased by alloying with Ti, Ni, Cu, Fe, Co, or H_2, except by use of amounts so great that burning properties were deleteriously affected.

Acknowledgments

The authors wish to thank the Frankford Arsenal, under whose sponsorship a part of this research was carried out, and the Foote Mineral Company, for permission to publish these results. Mr. Thomas Stevenson, of the Pitman-Dunn Laboratory of the Frankford Arsenal, has provided many suggestions relevant to the course of the research and supplied spark evaluations of all samples reported herein. Frequent stimulating discussions with Mr. Charles L. Scheer of this laboratory contributed to the progress of the work, and Mr. Anthony C. Demos carried out several of the experimental phases of the research.

Any discussion of this paper will appear in a Discussion Section, to be published in the December 1953 issue of the Journal.

References

1. J. H. deBoer, *Foote Prints* **3**, No. 2, 1 (1930).
2. W. J. Kroll and W. W. Stephens, *Ind. Eng. Chem.*, **42**, 395 (1950).
3. R. J. Brumbaugh, *Ind. Eng. Chem.*, **43**, 2878 (1951).
4. D. B. Alnutt and C. L. Scheer, *Trans. Electrochem. Soc.*, **88**, 195 (1945).
5. K. S. Pitzer and S. G. English, *Chem. Eng. News*, **29**, 4836 (1951).
6. L. F. Ehrke and C. M. Slack, *J. Appl. Phys.*, **11**, 129 (1940).
7. W. Espe, M. Knoll, and M. P. Wilder, *Electronics*, **23**, 80 (1950).
8. M. Pipkin (to the General Electric Co.), U. S. Pat. 2,285,125, June 2, 1942.
9. G. H. Chambers, *Metals & Alloys*, **4**, 199 (1933).
10. U. S. Government Specifications JAN-Z-399A, Aug. 13, 1948.
11. D. Hart and W. R. Tomlinson, Jr., *Metal Progr.*, **59**, 788 (1951).
12. German Pat. 441,639, (to the Westinghouse Lamp Company), July 24, 1924.
13. J. H. deBoer and J. D. Fast, *Z. anorg. u. allgem. Chem.*, **187**, 177 (1930).
14. W. C. Lilliendahl and H. C. Rentschler, *Trans. Electrochem. Soc.*, **91**, 285 (1947).
15. P. S. Roller, *Proc. Am. Soc. Testing Materials*, **32**, Part II, 607 (1932).
16. A. Klein, pp. 52–65 in *ASTM Symposium on New Methods for Particle Size Determination in the Subsieve Range*, March 4, 1941.
17. I. Hartmann, *Ind. Eng. Chem.*, **40**, 752 (1948).
18. W. C. Krumbein and F. J. Pettijohn, "Manual of Sedimentary Petrography," p. 147, Appleton-Century-Crofts, Inc., New York (1938).
19. U. S. Government Specifications W-L-122, Federal Standard Stock Catalog Section IV, Part 5, Feb. 2, 1945.
20. F. B. Litton, *Metal Progr.*, **60**, 83 (1951).
21. E. A. Gulbransen and K. F. Andrew, *J.* (*and Trans.*) *Electrochem. Soc.*, **96**, 364 (1949).
22. H. Eyring and B. J. Zwolinski, *Record Chem. Progr.*, **8**, 87 (1947).
23. T. E. Leontis and F. N. Rhines, *Trans. Am. Inst. Mining Met. Engrs.*, **166**, 265 (1946).
24. W. M. Fassell, Jr., L. B. Gulbransen, J. R. Lewis, and J. H. Hamilton, *J. Metals*, **3**, 522 (1951).
25. I. Hartmann, J. Nagy and M. Jacobson, "Explosive Characteristics of Titanium, Zirconium, Thorium, Uranium, and their Hydrides," U. S. Bureau of Mines, Repts. Invest. 4835 (1951).
26. P. H. Emmett, pp. 95–105 in *ASTM Symposium on New Methods for Particle Size Determination in the Subsieve Range*, March 4, 1941.
27. W. G. Guldner and L. A. Wooten, *J.* (*and Trans.*) *Electrochem. Soc.*, **93**, 223 (1948).
28. E. A. Gulbransen and K. F. Andrew, *J. Electrochem. Soc.*, **97**, 383 (1950).
29. "Zirconium," National Safety Council Industrial Data Sheet D-Chem. 45.
30. W. C. Fink, *Sylvania Technologist*, **5**, 7 (1952).

Alkaline Earth Orthophosphate Phosphors[1]

KEITH H. BUTLER

Sylvania Electric Products Inc., Salem, Massachusetts

ABSTRACT

The characteristics of new phosphors, comprising orthophosphates of calcium, strontium, and barium, and their mixtures are described. The primary (absorbing) activator is tin dissolved in the matrix and with this activator alone strontium, barium, and alpha calcium phosphate emit either in the long wave ultraviolet or the blue regions of the spectrum, while beta calcium phosphate emits mainly in the red. Introduction of manganese as a secondary activator into beta calcium phosphate or into the mixed calcium-strontium phosphate gives deep red emission. Variable color can be obtained by varying the manganese content. Beta calcium phosphate, tin activated, has an efficiency of 45 lpw in 40 watt fluorescent lamps and their color is close to 3500° White. It gives outstandingly good color rendition and represents an improvement over the red phosphor now used in the Deluxe line of lamps.

INTRODUCTION

Although halide-free phosphate phosphors emitting visible light have received some attention in the patent literature (1–3), other published information is rather scanty. Huniger and Panke are quite indefinite in their description of the matrix materials, but from the context it seems probable that they were working with meta phosphates. Tin-activated calcium phosphate, strontium phosphate, or barium phosphate were all listed as giving a medium fluorescence of blue color. McKeag deals with pyrophosphates of strontium or barium, activated by tin or tin and manganese. Kroger (4) has mentioned the preparation of doubly activated orthophosphates of calcium and strontium, containing the combinations Ce-Mn and Sn-Mn. Froelich and Margolis (5) have also published an excellent discussion of calcium orthophosphate, activated by cerium and manganese, which emits deep red light. Henderson and Ranby (6) have described a blue-green emitting barium pyrophosphate, activated by a rather large amount of titanium.

In considering the alkaline earth phosphates as phosphors, it is important to recognize clearly the multiplicity of crystal structures which may be encountered and to specify exactly which crystal structure is being used in the particular phosphor. The best summary on the crystal structures of the calcium phosphates is that of Bale, Bonner, and Dodge (7), who give x-ray powder diffraction patterns of 11 different materials. There are no equally thorough surveys of either the barium or strontium phosphate systems, though Zachariasen (8) has proposed a crystal structure for the two orthophosphates.

The present paper discusses the preparation and properties of phosphors made from the orthophosphates of calcium, strontium, and barium or from mixed orthophosphates, employing tin or tin and manganese as activators.

No previous work has been published dealing with orthophosphate phosphors,* activated by tin alone, and only the single reference by Kroger has been found for orthophosphate phosphors containing both tin and manganese. Kroger's work was limited to preparation of two specific phosphor compositions by firing in wet nitrogen, which is not suitable for most of the phosphors described in the present paper.

The primary activator in these orthophosphate phosphors is stannous ion in solid solution in the lattice, probably replacing calcium.[2] It need be present only in low concentration while the secondary activator, manganese, must be present in larger amounts before its emission will be appreciable.

METHOD OF PHOSPHOR PREPARATION

The basic raw materials used in the preparation of all of the phosphors were the secondary phosphates and the carbonates of the alkaline earths, with the activators being added generally as stannous oxide and manganous carbonate. The secondary phosphates were made by precipitation, with purified ammonium monohydrogen phosphate, of a pure chloride or nitrate solution. A small amount of am-

[1] Manuscript received July 21, 1952. This paper was prepared for delivery before the Philadelphia Meeting, May 4 to 8, 1952.

[2] In this paper "primary activator" is used for the activator capable of absorbing exciting radiation and capable also of emission. The energy absorbed may be transferred to the "secondary activator" which is not capable of absorbing the exciting radiation directly, but which may furnish the main visible emission band.

*Note added in proof: Th. P. J. Botden, has published [*Philips Research Rpts.*, **7**, 197 (1952)] some data on strontium orthophosphate activated by tin.

monium chloride was sometimes added to the blend of raw materials to catalyze the diffusion of the activators into the lattice.

The powdered raw materials were dry blended and hammer milled to insure intimate mixing before firing. The blends were fired in an electrically heated furnace, in open silica crucibles, to form the orthophosphates containing the activators in solid solution in their oxidized form. These nonfluorescent white or pink powders were then converted to phosphors by firing and cooling in a controlled atmosphere, which consisted of a mixture of hydrogen with oxygen-free nitrogen. The exact mixture used was determined by the firing temperature and by the composition of the phosphor, but it generally contained from 0.5 to 10 per cent hydrogen by volume. The color of light emitted was generally independent of the composition of the ambient atmosphere, but brightness was low either with very low hydrogen content or with excessive hydrogen content, due in the first case to insufficient stannous ion being formed and in the second case to reduction to metallic tin. The temperature for the initial firing ranged from 1040° to 1200°C, while that of the second firing ranged from 925° to 1200°C.

The firing method, using carefully controlled reducing atmospheres, is quite different from those previously described in the literature. In the past, either an inert atmosphere, such as nitrogen, has been relied upon to prevent oxidation of the activators, or a strong reducing atmosphere, such as dry or wet hydrogen, has been used to insure complete reduction of the activators. Neither atmosphere is fully effective with the tin-activated phosphates, since nitrogen does not prevent oxidation by the water vapor or CO_2 evolved during firing, and pure hydrogen gives metallic tin. In contrast, controlled small amounts of hydrogen serve to reduce the stannic ion to stannous ion without formation of the free metal.

While the phosphors are designated as orthophosphates, they generally contain less than the stoichiometric amount of the alkaline earths, as materials with the theoretical amount do not fluoresce well.

The phosphors made with tin as the only activator have emission colors determined solely by the crystal structure of the matrix, with concentration of the activator having no effect. When manganese is introduced as a second activator, the emission color becomes dependent on the manganese concentration, since the emission band due to tin is gradually suppressed, while that due to manganese builds up, as the concentration increases.

The following sections of this paper will describe briefly the outstanding characteristics of the various phosphors, classified according to the alkaline earth metals used to form the orthosphosphate. The ultraviolet emission of some of the individual phosphors is described in a separate section.

The composition is expressed as gram-atoms of each metal for each two gram-moles of the PO_4 radical. Thus, a typical calcium strontium orthophosphate would have the composition:

Element	Gram-atoms
Ca	1.44
Sr	1.44
P (as PO_4)	2.00
Sn	0.04
Mn	0.04

TABLE I

Gram-atoms						Firing conditions		Figure
Ca	Sr	Ba	P (as PO_4)	Sn	Mn	% H_2	°C	
2.88	—	—	2.00	0.005	—	1.8	1200	1 (Alpha-Sn)
2.88	—	—	2.00	0.040	—	2.8	1200	1 (Beta-Sn)
2.84	—	—	2.00	0.020	0.080	3.6	1200	1 (Beta Sn-Mn)
—	0.00	2.88	2.00	0.040	—	2.8	1150	2 A
—	0.88	2.00	2.00	0.040	—	2.8	1040	2 B
—	2.00	0.88	2.00	0.040	—	2.8	1150	2 C
2.88	—	—	2.00	0.010	—	2.8	1175	3
2.64	—	0.24	2.00	0.040	—	2.8	1040	3
2.00	—	0.88	2.00	0.040	—	2.8	1175	3
2.66	0.22	—	2.00	0.040	—	1.8	1200	4
2.00	0.88	—	2.00	0.040	—	1.8	1120	4
2.00	0.88	—	2.00	0.040	0.00	1.8	1200	5
2.00	0.88	—	2.00	0.040	0.01	1.8	1200	5
2.00	0.88	—	2.00	0.040	0.08	1.8	1200	5
2.80	—	—	2.00	0.005	—	2.8	1175	6 (Alpha)
2.80	—	—	2.00	0.005	—	2.8	1065	6 (Beta)
1.60	1.20	—	2.00	0.020	—	0.3	1090	7
2.00	—	0.88	2.00	0.010	—	0.6	1175	8
2.88	—	—	2.00	0.005	—	1.4	1200	8
—	2.80	—	2.00	0.040	—	0.6	1200	8
—	—	2.88	2.00	0.040	—	0.6	1150	8

Table I lists the composition and final firing conditions of the phosphors for which emission curves are given in the accompanying figures. Except for tricalcium phosphate, as discussed below, nearly identical emission curves are obtained with a wide range of hydrogen concentrations and firing temperatures. The firing time for the controlled atmosphere firing was one hour, using a porcelain boat in a 1½-in. x 30-in. silica tube.

Calcium Orthophosphate Phosphors

Three different types of phosphors have been made, based on tricalcium phosphate, and their characteristics are listed briefly in Table II. The emission curves of typical materials are shown in Fig. 1.[3]

The alpha form of the phosphate is quite readily produced by firing at temperatures above 1175°C, with low amounts of tin present and compositions near the stoichiometric amounts. Deviations from these conditions lead to the formation of the beta form, and the production of this can be made certain by the use of rather large amounts of tin and control of the atmosphere so as to only partially reduce the stannic ion. Apparently, the stannic ion inhibits the conversion to the alpha form at temperatures below

TABLE II

Crystal structure	Activators	Emission	Peak wavelength
High temp (Alpha)	0.005 Sn	Blue	4900
Low temp (Beta)	0.04 Sn	White	6300
Low temp (Beta)	0.02 Sn + 0.08 Mn	Orange	6500

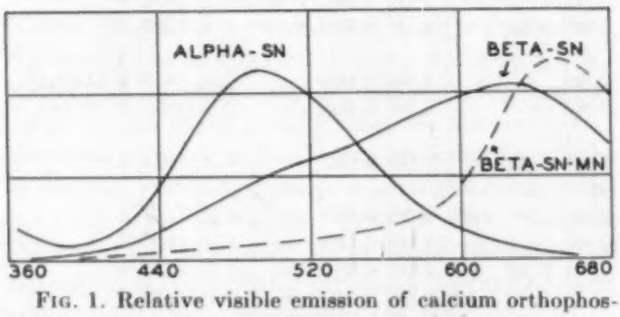

Fig. 1. Relative visible emission of calcium orthophosphates activated by tin and by tin and manganese.

1200°C. Manganese also inhibits the conversion to the alpha form and it has proved rather difficult to obtain alpha tricalcium phosphate containing tin and manganese. However, this phosphor has a very weak fluorescence and is not of great interest.

The reduction processes, converting stannic ion to stannous ion and stannous ion to metallic tin, are sensitive to temperature, and the ambient atmosphere employed during firing must be changed in ratio of hydrogen to nitrogen to suit the exact time and temperature of firing.

With tin contents between 0.01 and 0.04 gram-atoms per mole of calcium phosphate, it is readily possible to produce phosphors of variable color ranging from blue to white, with the emission depending on the relative proportions of the two crystal structures present in the final product.

The visible emission of the alpha form of the phosphor, activated by tin, is a single band with a Gaussian distribution of energy against wave number. In addition, there is an ultraviolet emission band.

The visible emission of the beta form, tin-activated, is somewhat more complex and it may be analyzed into two subbands with Gaussian distribution of energy, the peaks of these subbands lying at 6300 and 4950 Å.

The introduction of manganese into the tin-activated beta structure apparently suppresses the tin emission as the concentration of manganese increases, with the development of a new emission band peaking at 6500 Å. Thus the result of the manganese addition is a gradual shift from a white to an orange-red emission. With manganese concentrations above 0.15 gram-atoms, the emission becomes quenched and intensity drops off.

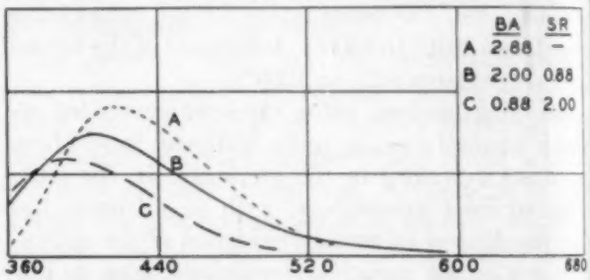

Fig. 2. Relative visible emission of tin-activated barium-strontium orthophosphates.

Strontium and Barium Orthophosphate Phosphors

At the firing temperatures used for the preparation of these phosphors, only one crystal form of strontium orthophosphate and barium orthophosphate was detected, confirming previously reported data. Both phosphors show relatively simple emission spectra, that of barium orthophosphate lying in the visible with the peak at about 4150 Å as shown in Fig. 2. The color of the emission is independent of the tin concentration, but the efficiency falls off at either very low or very high concentrations. The control of the tin reduction also becomes difficult at concentrations above 0.08 gram-atoms and the powders are frequently grayish, unless the ambient atmosphere during firing is correctly chosen.

The emission of strontium orthophosphate lies completely in the ultraviolet and will be described in a later section.

Addition of manganese to the strontium phosphate results in rather poor emission in the visible with the

[3] In Fig. 1 to 5 the relative energy scale is the same and 2537 Å radiation is used for excitation.

effect of the manganese being mainly that of suppressing the emission due to tin, though it does introduce a band peaked at 6100 Å. Barium phosphate will not dissolve manganese.

Mixed Orthophosphate Phosphors

Use of a mixture of the alkaline earth metals in place of the single metals results in slight changes with certain mixtures and in more radical changes in the emission spectra for other systems.

Strontium-Barium Phosphates

The effect of replacing a part of the barium, in barium orthophosphate, by strontium is relatively slight with a gradual shift in the peak of the emission curve. Typical emission curves are given in Fig. 2. The change in position of the peak is quite gradual through most of the range, but as the pure strontium phosphate is approached, the change in peak emission becomes more rapid.

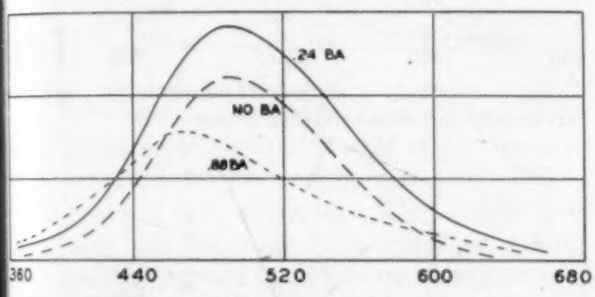

Fig. 3. Relative visible emission of tin-activated calcium-barium orthophosphates.

Strontium-Barium-Calcium Phosphates

Tin-activated phosphors containing all three of the alkaline earth metals generally gave very poor emission when moderate amounts of any of the three components were present.

Calcium-Barium Phosphates

When there is gradual replacement of calcium by barium in the alpha phosphate there is at first little change in the emission spectrum or in the crystal structure, although there is a definite change in physical properties, with evidence of a eutectic for the composition containing 2.44 gram-atoms of calcium and 0.44 gram-atom of barium. Further replacement leads to changes in both emission spectrum and crystal structure, as evidenced by powder diffraction patterns. With 2.00 gram-atoms of calcium and 0.88 gram-atom of barium, only the new powder diffraction pattern is found, and the emission curve peaks at 4700 Å. Further increase in the barium content leads to decreased emission, until the pure barium orthophosphate is approached. Typical curves are shown in Fig. 3.

Like many other systems containing barium, manganese is not soluble in the calcium-barium phosphates and useful phosphors containing manganese have not been made.

Calcium-Strontium Phosphates

This system shows rather radical changes in the emission spectra as the composition of the mixture is varied.

Starting with the beta form of tricalcium phosphate, which has a red emission band with subbands peaked at 6300 and 4950 Å, the apparent effect of strontium substitution up to 0.88 gram-atom is a suppression of the 4950 subband, without major change in the 6300 subband, and the development of a new emission band at 4000 Å. While the 6300 subband shows no major change, it does shift position slightly from 6300 to 6150 Å as shown in Fig. 4. The emission color thus shifts from a white to a red, because of the suppression of the 4950 sub-

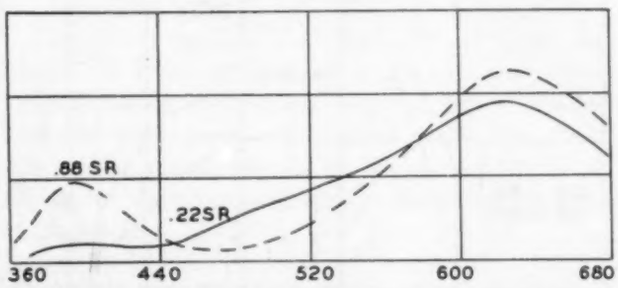

Fig. 4. Relative visible emission of tin-activated calcium-strontium orthophosphates.

band and the low visual effectiveness of the band at 4000 Å. This change in emission occurs without change in crystal structure other than a slight expansion of lattice.

Addition of manganese to a phosphor containing 2.00 gram-atoms of calcium and 0.88 gram-atom of strontium, like additions to beta calcium phosphate, results in a gradual suppression of the tin emission at 4000 Å, while the change in the red emission band may be interpreted as a suppression of the tin band at 6150 Å and the development of a new manganese band peaking at 6350 Å. This manganese band is considerably sharper than that due to tin, so the emission color is deep red. Fig. 5 shows emission curves for phosphors containing 2.00 gram-atoms of calcium and 0.88 gram-atom of strontium.

With tin activation, further increase in the strontium content above 0.88 gram-atom results in the development of a new type of crystal structure which might be described as a transition structure between calcium and strontium phosphates. However, this change of structure does not cause any marked change in the emission spectra. Surprisingly,

the typical red emission spectrum persists even with compositions containing as much as 2.60 gram-atoms of strontium with 0.20 gram-atom of calcium, even

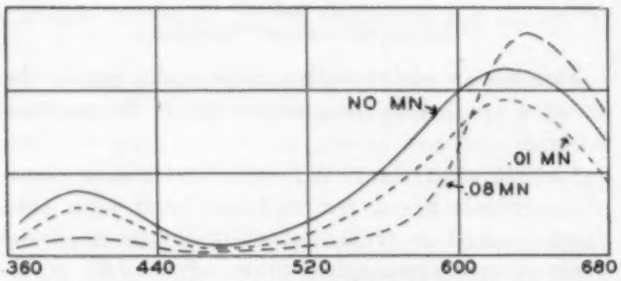

FIG. 5. Relative visible emission of calcium-strontium orthophosphate activated by tin and manganese.

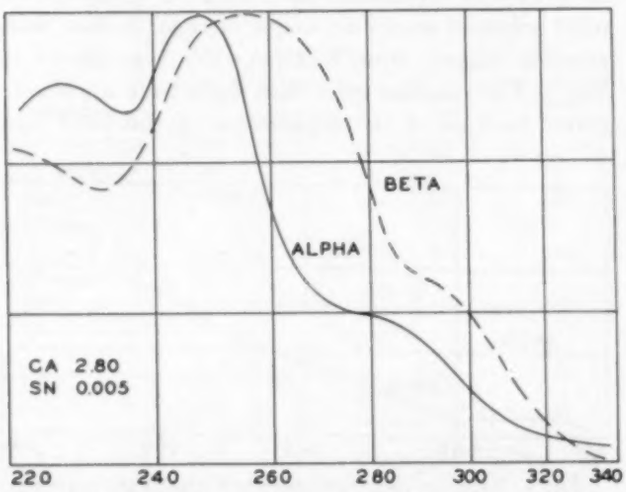

FIG. 6. Normalized reiative excitation spectra of alpha and beta calcium orthophosphate activated by tin.

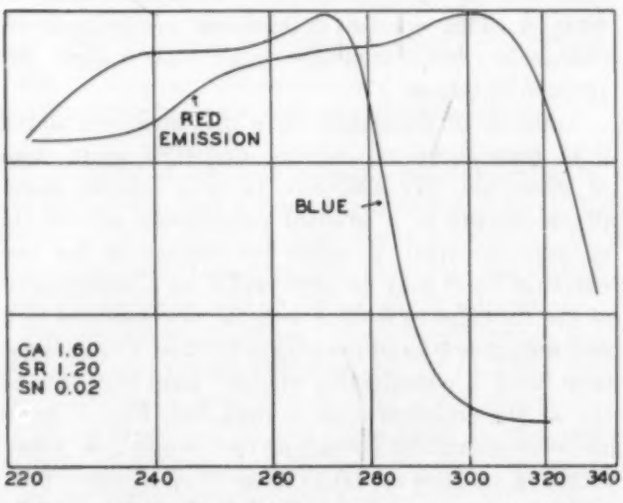

FIG. 7. Normalized relative excitation spectra of calcium-strontium orthophosphate for red and blue emission bands.

though this shows the powder diffraction pattern of strontium orthophosphate. Beyond this point, there is a sharp transition to the typical ultraviolet emission of the tin-activated strontium orthophosphate.

EXCITATION SPECTRA

A rather limited amount of work has been done on the excitation spectra of these phosphors and data on these spectra will be reported in a later paper. The excitation spectra are quite complex in their dependence on composition and show a multiplicity of peaks, in some cases, over a wavelength range from 2200 to 3200 Å. In general, the peak of the excitation curves lies close to 2537 Å, so that the efficiency of excitation by the low-pressure mercury arc is excellent. The results on

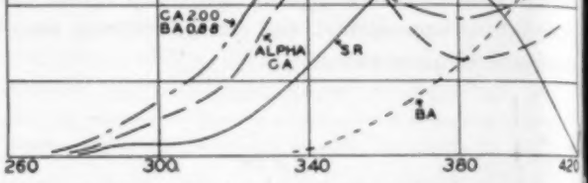

FIG. 8. Normalized ultraviolet emission spectra of various orthophosphates activated by tin.

FIG. 9. Emission spectra, omitting mercury lines, of 40T12 Cool White fluorescent lamps. A, major component $CaSiO_3$:Pb,Mn; B, major component $Ca_3(PO_4)_2$:Sn.

the mixed calcium strontium orthophosphates activated by tin are especially interesting since they show different excitation spectra for the red and the blue emission bands. For example, radiation of 3000 Å will excite red emission efficiently but will not cause appreciable blue emission. Some typical normalized excitation curves are given in Fig. 6 and 7.

ULTRAVIOLET EMISSION SPECTRA

As mentioned previously, some types of tin-activated phosphate phosphors show emission in the ultraviolet. Typical examples are shown in Fig. 8. In this figure, the ultraviolet emission curves have been normalized since our method of measurement

did not permit accurate intercomparison of different phosphors. However, it should be noted that the emission was much weaker than that of lead-activated barium disilicate, the best of the blacklight phosphors.

Applications

A number of these phosphors offer considerable promise for use in fluorescent lamps, especially in Deluxe types, because of the large amount of deep red light emitted and the relatively high efficiency. Some of the blue emitting phosphors are also of interest as possible replacement for certain tungstates.

The properties of typical red phosphors when made into 20 watt lamps are listed below:

Alkaline earths	Activators	100 hr lpw	x	y
Calcium (Beta).....	Sn	35	0.417	0.384
Calcium (Beta).....	Sn, Mn	21	0.420	0.345
Calcium + strontium....	Sn	29	0.444	0.363
Calcium + strontium....	Sn, Mn	21	0.465	0.339

The beta calcium phosphate, tin-activated, gives lamps with a color between that of one of the soft white lamps now on the market, and 3500° White, and by blending with magnesium tungstate and zinc orthosilicate can be made to match Cool White. This improved Deluxe Cool White has a very smooth output curve for the phosphor component, with an unusually large amount of deep red light, as shown in Fig. 9. The measured output in 40 watt lamps has reached 45 lpw at 100 hours and the color rendition obtained is exceptionally close to that with natural daylight.

Conclusion

The system of phosphors described in this paper is not only of considerable practical interest as an addition to the growing group of deep red phosphors for fluorescent lamp use, but also of great theoretical interest because of the striking differences in emission and excitation characteristics caused by changes in crystal structure or by replacement of one alkaline earth metal by another.

At present it seems that the various emission colors obtained with tin as the only activator can be interpreted as transitions between the $^1S_0$ ground state and the $^3P_1{}^0$ or $^1P_1{}^0$ excited states with the transition probabilities and the exact location of the absorption and emission bands being determined mainly by the crystal structure of the matrix. The phosphors containing both tin and manganese, in their general behavior, resemble calcium silicate activated by lead and manganese, or calcium halophosphate activated by antimony and manganese. All are, therefore, sensitized phosphors in which the primary activator is present in low concentration. They are unlike the other well-known systems activated by cerium and manganese, where the primary activator, cerium, must be present in high concentration.

It is expected that a detailed study of the excitation and emission spectra of these new phosphors will throw further light on the mechanisms of fluorescence, and work along these lines is in progress. Further interpretation of their behavior must be deferred until this is completed.

Acknowledgments

The author would like to thank Mr. R. Vogel and Mr. A. J. Oszy for data on excitation and ultraviolet emission spectra, and Mrs. V. M. B. Hannaford for x-ray powder diffraction data. He would like also to thank Mr. O. H. Biggs and Dr. E. F. Lowry for their encouraging interest in the progress of the work.

Note added in proof—See p. 250, column 2: Th. P. J. Botden has published [Philips Research Rpts., **7**, 197 (1952)] some data on strontium orthophosphate activated by tin.

Any discussion of this paper will appear in a Discussion Section, to be published in the December 1953 issue of the Journal.

REFERENCES

1. M. Huniger and H. Panke, U. S. Pat. 2,270,124, Jan. 13, 1942; 2,241,950, May 13, 1941; 2,241,951, May 13, 1941.
2. H. C. Froelich and J. M. Margolis, U. S. Pat. 2,575,754 and 2,575,755, Nov. 20, 1951.
3. A. H. McKeag, S. African Pat. 1974/50/2793/51.
4. F. A. Kroger, *Physica*, **15**, 801 (1949).
5. H. C. Froelich and J. M. Margolis, *J. Electrochem. Soc.*, **98**, 400 (1951).
6. S. T. Henderson and P. W. Ranby, *J. Electrochem. Soc.*, **98**, 479 (1951).
7. W. F. Bale, J. F. Bonner, H. C. Dodge, H. Adler, A. R. Wreath, and R. Bell, *Ind. Eng. Chem. Anal. Ed.*, **17**, 491 (1945).
8. W. H. Zachariasen, *Acta Cryst.*, **1**, 263 (1948).

Divisions of the Society

Battery
EUGENE WILLIHNGANZ, Chairman
N. C. CAHOON, Vice-Chairman
E. J. RITCHIE, Sec.-Treas.
The Eagle-Picher Company
Joplin, Mo.

Corrosion
FRED W. FINK, Chairman
W. D. ROBERTSON, Vice-Chairman
HAROLD A. ROBINSON, Sec.-Treas.
616 E. Grove Street
Midland, Mich.

Electric Insulation
THOMAS D. CALLINAN, Chairman
JOHN J. CHAPMAN, Vice-Chairman
RALPH A. RUSCETTA, Sec.-Treas
11 Constitution Road
Pittsfield, Mass.

Electrodeposition
M. L. HOLT, Chairman
C. A. SNAVELY, Vice-Chairman
SIDNEY BARNARTT, Sec.-Treas.
Westinghouse Research Labs.
East Pittsburgh, Pa.

Electronics
J. R. MUSGRAVE, Chairman
A. L. SMITH, Vice-Chairman
D. M. WROUGHTON, Vice-Chairman
MEIER SADOWSKY, Vice-Chairman
C. W. JEROME, Sec.-Treas.
Sylvania Electric Products Inc.
Salem, Mass.

Electro-Organic
C. L. WILSON, Chairman
H. M. SCHOLBERG, Vice-Chairman
STANLEY WAWZONEK, Sec.-Treas.
State University of Iowa
Iowa City, Iowa

Electrothermic
C. H. CHAPPELL, Chairman
A. E. PAVLISH, Vice-Chairman
I. E. CAMPBELL, Sec.-Treas.
Battelle Memorial Institute
Columbus, Ohio

Industrial Electrolytic
DEAN O. HUBBARD, Chairman
FRED W. KOERKER, Vice-Chairman
A. R. ORDAN, Sec.-Treas.
Niagara Alkali Company
Niagara Falls, N. Y.

Theoretical Electrochemistry
WALTER J. HAMER, Chairman
PAUL FUGASSI, Vice-Chairman
A. J. DE BÉTHUNE, Sec.-Treas.
Boston College
Boston, Mass.

Local Sections of the Society

Chicago
SIMON P. GARY, Chairman
HOWARD T. FRANCIS, Vice-Chairman
WERNER JACOBSON, Treasurer
ROBERT R. BANKS, Secretary
Armour Research Foundation
Chicago, Ill.

Cleveland
L. E. PUCHER, Chairman
N. C. CAHOON, Vice-Chairman
W. H. STOLL, Treasurer
J. M. MARGOLIS, Secretary
3628 Blanche Road
Cleveland, Ohio

Detroit
GLENN COLEY, Chairman
DAN TRIVICH, 1st Vice-Chairman
WRIGHT WILSON, 2nd Vice-Chairman
GERALD V. KINGSLEY, Sec.-Treas.
12083 Ward Avenue
Detroit, Mich.

Midland
H. A. ROBINSON, Chairman
H. H. ROTH, Vice-Chairman
W. R. PERRY, Sec.-Treas.
Chlorine Dept., The Dow Chemical Co.
Midland, Mich.

New York Metropolitan
A. C. LOONAM, Chairman
HERBERT BANDES, Vice-Chairman
F. A. LOWENHEIM, Sec.-Treas.
Metal & Thermit Corp.
Rahway, N. J.

Niagara Falls
MORTON S. KIRCHER, Chairman
HARRY R. OSWALD, Vice-Chairman
MILTON JANES, Sec.-Treas.
National Carbon Company
Niagara Falls, N. Y.

Pacific Northwest
G. L. PUTNAM, Chairman
GLENN WARE, Vice-Chairman
J. B. HEITMAN, Sec.-Treas.
604 North Carr Street
Tacoma 3, Wash.

Philadelphia
JOHN F. GALL, Chairman
J. F. HAZEL, Vice-Chairman
GEORGE F. TEMPLE, Treasurer
EDGAR L. ECKFELDT, Secretary
Leeds & Northrup Co.
Philadelphia, Pa.

Pittsburgh
M. T. SIMNAD, Chairman
R. D. WILLIAMS, Vice-Chairman
ROBERT A. WOOFTER, Sec.-Treas.
Jones & Loughlin Steel Corp.
Pittsburgh, Pa.

San Francisco
EDWARD B. SANIGAR, Chairman
GEORGE B. SCHEER, Vice-Chairman
R. F. BECHTOLD, Sec.-Treas.
The Dow Chemical Co.
Pittsburg, Calif.

Washington-Baltimore
R. S. DEAN, Chairman
S. EIDENSOHN, Vice-Chairman
FIELDING OGBURN, Sec.-Treas.
9607 Riley Place
Silver Spring, Md.

India
M. S. THACKER, Chairman
CHARAT RAM, Vice-Chairman
K. RAJAGOPAL, 2nd Vice-Chairman
J. BALACHANDRA, Sec.-Treas.
Indian Institute of Science
Bangalore, India